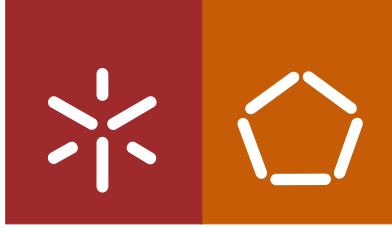


**Universidade do Minho**  
Escola de Engenharia

Manuel José Leal Zamith de Passos

## **A Radiofrequency Identification System for the 60 GHz ISM Band**



**Universidade do Minho**  
Escola de Engenharia

Manuel José Leal Zamith de Passos

## **A Radiofrequency Identification System for the 60 GHz ISM Band**

Dissertação de Mestrado  
Mestrado Integrado em Engenharia Biomédica  
Ramo de Eletrónica Médica

Trabalho efetuado sob a orientação do  
**Professor Doutor Paulo Mateus Mendes**

julho de 2015

## DECLARAÇÃO

Nome: Manuel José Leal Zamith de Passos

Endereço eletrónico: manueljosezamith@gmail.com

Telefone: +351 912096755

Cartão do Cidadão: 14170502

Título da dissertação: A Radiofrequency Identification System for the 60 GHz ISM Band

Orientador: Professor Doutor Paulo Mateus Mendes

Ano de conclusão: 2015

Mestrado Integrado em Engenharia Biomédica

Ramo de Eletrónica Médica

É AUTORIZADA A REPRODUÇÃO INTEGRAL DESTA DISSERTAÇÃO APENAS PARA EFEITOS DE INVESTIGAÇÃO, MEDIANTE DECLARAÇÃO ESCRITA DO INTERESSADO, QUE A TAL SE COMPROMETE.

Universidade do Minho, \_\_\_\_/\_\_\_\_/\_\_\_\_

Assinatura:

# AGRADECIMENTOS

Esta dissertação simboliza o concluir de uma etapa de cinco anos. Cinco anos na cidade de Braga que me transformaram como estudante e me enriqueceram como pessoa. Englobar numa ou duas páginas as pessoas que contribuíram para o meu crescimento é sem margem para dúvida uma tarefa pesada, destinada a fracasso. Espero, ainda assim, que estas me continuem a acompanhar nas futuras etapas que se avizinham.

Quero agradecer, em primeiro lugar, ao Professor Doutor Paulo Mendes, orientador deste trabalho, pelo desafio que me lançou, pela disponibilidade a todas as horas, pela experiência e pela compreensão nas vezes em que nem tudo corria como esperado. Obrigado também pela integração no projeto PTDC/EEI-TEL/2881/2012, patrocinado pela Fundação para a Ciência e Tecnologia, Programa Operacional Temático Fatores de Competitividade (COMPETE) e Fundo Comunitário Europeu FEDER.

Um grande agradecimento aos meus colegas de laboratório de Gualtar, pela boa disposição, pelo ambiente de ajuda constante e pelo alento que me deram num ano que não foi fácil. Quero destacar o Adriano e o Hugo, companheiros desde o primeiro ano. Obrigado pela amizade, pela empatia e pelas batalhas diárias que me ajudaram a ultrapassar.

A todos os que entraram comigo nesta viagem em 2010, é impossível enumerar os motivos da minha eterna gratidão. Amizade incondicional foi sempre uma característica que vi neste grupo e em mais nenhum. Tenho a certeza que nunca vos vou perder como amigos e que todas as aventuras vão perdurar na nossa memória. Macedo e França, não posso deixar de vos evidenciar porque é a vós que recorro sempre, para o bem e para o mal.

À restante família de Biomédica só tenho a agradecer tudo o que fazem para tornar este curso único. Aos meus eternos “engenheiros”, obrigado por me ensinarem a ser estudante. Aos meus caloiros, obrigado pela gritaria e pela dedicação. Destes últimos, agradeço a três em especial: Bia, Américo e Rei, obrigado por me ensinarem que as pequenas coisas às vezes são as maiores.

Bia e Pi, amigos da cidade berço, estou-vos grato por me fazerem perceber que as amizades, quando são verdadeiras, resistem ao teste do tempo. Foram inúmeros os desabafos que vos fiz. Vocês permitiram-me sempre escapar em alturas difíceis, e festejar em épocas de entusiasmo.

Ao meu irmão agradeço o exemplo que sempre me forneceu. Obrigado por me pores debaixo do teu braço quando precisei, por constantemente me explicares coisas que não

entendo, pelas intermináveis discussões que só me enriquecem. Espero continuar a discordar de ti por muitos mais anos. Nunca mudes, porque como tu não há igual.

Ao meu pai pela força de vontade e de decisão. Obrigado por me mostrares que na perseverança há uma grande virtude. Obrigado por seres assertivo quando me notas inseguro e por me dares tudo o que preciso, sem eu nunca te pedir.

Sobre a minha mãe podia escrever parágrafos intermináveis. Obrigado pelo amor, pelo carinho e por eliminares as minhas fraquezas. Obrigado por me obrigares a perspetivar e por me colocares no caminho certo quando, insistentemente, me desvio. Este ano teria sido muito mais difícil, não fosses tu. Tudo o que serei nesta vida a ti se deverá.

À minha restante família, avós, tios e primos agradeço a preocupação, o interesse e o ambiente inigualável a que me habituaram.

Por último, mas não menos importante, à Rita, que foi um pilar nos meses mais complicados do meu percurso académico. Trazes-me novo alento e obrigas-me a sair dos meus pensamentos, que são o meu pior inimigo. Obrigado por me salvares e por não desistires de mim. Se concluí esta dissertação, a ti o devo.

# RESUMO

Foi notável, no decorrer da passada década, o crescente interesse em sistemas sem fios de banda larga que comunicam usando ondas milimétricas. Este esforço continuado tem sido motivado pelas oportunidades que se preveem para as tecnologias nesta banda de frequências relativamente ao mercado da eletrónica de consumo.

Esta banda de frequências pode alterar a maneira como tiramos partido das comunicações sem fios em casa devido às suas características peculiares. Os 60 GHz estão posicionados num pico de absorção do oxigénio, o que significa que existe uma alta atenuação atmosférica. Esta qualidade permite uma elevada “reutilização” de frequência, assim como uma segurança acrescentada, como consequência da dificuldade de escuta entre canais. Além disso, a operação em frequências tão elevadas permite o desenvolvimento de agregados de antenas ultrapequenos e dispositivos com níveis de integração sem precedência, para uso em aplicações que exigem equipamentos miniaturizados.

Nesta dissertação, utiliza-se a tecnologia de ondas milimétricas a fim de implementar um sistema de identificação por radiofrequência (RFID) e mostra-se de que maneira pode ser usado para a deteção de instrumentos e esponjas retidas no decorrer de cirurgias.

Corpos retidos depois de uma intervenção cirúrgica são considerados erros evitáveis. Contudo, a documentação existente mostra que continuam a ser uma ocorrência em hospitais de todo o mundo, uma vez que as medidas de prevenção atuais dependem do desempenho humano.

Abordagens baseadas em tecnologia, nomeadamente por identificação por radiofrequência são a solução lógica para o problema. Colocando um pequeno rótulo (*tag*) no instrumento cirúrgico, este poderia ser identificado por um dispositivo de leitura numa estação base.

Fez-se um estudo da influência das esponjas cirúrgicas e do seu conteúdo em água na propagação das ondas de alta frequência, provando-se o potencial dos sistemas de ondas milimétricas para a aplicação em mão.

O estabelecimento de uma conexão nos 60 GHz foi bem sucedido até uma distância de 5 metros usando um conversor de bandas comercial sem o uso de antenas. Além disso, uma estratégia de *multiplexing* de frequência foi usada para codificar uma sequência binária no sinal. Para mais, montou-se um sistema de *downconversion* e retificação usando componentes

*off-the-shelf* e DIP para uma conversão de RF para DC, a fim de reproduzir a sequência transmitida na recepção.

O sistema RFID que foi implementado e validado poderá ser alvo de miniaturização, numa tentativa de melhorar as características da solução proposta, especialmente quando se considera as pequenas dimensões da instrumentação cirúrgica num aspeto geral.

# ABSTRACT

Over the past decade, there has been an increasing interest in mm-wave wireless broadband systems and enabling technologies. This consistent effort has been motivated by the foreseen opportunities for V-band (40 to 75 GHz) technology in the market of broad consumer electronics.

This frequency band could change the way we experience wireless communication at home due to some unique features. 60 GHz is placed in an oxygen absorption peak, meaning high attenuation takes effect, adding advantages such as high frequency reuse and improved security due to the difficulty of eavesdropping. Also, and on a more relevant note, mm-wave operation allows for the development of unprecedented ultra-small antenna arrays and integrated transceiver modules for applications where small footprint devices are of utmost importance.

In this dissertation we apply millimetre-wave technology to implement a radiofrequency identification system and show how it can be used for tracking retained surgical instruments and sponges.

Retained foreign bodies after operative interventions are considered a preventable mistake. However, literature shows that they're still an occurrence in hospitals worldwide because current prevention methods rely on human performance.

Technology-supported approaches, namely by radiofrequency identification (RFID), is a logical solution to the problem. By placing a small tag in the surgical objects, they could be identified by a reader device in a base-station.

Establishment of 60 GHz link was successful up to distances of 5 meters using a commercial V-band converter without the usage of antennas. A frequency multiplexing strategy was used to code a binary sequence into the signal. Also, a downconversion and rectification system was employed using off-the-shelf and DIP components for RF-to-DC conversion, in order to reproduce the transmitted sequence at reception.

A feasibility study was made in relation to the sponge's influence, according to water content, in wave propagation, proving the undeniable potential of mm-wave technology for the application at hand.

The system that was implemented and validated could possibly be a target for miniaturization, improving the proposed solution, considering the small sizes of surgical instruments in general.





# TABLE OF CONTENTS

Agradecimientos.....	iii
Resumo.....	v
Abstract.....	vii
List of Figures.....	xi
List of Tables.....	xiii
List of Abbreviations and Acronyms.....	XV
Chapter 1 Introduction.....	1
1.1 Retained Surgical Instruments.....	1
1.2 Technology-supported Approaches.....	5
1.3 Motivation.....	7
1.4 Contributions.....	8
1.5 Outline and Structure.....	10
Chapter 2 mm-Waves for Short Range Communication.....	11
2.1 Small-size, Highly Integrated Transmitters and Receivers.....	11
2.2 Available Bandwidth.....	19
2.3 Industrial Standards for the 60 GHz ISM Band.....	19
2.4 Atmospheric Factors.....	20
2.5 Propagation.....	21
2.6 RFID Based on Millimetre Waves.....	24
2.7 Examples of RFID Devices for the 60 GHz ISM Band.....	26
Chapter 3 Automatic Identification Systems.....	29
3.1 Types of Tags.....	30
3.1.1 Active Tags.....	31
3.1.2 Passive Tags.....	31
3.2 Role of the Reader.....	32
3.3 Accessing Multiple Tags Simultaneously.....	33
3.3.1 Conflict-free Access Protocols.....	34
3.3.2 Aloha Protocols.....	35

3.3.3	Carrier Sensing Protocols.....	36
3.3.4	Collision Resolution Protocols.....	37
Chapter 4	Implementation of an RFID System Using mm-Waves.....	39
4.1	Communication Protocol.....	40
4.2	Hardware .....	41
4.2.1	Block Diagram of the RFID System .....	42
4.2.2	IF Signal Generation and Modulation.....	44
4.2.3	V-band Converter by Sivers IMA .....	45
4.2.4	Decoding the Intermediate Frequency Signal .....	47
4.2.5	Control Unit of the RFID System .....	50
4.3	Software.....	52
4.3.1	Program for the Microcontrollers.....	52
4.3.2	Configuration of the Converter's Control Board .....	58
4.4	Suggested Protocol for Implementation in an Operating Room.....	59
Chapter 5	RFID System Characterization.....	61
5.1	60 GHz Link between Tag and Reader .....	61
5.2	Downconversion to 5 MHz and Rectification Circuit .....	65
5.3	Microcontroller Communication .....	69
5.4	Case study.....	70
Chapter 6	Conclusions and Future Work.....	75
6.1	Conclusions .....	75
6.2	Future Work.....	77
References	.....	79
Appendices	.....	89
Appendix A: Assembling the RFID system .....		89
Digital Lab Connections .....		89
V-band Converter boards.....		89
Voltage Controlled Oscillators and Mixers .....		91
Coaxial Amplifiers.....		93
Decoding Circuit in Breadboard .....		93
Microcontroller Units.....		94

# LIST OF FIGURES

<b>Figure 1</b> – Different foreign bodied retained during surgery: <b>a)</b> Retained needle detected by a CT scan to the pelvis; <b>b)</b> Retained clamp detected by an abdominal radiograph; <b>c)</b> Retained opaque sponge detected by an abdominal radiograph.....	2
<b>Figure 2</b> – Photograph the implemented RFID system. ....	8
<b>Figure 3</b> – Block diagram (in perspective) of the implemented RFID system, showing the separate components. ....	9
<b>Figure 4</b> – Frequency spectrum and available bandwidth. ....	19
<b>Figure 5</b> – Specific water vapour and oxygen attenuation values according to frequency. T=20 °C, p = 1atm, h = 0 Km. ....	21
<b>Figure 6</b> – Basic components on a simple RFID system.....	30
<b>Figure 7</b> - Simple representation of the backscattering principle.....	32
<b>Figure 8</b> – Overview of the system’s components. ....	39
<b>Figure 9</b> – Communication diagram for a link at the 60 GHz ISM band with the assembled setup. ....	40
<b>Figure 10</b> – Diagram of the communication protocol between reader and tag. ....	41
<b>Figure 11</b> – Diagram showing an overview of the full RFID system. ....	42
<b>Figure 12</b> – Output RX power according to distance for a power input of 20 dBm. ....	43
<b>Figure 13</b> – VCOs used for signal generation. ....	44
<b>Figure 14</b> – <b>a)</b> Picture of the Sivers IMA FC1005V00 and control board; <b>b)</b> Sketch with pin diagram; <b>c)</b> Block diagram. ....	46
<b>Figure 15</b> – Basic principle of downconversion.....	47
<b>Figure 16</b> – Photograph of the downconversion unit. ....	48
<b>Figure 17</b> – Block diagram of the decoding circuit.....	48
<b>Figure 18</b> – Implemented DIP decoding circuit. ....	49
<b>Figure 19</b> – Schematic of the decoding circuit.....	49
<b>Figure 20</b> – Connection diagrams of the control unit: <b>a)</b> Reader; <b>b)</b> Tag. ....	51
<b>Figure 21</b> – Flowchart of the main function of the Microcontroller Unit (Reader). ....	54
<b>Figure 22</b> – Flowchart of the Interrupt Service Routines of the Microcontroller Unit (Reader): <b>a)</b> Timer Compare Match; <b>b)</b> Pin Change; <b>c)</b> External Interrupt. ....	55
<b>Figure 23</b> – Flowchart of the main function of the Microcontroller Unit (Tag) .....	57

<b>Figure 24</b> – Flowchart of the Interrupt Service Routines of the Microcontroller Unit (Tag): <b>a)</b> Timer Compare Match; <b>b)</b> External Interrupt. ....	58
<b>Figure 25</b> – Example of converter configuration: <b>a)</b> TX module; <b>b)</b> RX module. ....	59
<b>Figure 26</b> – Assembled setup for a link at the 60 GHz ISM band. ....	61
<b>Figure 27</b> – Setup used to implement the link at 58 GHz, with different blocks differentiated. ....	62
<b>Figure 28</b> – Output intermediate frequency RX power according to: <b>a)</b> Increasing distances separating tag and reader; <b>b)</b> Different rotation angles at a fixed distance of 4 m. ....	63
<b>Figure 29</b> – Comparison between calculated and experimental values for the RX output power according to distance. ....	64
<b>Figure 30</b> – Setup used to implement the link at 58 GHz at different angles, with different blocks differentiated. ....	65
<b>Figure 31</b> – Spectral Characterization of the Downconversion block. ....	66
<b>Figure 32</b> – Characterization of the Rectification block. ....	68
<b>Figure 33</b> – Connection diagram to test the communication between control units. ....	69
<b>Figure 34</b> – Communication between reader and tag. Channel 1: output from tag; Channel 2: output from reader. ....	70
<b>Figure 35</b> – Illustration of the placement of the tags and reader. ....	71
<b>Figure 36</b> – Laboratory facilities where the measurements were conducted. ....	72
<b>Figure 37</b> – Materials used: <b>(left)</b> Cotton ball; <b>(right)</b> PVA sponge;. ....	73
<b>Figure 38</b> – Proposed integration solution: <b>a)</b> Artistic view; <b>b)</b> Three-dimensional view.....	77
<b>Figure 39</b> – Connections of the control unit. ....	89
<b>Figure 40</b> – Connection diagram of the converter board. ....	91
<b>Figure 41</b> – Schematic of the decoding circuit. ....	94

# LIST OF TABLES

<b>Table 1</b> – Most common explanations for falsely correct counts.....	4
<b>Table 2</b> – State-of-the-art of small, highly integrated transmitters and receivers. ....	8
<b>Table 3</b> – Summary of the research presented in section 2.1. ....	17
<b>Table 4</b> – Attenuation for different solid materials.. ....	24
<b>Table 5</b> – Transmission frequency bands used on RFID systems. ....	24
<b>Table 6</b> – Power and Frequency Budget (VCOs). ....	42
<b>Table 7</b> – Power and Frequency budget (downconversion unit). ....	44
<b>Table 8</b> – Interrupts of the reader device program. ....	53
<b>Table 9</b> – Interrupts of the tag device program ....	56
<b>Table 10</b> – IF output power measurements with tag placed in the ground.....	73
<b>Table 11</b> – IF output power measurements with tag placed at reader’s height ....	74
<b>Table 12</b> – Com-port settings for converter configuration ....	90
<b>Table 13</b> – Configuration example for the converter boards.....	90
<b>Table 14</b> – Connection summary of the VCOs.....	92
<b>Table 15</b> – Connection summary of the mixers.....	93
<b>Table 16</b> – Connection summary of the amplifiers ....	93
<b>Table 17</b> – Decoding circuit’s connection summary ....	94
<b>Table 18</b> – Microcontroller units’ connection summary ....	95



# LIST OF ABBREVIATIONS AND ACRONYMS

ACK	Acknowledgement
ACS	American College of Surgeons
AM	Amplitude Modulation
AORN	Association of periOperative Registered Nurses
ASK	Amplitude Shift Keying
Auto-ID	Automatic Identification
BMI	Body Mass Index
BPSK	Binary Phase Shift Keying
CMOS	Complementary Metal-oxide-semiconductor
CRP	Collision Resolution Protocol
CSMA	Carrier Sensing Multiple Access
CT	Computed Tomography
DC	Direct Current
DIP	Dual In-line Package
EAS	Electronic Article Surveillance
FDMA	Frequency Division Multiple Access
FM	Frequency Modulation
GPS	Global Positioning Service
HEMT	High-electron-mobility Transistor
HF	High Frequency
HJFET	Heterojunction Field Effect Transistor
HTCC	High Temperature Co-fired Ceramic
HW	Hardware
IC	Integrated Circuit
IEEE	Institute of Electrical and Electronics Engineers
ISR	Interrupt Service Routine
IF	Intermediate Frequency



ISM	Industrial, Scientific and Medical
JCAHO	Joint Commission for the Accreditation of Hospitals
LCP	Liquid Crystal Polymer
LED	Light-emitting Diode
LNA	Low-noise Amplifier
LO	Local Oscillator
LOS	Line-of-sight
LTCC	Low Temperature Co-fired Ceramic
MCU	Microcontroller Unit
mm-wave	Millimetre Wave
mHEMT	Metamorphic High-electron-mobility Transistor
MMIC	Monolithic Microwave Integrated Circuit
MMID	Millimetre Wave Identification
NLOS	Non-line-of-sight
OOK	On-off Keying
OR	Operating Room
PA	Power Amplifier
PCB	Printed Circuit Board
pHEMT	Pseudomorphic High-electron-mobility Transistor
PLL	Phase-locked Loop
QAM	Quadrature Amplitude Modulation
RF	Radiofrequency
RF-DAC	Radiofrequency Digital-to-analogue Converter
RFDS	Radiofrequency Detection System
RFID	Radiofrequency Identification
RSI	Retained Surgical Instruments
RX	Reception
SNR	Signal-to-noise Ratio
SW	Software
TDMA	Time Division Multiple Access
TX	Transmission
UHF	Ultra High Frequency
VCO	Voltage-controlled Oscillator

# CHAPTER 1 INTRODUCTION

Medical errors can be defined as the failure of a planned action to be completed as intended or the use of a wrong plan to achieve an aim. Preventable medical errors have always been an occurrence in hospitals all around the world [1].

The extreme complexity and diversity of the tasks involved in medical care leads to these mistakes and the fact that they happen infrequently, makes it hard for some institutions to study them further and identify risk patterns [2]. In the present chapter, we take a look at the medical error at hand, which happens when a surgical instrument or sponge is misplaced inside a patient's body during the course of surgical procedures. Recent literature continues to focus on risk factors, prevention methods, complications and technological trends, making us believe that retained surgical instruments (RSI) are a recurring problem [3]–[5]. Despite the efforts to minimize the occurrence of RSIs, zero incidence remains elusive.

Furthermore, we present automatic detection through a radiofrequency identification system as a mitigation of this problem, as well as what the motivations of this study and the scientific contributions that were made.

## 1.1 Retained Surgical Instruments

---

One persistent and poorly understood error is the misplacement of surgical instruments and sponges inside patients' bodies in the course of surgery. Despite being a rare event, it can lead to serious consequences for the patients and the medical care facility as well. There are reports of retained instruments in different surgical procedures such as prostatectomy, thyroidectomy,

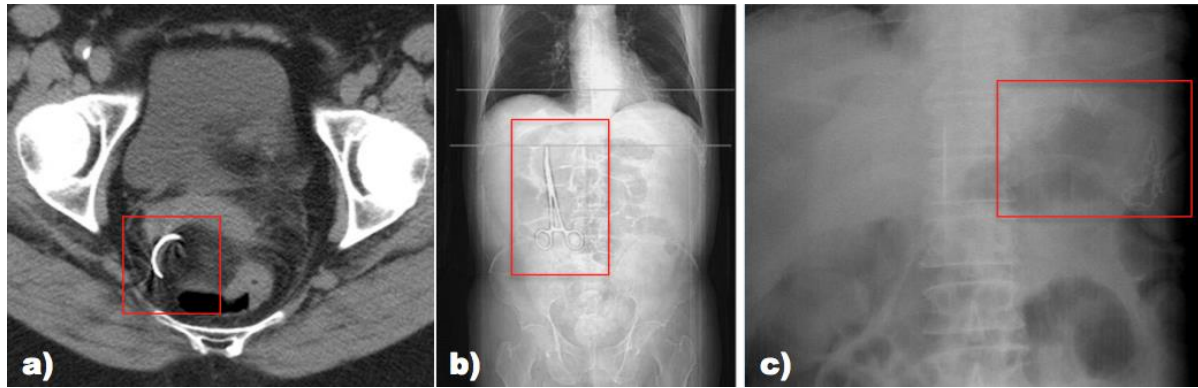


**Figure 1** – Different foreign bodies retained during surgery: **a)** Retained needle detected by a CT scan to the pelvis; **b)** Retained clamp detected by an abdominal radiograph; **c)** Retained opaque sponge detected by an abdominal radiograph. Adapted from [6].

cardiothoracic surgery (eg. sponges in the lung parenchyma, pleural space, and pericardium), neurosurgery (eg. sponges in the neck, spine), and orthopaedic surgery [6].

The incident of a foreign body varies from 1 in 5000 to 1 in 18000 overall, and up to 1 in every 1000 intra-abdominal operations [2], [3], [7]–[9], although no body cavity has been exempt. This roughly translates to one case per year in a hospital that conducts at least 10,000 cases per year [6]. Furthermore, mortality rates that result from unintended retained foreign bodies are as high as 11% to 35% [10]. **Figure 1** illustrates three different examples of foreign objects left behind in surgical procedures.

There are documented records of all kinds of retained objects, such as prosthesis, surgical clamps and needles [6] and even an asepto bulb [11]. However, surgical sponges and gauze sum up to about half of the claims for foreign retained bodies (48% to 69%) [12].

The relative rarity of this event does not diminish its physiological and psychological effects on patients and their families [7]. Plenty of complications can take place after a surgery in which a foreign body was retained, such as perforations, sepsis and even death [2], [8].

As an example, a gossypiboma, which is the name given to a retained surgical swab or sponge [13] can present itself in an immediate or a delayed phase. Early symptoms like nausea, vomiting, rectal bleeding and altered bowel habits can indicate an abscess formation or a fistula in the acute phase. Secondary to the exudative inflammatory reaction, the patient can also present fever, anorexia and weight loss. In this phase, it's not abnormal to detect penetration through the wall of a neighbouring organ, with migration into the organ. This results in obstruction or gastrointestinal haemorrhage from erosion of blood vessels [13].

The discovery of the misplaced items inside the patients' bodies most commonly happens through a postoperative x-ray [12]. However, ultrasound, magnetic resonance imaging and

computed tomography (CT) have also been used for diagnosis and the last mentioned has proven to be the most reliable method for detection of retained surgical instruments.

As so, the need for a follow-up surgery to remove the foreign body and drain the associated infectious collection is frequent [12] and the disclosure of an RSI to the patient is mandatory by law [4]. Moreover, the risk that disclosing a medical error (especially a preventable one) to a patient, cannot be disregarded, as it could prompt a lawsuit [14].

As can be immediately concluded, these situations can present serious complications, not only to the patients involved, but also to the medical facilities and professionals. In the case of a medical liability claim, defending the surgical team can be difficult and expensive [7], [12], [15]. In a study demonstrating the prevalence of 40 cases in a 7-year period, an expenditure of about \$500,000 for defence costs and \$2,000,000 for indemnity payments indicates the significance of the problem [12].

In addition, avoidable mistakes made in an operating room (OR) can attract wide critical press coverage [2] and represent significant organizational and personal embarrassments [7]. Yet, these errors persist.

Procedures to try to prevent these events are in effect in ORs all across the world. Guidelines have been promulgated by the American College of Surgeons (ACS), the Association of periOperative Registered Nurses (AORN), and oversight and regulatory agencies such as the Joint Commission for the Accreditation of Hospitals (JCAHO) [2], [6]. Nevertheless, it's up to every individual facility to develop their policy as an attempt to improve the provided service.

In most hospitals, current prevention measures include a surgical count performed by members of the surgical team [2], [6], [10], [13]. These counts are normally performed by registered nurses and technicians and, according to the most recent guidelines published by the AORN, counting should be done:

- ✓ Before the procedure, to establish a baseline and identify manufacturing faults;
- ✓ When new items are added to the field;
- ✓ Before closure of a cavity within a cavity (eg. uterus);
- ✓ At skin closure;
- ✓ At the time of permanent relief of the person responsible for counting [16].

Despite this, however, errors keep occurring. Counting is heavily dependent on human performance and is subject to inherent error. There are three separate circumstances where reliance on counting can mislead: either no count is performed, or there is miscount (cases where the count is incorrect) or falsely correct counts [6], [13]. The last one is the most common

occurrence of the three and makes the surgical count an unsafe practice. In fact, a study in [9] found that 66% of RSIs occurred when the count was claimed as correct and in [17] it's demonstrated that the sensitivity of surgical counts adds up to about 77%.

Adding to this, existing protocols have been criticized for interfering with the surgical flow [7]. **Table 1**, collected from [12], shows the diversity of explanations given by medical professionals when confronted on why these errors occur. In addition, in a study from 2013 [3], it is stated that the three main obstacles to reducing the incidence of RSIs are identifying lost items, reducing the rate of falsely correct counts and improving team attentiveness and compliance with recommended procedures.

We can safely conclude that these problems are unsolvable, as human mistake is always an important variable. Technology-supported approaches should be considered.

*Table 1 – Most common explanations for falsely correct counts.*

***Explanations given for incorrect counts***

---

*Team fatigue*

*End of shift*

*Adherent sponges*

*System problem*

*Surgeon declined repeat count*

*Falsely negative intraoperative x-ray*

*Excessively bloody procedure*

*Incorrect package count*

*Conversation in the OR*

*Registered nurse left the OR*

*No count performed*

*Sponge looked for, not found*

Nonetheless, other risk factors associated with RSIs include emergency surgery, high body mass index (BMI), unexpected changes in procedures and long duration of surgery [15].

Other recommendations state that only radiography-detectable sponges are to be used and that they should be counted once at the beginning and twice at the end of every open-cavity procedure. If a count is incorrect, that is, if all materials are not accounted for, manual or radiography oriented exploration is to be performed [2], [16].

There is a significant amount of data proving that radiography is not a reliable way to ensure

that an RSI does not occur, especially for sponges and needles. In [9], only 67% of the objects left in patients during surgery were identified by an intraoperative X-ray and in [12] 10,3% of retained sponges were falsely reported as negative in radiography results. As so, not only do intraoperative imaging techniques provide suboptimal information, they're also time consuming, expensive, and expose patients to unnecessary radiation. The cost of performing routine intraoperative radiographies to prevent retained instruments is estimated to be 11,5 million dollars for every harmful detected object [15].

## **1.2 Technology-supported Approaches**

---

The need for an automatic solution to this problem is imminent, as it would substantially reduce the unavoidable human mistake from this equation. In 2005, electronic article surveillance (EAS) applied to surgical sponges was introduced in [18]. This technology is commonly used in commercial applications to prevent theft in stores. This system proved an initial assessment of using electronic detection systems to possibly prevent retention of sponges.

An electronic system in which barcodes are applied to the swabs is already an FDA-approved solution. These represent two-dimensional data matrixes that grant each sponge a unique identifier. A scanner can be located in close proximity to the back table so that sponges can be counted as they are passed off the table, in a “grocery store” checkout fashion. Every instrument must be passed through the device in the beginning and end of the procedure [19]. This barcode solution is already available in the market and improves the reliability of surgical counting, as proved in a randomized trial from 2008 [20]. In this study, 300 general surgery operations were performed comparing a traditional counting system to a bar-coded sponge system. Outcome was improved, as about twice of the RSIs were detected and medical professionals seemed open to adopting the system. However, human mistake is still a problem in this methodology implies a learning curve, demanding training for all the surgical professionals. Also, surgery time was noted to require 12 minutes more on average (average surgery duration of 2,90 hours).

As another alternative, the use of radiofrequency detection systems (RFDS) holds great promise in this issue and there is application in the market already, by RF Surgical Systems, Inc. [21]. That system uses a passive RF tag embedded in sponges that can be detected if a wand is within 24 inches of it. This wand is connected to a detection console that generates an audible

and visible alarm when the tag is detected.

In 2011 [22] and 2013 [23] complete cross-over studies were performed that proved this method's level of accuracy surpasses any other and should be seriously considered when redesigning health care systems in order to enhance patient safety. Nevertheless, implementation of this system also requires training for the staff and is viewed as complementary to manual counting. Also, each tag contains no specific information about the surgical instrument where it's placed, so the system cannot distinguish between instruments; rather, it can only identify whether the tag is within reach, inside the patient or in any other place in the OR. In addition, the system cannot count tags, as the signal will have the same intensity whether there are 1 or 5 sponges to be detected.

An RFID system should be able to both count and detect, gathering the advantages of bar-coding and RFDS. This technology is faced as the most promising, given its unobtrusiveness and easy integration in healthcare systems. RFID does not require focused passing through scanners (unlike bar-coded methodologies) and it enables faster and simultaneous scanning of multiple items, minimizing human intervention in task performance [24].

ClearCount Medical [25] developed an RFID system that embeds a unique identification chip into each surgical sponge. There is a separate computer console with a scanning bucket into which used sponges are introduced.

Unopened packages of sponges are placed on a front panel to be electronically counted. Then the sponges are opened and placed on the sterile field. As used sponges are retrieved, the scanning bucket will count them individually. If there is a miscount, a wand that is attached to the bucket by a cord is used for inspection.

The passive chip is about 10 mm<sup>2</sup> which makes it noticeable and too large to fit through minimally invasive surgery trocars [26]. Also, the need to use a large wand attached to a main device by a cord can disrupt surgical flow, as well as be time consuming.

A clinical evaluation was made in 2006 [27] to prove the feasibility of ClearCount Medical's system, and it showed promising results. However, this early study lacked power to detect sensitivity and specificity and did not account for variability in the patients (such as weight and BMI), so there is still limited information about the accuracy and effectiveness of this technology [15].

One relevant concern in relation to the use of technology-supported approaches as part of surgical protocol is the financial investment. A recent report (2014) [15] featuring a cost-benefit analysis of radiofrequency technology showed that, in fact, the use of RF devices could represent a high initial cost because of the price of detectable sponges and wands. However,

one should account for the costs saved and avoided.

Decreased use of radiography equipment could save the hospital a lot of money, because of technician and radiologist fees. Also, avoided costs concerning readmission of patients, unnecessary follow-up surgical procedures and legal costs are a consequence of using more efficient equipment. The study concluded that hospitals could potentially save thousands of dollars annually.

However, no detection system has been assessed as a replacement for manual counting protocols and procedures, as current official recommended preventive measures don't yet include technology-supported approaches.

### 1.3 Motivation

---

“Never events” like RSIs are considered to be “avoidable”, however, current measures to prevent them consist of protocols and recommendations, which are also dependable on human performance. It's obvious that an automatic solution based on technology would be a step towards erasing human error from the equation and saving patients from complications resulting from these mistakes.

Millimetre waves represent frequencies between 30 and 300 GHz and are a trend in the electronics engineering and investigation world; as they could be an answer to the bandwidth shortage of wireless systems, as well as provide very large data rate links. However, for this dissertation, we're interested in other differentiating characteristics that make this band unique, such as allowing high-frequency reuse and the miniaturization of antennas to extremely small sizes.

Recent developments in mm-wave technology prove communications in the 60 GHz band could be the solution for the development of miniaturized devices for indoor communications. **Table 2** shows examples present in the most recent literature. These examples show how very small-sized devices with low power consumption for the 60 GHz band are a reality already. A more complete study is presented in section 2.1.

Since millimetre wave technology can be advantageous and present itself as a feasible solution to the RSI problem, the aim of this dissertation is to develop an RFID system working in the 60 GHz ISM band, which can be used to automatically identify objects inside of a room such as an operating room.



**Table 2** – State-of-the-art of small, highly integrated transmitters and receivers.

<i>Reference</i>	<i>Year</i>	<i>Technology</i>	<i>RX/TX</i>	<i>P<sub>OUT</sub>(dBm)</i>	<i>P<sub>C</sub>(mW)</i>	<i>Size (mm<sup>2</sup>)</i>
[28]	2012	40 nm CMOS	Single TX and RX IC	10,2	TX: 1820 RX: 1250	0,7
[29]	2014	65 nm CMOS	Single TX and RX IC	N/A	TX: 251 RX: 220	4,2
[30]	2014	40 nm CMOS	TX	10	75	2,38

*P<sub>OUT</sub>* – Output power of device.

*P<sub>C</sub>* – Power consumption of device.

## 1.4 Contributions

All components of an RFID system using mm-wave communication were implemented and feasibility of such system to mitigate RSI was proved. **Figure 2** shows the implemented full system and **Figure 3** illustrates a block diagram for better comprehension of the different components.

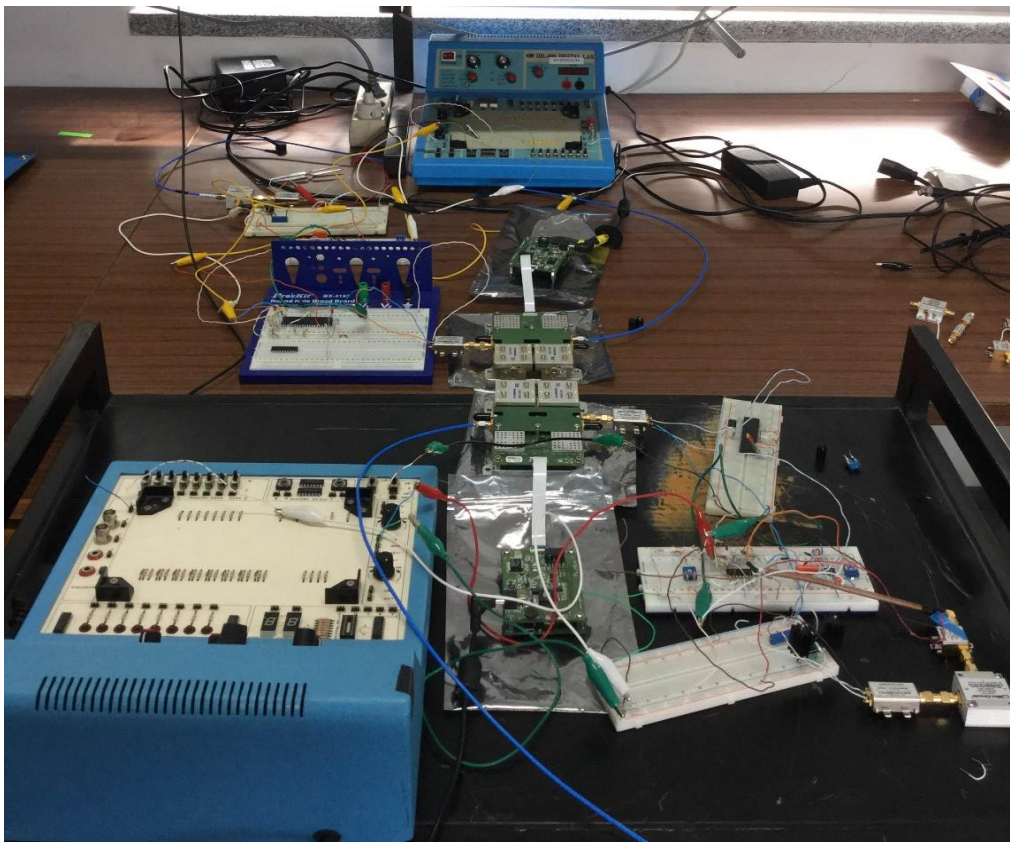


**Figure 2** – Photograph the implemented RFID system.

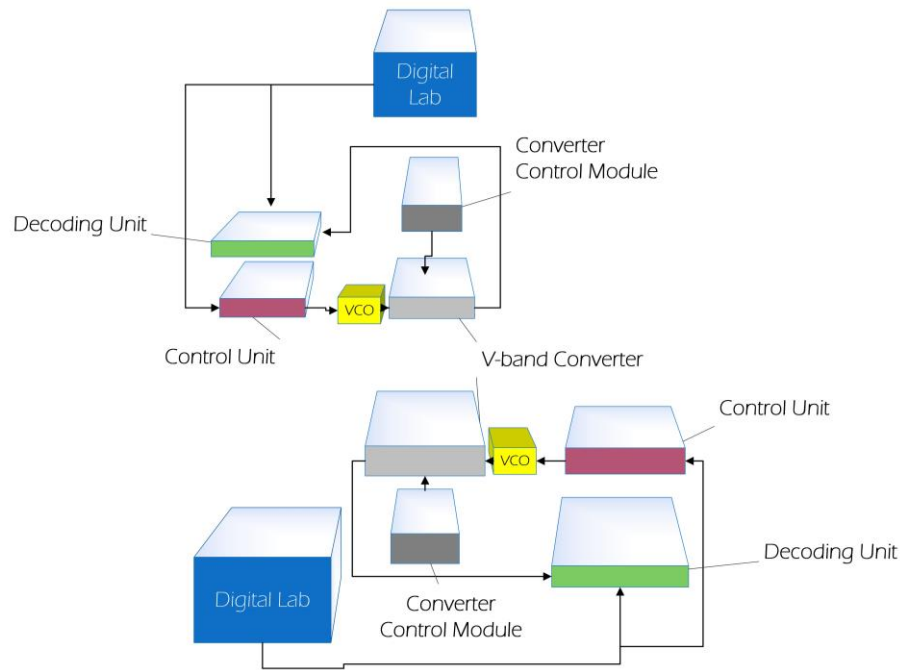


**Figure 3** – Block diagram (in perspective) of the implemented RFID system, showing the separate components.

The tag and reader devices consist of V-band converters by Sivers IMA that allow a link in the 60 GHz band to be made. Downconversion and decoding circuits were implemented using DIP and *off-the-shelf* components.

For intermediate frequency signal generation, VCOs were used, whose tune voltage was controlled by a microcontroller, allowing for a frequency multiplexing modulation strategy.

In addition, a case study is presented in order to study the influence of the most commonly used materials for surgical sponges, as well as the effect of water content in the power attenuation of the signal.

This dissertation also contributes with a general analysis of the developments made concerning highly integrated transceiver technology for the 60 GHz ISM band between 1997 and 2014.

Additionally, this study has also contributed to the following publications:

- H. Dinis, M. Zamith, J. Fernandes, J. Magalhães, and P. M. Mendes, “On-Chip, Efficient and Small Antenna Array for Millimetre-Wave Applications,” in International Workshop on Antenna Technology (iWAT2015), 2015;
- Zamith and P. M. Mendes, “Towards an RFID microsystem for surgical instrument detection using millimetre waves,” in 2015 IEEE 4th Portuguese Meeting on Bioengineering (ENBENG), 2015, pp. 1–5;

- M. Zamith, J. Magalhães, P. Anacleto, and P. M. Mendes, “60 GHz On-Chip Antenna Array with Efficiency Improvement Using 3D Microfabrication Technology,” in 9th European Conference on Antennas and Propagation (EuCAP2015), 2015;
- H. Dinis, M. Zamith, P. M. Mendes, “Performance Assessment of an RFID System for Automatic Surgical Sponge Detection in a Surgery Room,” in 37th Annual International Conference of the IEEE Engineering in Medicine and Biology Society (EMBC), 2015. *Accepted*;
- H. Dinis, M. Zamith, J. Fernandes, J. Magalhães, P. M. Mendes, “On-Chip, Efficient and Small Antenna Array for Millimetre-Wave Applications”, Forum of Electromagnetic Research Methods and Application Technologies (FERMAT), vol. 17, 2016. *On-line*.

## 1.5 Outline and Structure

---

This dissertation is divided into six chapters. They're enumerated as follows:

The present chapter explains the recurring problem of RSIs, as well as the motivations and contextualization of the developed research project. In addition, contributions and scientific publications are totalled.

In Chapter 2, we explain the physical aspects that make mm-wave an advantageous technology for indoors, short-range communications, focusing on RFID. In addition, the state-of-the-art in on-chip, highly integrated transceiver devices is detailed.

Chapter 3 presents an overview of the mandatory components of a typical RFID system. Also, an overview of the existing multiple access protocols is presented.

Chapter 4 focuses on the implementation of the blocks that constitute the RFID system, as well as the explanation of the strategies used.

In Chapter 5, we explain the feasibility tests that were performed, their outcome and the main challenges and obstacles encountered.

Chapter 6 gives an overall conclusion, with an emphasis on future directions for this investigation process.

# CHAPTER 2

# MM-WAVES FOR SHORT RANGE COMMUNICATION

Such as several other technological advances, millimetre-wave technology was fostered by military needs, from the seventies all throughout the nineties, mainly because of radar applications [31]. This technology allowed the successful use of seekers for terminal guided submissions or terrain mapping and its widespread use allowed breakthroughs in mm-wave circuit engineering [31].

Nowadays, millimetre-wave (mm-wave) technology for the 60 GHz ISM band is one of the most exciting opportunities for communication systems and is no longer “just around the corner”. This band is, in fact, the beginning of a big trend, and consumer demand for these applications is expected to result in millions of 60 GHz communication devices sold [32], [33].

In this chapter, we take a look at what makes the 60 GHz ISM band so special and the problems that have to be overcome in order to work with it efficiently. In addition, we present some of the main applications and trends that stride towards high efficiency miniaturized devices.

## **2.1 Small-size, Highly Integrated Transmitters and Receivers**

---

The 60 GHz ISM band offers a great opportunity for the design of small, cheap, and power

---

efficient devices for wireless communication. Devices such as these, if small enough, have the potential to be used in applications where miniaturization is a demand, like attachment to surgical instruments and sponges, for radiofrequency identification. In this subchapter, we will discuss the latest developments on highly integrated transmitter and receiver circuits, as well as the most influential and pioneering works in this field, in a *state-of-the-art* type of structure. We also try to present a perspective on how mm-wave devices were introduced into the global market and how they garnered the interest of large multinational companies like SiBEAM and IBM.

Despite not being the targeted goal of this dissertation, it's noticeable that the search for high data-rate communication for applications, such as live video streaming or next generation cellular networks [34]–[38], has motivated researchers to focus on technological developments in this particular band of the frequency spectrum, because of the available bandwidth.

What's desired for this type of device is a small, highly integrated chip, capable of establishing wireless communication over the vastest possible range. This device should, therefore, have a high output power without high-energy consumption.

Research for low-cost devices in mm-wave frequencies began in the 1990s, more specifically with the work of Ninomiya *et al.* [39] from the Fujitsu Laboratories in Japan. The authors utilized an InGaP/AlGaAs/GaAs HEMT process to fabricate two separate MMICs for transmitter and receiver devices. The module included a 15 GHz phase-locked loop (PLL), low-noise amplifier (LNA), mixer and frequency doublers in a total volume of  $150 \times 85 \times 18,1 \text{ mm}^3$ . However, the utilized technology does not integrate well with digital circuitry, which made it not viable for a low-cost consumer product. Only later developments in CMOS technology would allow the implementation of these ideas for the broad consumer market.

In 2002, also in Japan, Ohata *et al.* [40] from the NEC Corporation presented transmitter and receiver circuits operating in the 60 GHz band using a 150 nm AlGaAs/InGaAs HJFET process. The integrated circuit included a 30 GHz oscillator, frequency doubler, amplitude shift keying (ASK) modulator, filters and power amplifiers (PA). This research was motivated by the search for high-speed multimedia wireless communications that would allow for video streaming and provide evidence of the growing interest in the 60 GHz ISM band. Nevertheless, this device proved to still not be affordable enough for commercialization.

It wasn't until Doan *et al.*'s [41] contribution in 2004 that the complementary metal-oxide-semiconductor (CMOS) process was proved capable of 60 GHz operation. The authors presented some of the earliest work in the use of CMOS for highly integrated mm-wave systems, as they accepted the challenge implied by the requirement for new design

methodologies for this technology, as the wavelength (2,5 mm) in this band is of the size of the chip. They not only proved that 130 nm CMOS is capable of 60 GHz operation through careful modelling of active and passive components, but also opened the door for CMOS to become the emerging mm-wave technology for the future.

In the following year, the same investigators [42] from the Berkley Wireless Research Centre, USA, went one step further and compared 130 nm CMOS to other microwave technologies such as GaAs. They also successfully fabricated the first mm-wave CMOS amplifier operating at 60 GHz, improving the current *state of the art*.

Also in 2005, Gunnarsson *et al.* [43] from Ericsson of Sweden developed two separate MMICs for transmitter and receiver circuits that demonstrated an unprecedented level of integration for the time. The integrated circuits (IC), developed in 150 nm GaAs pHEMT technology, have an area of only 5 x 3,5 mm<sup>2</sup> and 5,7 x 5 mm<sup>2</sup> for transmission (TX) and reception (RX) ICs, respectively, and managed to incorporate a x8 frequency multiplier local oscillator chain. This particular component was a multifunction design by itself, consisting of a quadrupler, a feedback amplifier, a doubler and a buffer amplifier. This design aimed for high-speed wireless communication for voice, video and data, or as the authors called it, the “triple play”; however, incorporation of analogue with digital circuitry continued to be a problem.

Razavi [44] of the University of California at Los Angeles (UCLA) reported, in 2006, one of the first CMOS receiver circuits for the 60 GHz ISM band described in literature. The device incorporated LNA and mixer topologies for 130 nm CMOS technology and laid the groundwork for future innovation. The chip had a very small area of 0,3 x 0,4 mm<sup>2</sup>, excluding pads.

In the same year, Alldred *et al.* [45] pioneered the use of 90 nm CMOS technology through the development of a radio receiver chip. The authors managed to integrate a differential downconverter, two-stage LNA, mixer, local oscillator (LO) buffer and intermediate frequency (IF) buffer on an extremely small chip of 0,6 x 0,48 mm<sup>2</sup> that included pads. This work also excelled because of its low power consumption of only 60 mW, proving the low-power potential of CMOS for 60 GHz applications.

Also in 2006, Reynolds *et al.* [46] from the IBM T. J. Watson Research Centre published a study that proved to be a benchmark for integration technology, as a consequence of their efforts to reach multi Gb/s wireless communication. The authors developed a transmitter and receiver chipset that included PA, LNA, RF to IF and IF to RF mixers, quadrature IF to baseband and baseband to IF mixers, PLL and frequency tripler components, all in an area of 4 x 1,6 mm<sup>2</sup>. The chipset was developed in 130 nm SiGe BiCMOS technology and, despite being very power

consuming (about 10 times higher than Alldred *et al.*'s work), also demonstrated the feasibility of including antennas in-package.

In 2007, Gunnarsson *et al.* [47] updated their work from 2005, this time using a 150 nm GaAs mHEMT in the pursuit of multi Gb/s communication. Their work is a great example of how a “small” update in the technology can influence the performance of the devices. Separate TX and RX monolithic microwave integrated circuits (MMIC) were developed, as in [43], with higher output power (5,6 dBm compared to 5,2 dBm), half the DC power consumption and smaller areas (reduction of about 1,5 mm<sup>2</sup>). The devices exhibited the same level of integration.

Mitomo *et al.* [48] from Toshiba in Japan, also in 2007, developed a receiver device, using a 90 nm CMOS process, that integrated in package dipole antennas. This design would foreshadow future systems on chip, as it also integrated LNA, downconversion mixer and PLL synthesizer in a small area of 2,4 x 1,1 mm<sup>2</sup> (excluding pads). The on-chip receiver was very power efficient, as it only consumed 144 mW.

In the next year, Gilbert *et al.* [49] from SiBEAM developed a 90 nm CMOS fully integrated chipset that attempted introduction in the market, making it available for the consumer. This TX and RX transceiver device included LNA, PA, mixers, IF amplifiers, baseband amplifiers and also complete 60 GHz TX and RX smart antennas and beamformers. Moreover, it included an integrated crystal oscillator and frequency synthesizer. This was a very important step for the introduction of 60 GHz technologies to a wider audience.

2009 was a big year for 60 GHz technology. Dawn *et al.* [50] of the Georgia Institute of Technology developed two IF upconversion transmitters in 90 nm CMOS. The purpose of this paper was to show different approaches for low power and high performance applications. The low power single-ended transmitter integrated voltage-controlled oscillator (VCO), LO amplifier, mixer and PA in an area of 1,4 x 1,5 mm<sup>2</sup> with a power consumption of 76 mW, while the high performance differential transmitter had an area of 1,3 x 1,5 mm<sup>2</sup> and integrated VCO, mixer, marchand balun and three-stage PA. The last consumed a power of 112 mW.

In the same year, Parsa *et al.* [51] of the University of California at Los Angeles also documented a 90 nm CMOS transceiver device for the 60 GHz band, which included transmitter and receiver integrated in only one small chip. Active areas for RX and TX circuits were 0,19 and 0,2 mm<sup>2</sup> respectively. The authors introduced a new “half-RF” architecture, which incorporated a polyphase filter in the signal path to allow use of a 30 GHz LO to convert a signal from baseband to 60 GHz.

The potential offered by the 60 GHz band to achieve data rates as high as 6 Gb/s was demonstrated by Tomkins *et al.* [52] of the University of Toronto, also in the year of 2009. He

implemented a direct-conversion architecture, which was a revolutionary digital modulation technique (also called, “zero-IF”), on a chip that combined TX and RX. The chip included LNA, mixer, LO tree, frequency divider and binary phase shift keying (BPSK) modulator in an area of 1,28 x 0,81 mm<sup>2</sup>.

In 2010 and 2011, IBM and MediaTek made a significant investment in the 60 GHz communications field of study. This investment resulted in the fabrication of a prototype 60 GHz transmitter and receiver chips fabricated in 120 nm SiGe BiCMOS8HP. The devices included arrays of 16 planar antennas for use with the IEEE 802.15.3c standard. Firstly, Valdés-García *et al.* [53] documented a transmitter chip capable of non-line-of-sight (NLOS) links, with integrated beamformers, IQ calibration, frequency synthesizers, MSK modulation and digital control unit. However, this device proved to be very power consuming (3800 to 6200 mW from 2,7 V) and quite large sized, with an area of 44 mm<sup>2</sup>. Secondly, in the following year, Natarajan *et al.* [54] concluded this study by presenting a receiver device in the same technology that demonstrated the commercial interest even further. The receiver consumed 1800 mW at occupied an area of 6,08 x 6,2 mm<sup>2</sup>.

The work developed by IBM and Mediatech proved that hardware complexity is necessary to compensate for path loss and obstructions. High complex systems should focus on antenna arrays with beam steering algorithms, as opposed to directive antennas, which are a less efficient and space consuming solution for obtaining high read ranges.

The first examples of 65 nm CMOS applications for the 60 GHz ISM band came in 2011 with works such as Balankutty *et al.*'s [55] from Intel Corporation, who demonstrated a SiP (system in package) design for a transmitter device. This CMOS IC incorporated patch antennas, integrated on a low-temperature co-fired ceramic (LTCC) package. Integration included a distribution network for 60 GHz signals, phase shifters and PAs and proved the interest in “all-in-one”, smaller solutions (the device had an area of 16 mm<sup>2</sup>).

Growing corporate interest was demonstrated by works like Siligaris *et al.*'s [56] from CEA-Leti, also in 2011. The authors used a 65 nm CMOS process to develop a fully integrated transceiver designed for wireless high-definition video streaming over a 1 m range, operating by the WirelessHD standard. The device was incorporated in a high-temperature co-fired ceramic (HTCC) substrate along with glass antennas in an area of 2,8 x 3,3 mm<sup>2</sup>. Although still power consuming (TX consumed 357 mW and RX 454 mW), works like these proved 60 GHz communications technology was on the verge of market placement.

Still in 2011, Emami *et al.* [57] from SiBEAM developed a fully integrated 60 GHz phased array transceiver pair in 65 nm CMOS. This device included an embedded antenna array along



with dynamic phase shifters that allowed beam direction to be changed in real time. The author's strategy was to fabricate two different chips: one with 32 transmitters and 4 receivers and another with 32 receivers and 8 transmitters, as to allow asymmetric communication between the two. Although pioneering in several aspects, because devices were becoming "consumer ready", it's noticeable that power efficiency and area were still an issue. SiBEAM's transceiver consumed 1820 mW and had an area of 77,2 mm<sup>2</sup>.

In 2012, Vidojkovic *et al.* [28] from IMEC in Belgium was one of the first to document a transceiver device using a 40 nm CMOS technology. Their IC managed to incorporate LNA, RX mixer, baseband amplifier, PA and an LO synthesis circuit with a quadrature VCO, which used a 20 GHz reference in an unprecedented area for a fully integrated RX and TX device of 0,7 mm<sup>2</sup>. Vidojkovic *et al.* laid the groundwork for future innovation because, as well as small, this device was very power efficient, consuming 35 mW for the receiver and 90 mW for the transmitter.

Last year, Okada *et al.* [29] from the Tokyo Institute of Technology (Tokyo Tech) used a 65 nm CMOS process to reach a *state of the art* wireless link at 60 GHz, from a data rate standpoint. The authors used 64-QAM modulation to establish 28,16 Gb/s communication. The fully integrated transceiver required 251 mW for the transmitter and 220 mW for the receiver and had a total area of less than 4,2 mm<sup>2</sup>.

Finally, also in 2014, Khalaf *et al.* [30] from IMEC developed a 40 nm CMOS transmitter device that employed a digitally modulated polar TX architecture. The device integrated PA, RF-DAC, upconversion mixer and 60 GHz LO in an active 0,18 mm<sup>2</sup> area out of the 2,38 mm<sup>2</sup> from the test chip. The device required a power consumption of 75 mW.

It's safe to say that small, integrated solutions are a trending research topic, as far as wireless communications are concerned. The 60 GHz band offers such a possibility and, as we've seen, major companies are attempting to develop devices with high enough performance to make them available for the broad consumer market.

Technology has evolved in a way that these devices have become smaller and smaller, and digitally controlled algorithms have improved their performance, which leads us to believe that we may be on the verge of seeing "consumer ready" products in a near future. **Table 3** presents a brief summary of the publications that were discussed in this subsection.

*Table 3 – Summary of the research presented in section 2.1.*

Reference	Year	Technology	TX/RX	P <sub>OUT</sub> (dBm)	P <sub>C</sub> (mW)	Size (mm <sup>2</sup> )	Notes
[39]	1997	GaP/AlGaAs/GaAs HEMT	Separate RX and TX MMICs	2,3	N/A	150 x 85 x 18,1	Pioneering integration ideas. Incompatible with digital circuits.
[40]	2002	15 μm AlGaAs/InGaAs HJFET	Separate RX and TX MMICs	10,6	N/A	82 x 53 x 7	Expensive.
[43]	2005	150 nm GaAs pHEMT	Separate RX and TX MMICs	5,2	TX: 820 RX: 990	TX: 5 x 3,5 RX: 5,7 x 5	Unprecedented level of integration at the time.
[44]	2006	130 nm CMOS	RX	N/A	9	0,3 x 0,4 (no pads)	One of the first CMOS receiver circuits.
[45]	2006	90 nm CMOS	RX	N/A	60	0,6 x 0,48	Very low size and power consumption for a chip with pads included.
[46]	2006	130 nm SiGe BiCMOS	Single RX and TX chip	17	TX: 500 RX: 800	TX: 4 x 1,6 RX: 3,4 x 1,7	Antenna in-package. High power consumption.
[47]	2007	150 nm GaAs mHEMT	Separate RX and TX MMICs	5,6	TX: 420 RX: 450	TX: 4 x 3 RX: 5,5 x 4	Improvements from [43] in power consumption, gain and chip size.
[48]	2007	90 nm CMOS	RX	N/A	144	2,4 x 1,1 (no pads)	On-chip dipole antennas.
[49]	2008	90 nm CMOS	Single TX and RX chipset	N/A	N/A	N/A	Step towards commercial availability.
[50]	2009	90 nm CMOS	Two separate TX MMICs	TX <sub>1</sub> : 5,7 TX <sub>2</sub> : 8,6	TX <sub>1</sub> : 76 TX <sub>2</sub> : 112	TX <sub>1</sub> : 1,4 x 1,5 TX <sub>2</sub> : 1,3 x 1,5	Differentiated low power from high performance devices.
[51]	2009	90 nm CMOS	Single RX and TX chip	-7,2	TX: 78 RX: 36	TX: 0,2 (active) RX: 0,19 (active)	“Half-RF” architecture. Small size.
[52]	2009	65 nm CMOS	Single RX and TX chip	-0,7	TX: 131 RX: 101	1,28 x 0,81	Single CMOS chip (RX and TX combined). Zero-IF modulation technique.

## mm-Waves for Short Range Communication

Reference	Year	Technology	TX/RX	P <sub>OUT</sub> (dBm)	P <sub>C</sub> (mW)	Size (mm <sup>2</sup> )	Notes
[53]	2010	120 nm SiGe BiCMOS	TX	25,5	6400	6,5 x 6,75	Highly complex schemes and algorithms for improved performance. Focus on antenna arrays with been steering algorithms. Power consuming and large size.
[54]	2011	120 nm SiGe BiCMOS	RX	N/A	1800	6,08 x 6,2	
[55]	2011	65 nm CMOS SIP	TX	15	N/A	4 x 4	Highly integrated CMOS IC with patch antennas on LTCC package.
[56]	2011	65 nm CMOS	Single TX and RX chip	16	TX: 357 RX: 454	2,8 x 3,3	Incorporated glass antennas in an HTCC substrate.
[57]	2011	65 nm CMOS	Two different chips with RX and TX	28	TX: 1820 RX: 1250	Chip 1: 77,2 Chip 2: 72, 7	Embedded antenna array with dynamic phase shifters. 2 different chips. Power consuming.
[28]	2012	40 nm CMOS	Single TX and RX IC	10,2	TX: 1820 RX: 1250	0,7	First integrated transceiver in 40 nm CMOS allowed unprecedented area.
[29]	2014	65 nm CMOS	Single TX and RX IC	N/A	TX: 251 RX: 220	4,2	Highest data rate achieved.
[30]	2014	40 nm CMOS	TX	10	75	2,38	Polar TX architecture.

## 2.2 Available Bandwidth

After we discoursed about the developments in the implementation of integrated circuits capable of supporting mm-wave operation, we present a brief discussion about other physical aspects of 60 GHz communication.

In order to meet the exponential growth of mobile data of this generation, allocation of new spectrum is of paramount importance. As so, the availability of the 60 GHz band as unlicensed spectrum has spurred interest in wireless communication and could offer the desired bandwidth [58].

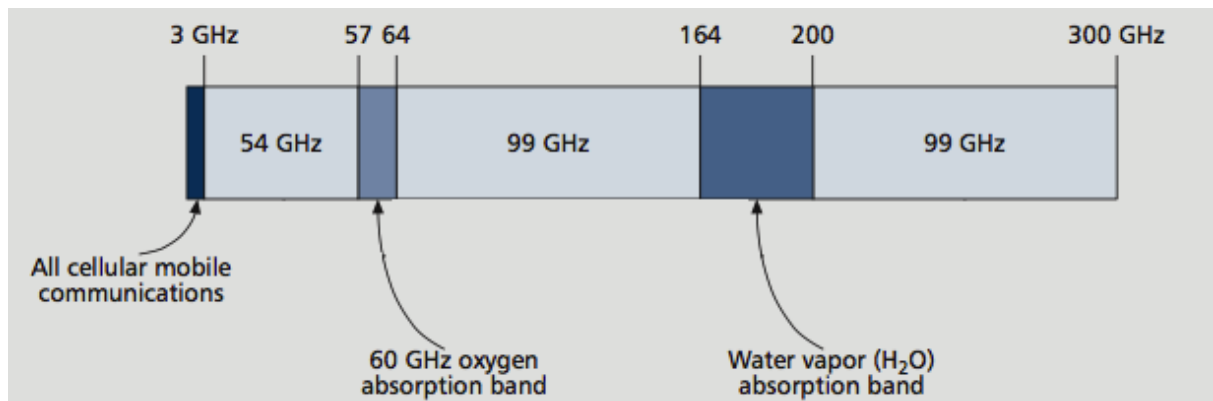


*Figure 4 – Frequency spectrum and available bandwidth. Adapted from [58]*

Almost all commercial applications for radio communications such as AM/FM radio, GPS, Wi-Fi and cellular have been contained in a narrow band of the radio-frequency spectrum (300 MHz – 3 GHz), an area generally referred to as “sweet spot” because of its favourable characteristics concerning propagation for long-range wireless communications [33], [58]. On the other hand, the portion of the RF spectrum above 3 GHz is largely unexploited for commercial use. Despite this, the 60 GHz band can provide very interesting characteristics concerning short-range connectivity and local networks, as we will see in the course of this chapter [58]. **Figure 4** provides a graphic overview of the available bandwidth.

## 2.3 Industrial Standards for the 60 GHz ISM Band

Industrial standardization reflects the commercial interest in mm-waves. Standards have already been issued such as WiGig, WirelessHD, ECMA-387 and IEEE 802.15.3c [32], [33], [58].

- Task group *c* has considered an alternative physical layer for the already available IEEE 802.15.3 standard for wireless personal networks (IEEE 802.15.3c);
- The European Computer Manufacturer Association has devised a 60 GHz technology standard for very high data-rate, short-range communications to support bulk data transfer such as video streaming;
- WirelessHD is an effort lead by industrial leaders to define wireless interface specifications for consumer electronic products;
- The Wireless Gigabit Alliance (WiGig) is a privately developed industrial consortium. It was based on the existing IEEE 802.15 standard and the two could possibly merge [33].

All these standards target short-range 60 GHz networks, which as very special characteristics, namely due to attenuation in the atmosphere, as we will see in the next section.

### 2.4 Atmospheric Factors

---

One of the limiting factors inherent to the use of millimetre waves is the considerable atmospheric attenuation caused by oxygen and water vapour [32], [59].

Gaseous absorption depends on gas pressure, temperature and density. Roughly speaking, when interacting with radio waves at a certain frequency, a forced rotation of the molecules is induced, which causes dissipation of part of the energy carried by the propagating field. Absorption is maximum in correspondence with the resonating frequencies of the gas molecules [59]. **Figure 5** shows the specific attenuation values for water and oxygen according to frequency. As is easily detected, the 60 GHz ISM band is located in a strong oxygen attenuation region.

Curiously, oxygen exhibits 45 distinct resonance peaks between 48 and 72 GHz, that all merge into a single attenuation curve at low altitudes due to molecular collisions. One other absorption line is exhibited at 119 GHz [59].

The maximum specific attenuation value for oxygen is about 15,5 dB/Km, where attenuation caused by water vapour can be neglected. As for water vapour, it exhibits three distinct absorption peaks at 22, 183 and 323 GHz. However, these must be carefully avoided when dealing with radio links because of a strong dependence on atmospheric conditions such as pressure and humidity [59].

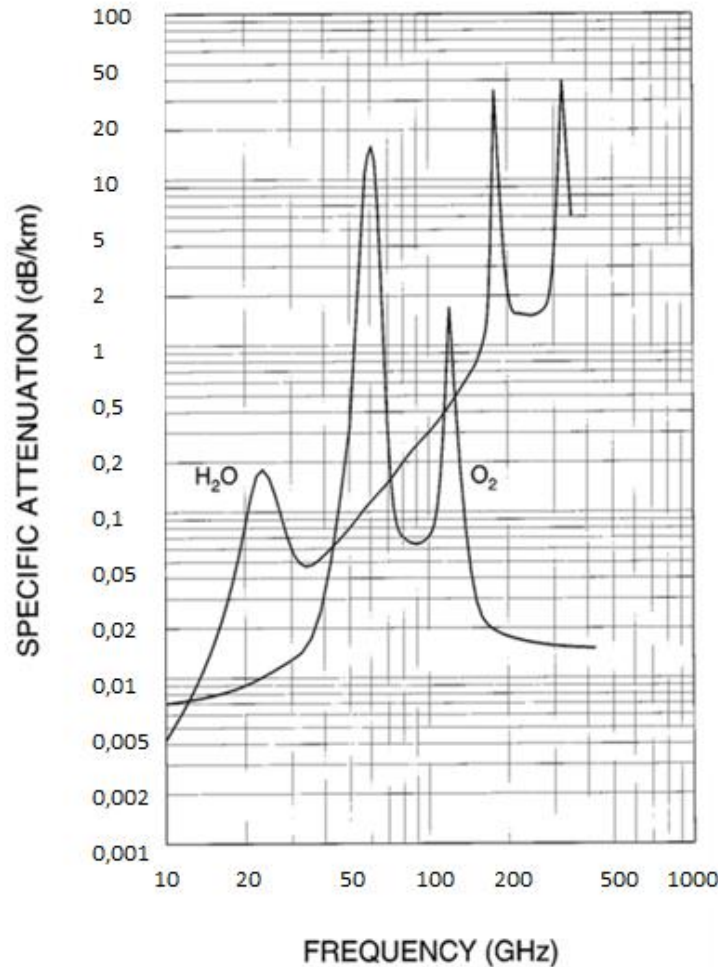


**Figure 5** – Specific water vapour and oxygen attenuation values according to frequency.  $T=20\text{ }^{\circ}\text{C}$ ,  $p = 1\text{ atm}$ ,  $h = 0\text{ Km}$ . Adapted from [59]

As we can see, sixty-gigahertz communication systems operate in an oxygen absorption peak. This severely limits link distances, making this band advisable for short-range communication. However, high atmospheric attenuation adds important advantages for short-range, indoor links like a high reuse factor and improved security conditions because of the difficulty of eavesdropping, as will be discussed in the next section [38].

## 2.5 Propagation

Microwave and millimetre wave communications are characterized by extremely complex multipath propagation phenomena [59]. As a consequence, the performance assessment of a communication system relies on simplified models, at least in a preliminary phase. A first class of such propagation models is based on the *Friis transmission equation*, introduced in

1946 [60], which states that in free space, the causes of path loss are merely frequency and distance, as shown in Equation (1):

$$\frac{P_{or}}{P_t} = \frac{1}{att} = \frac{1}{(4\pi d f/c)^2} \quad (1)$$

where  $c$  is the speed of propagation of the wave,  $f$  is the frequency,  $P_t$  is the transmission power,  $P_{or}$  is the received power in free space and  $d$  is the distance separating the receiver and the transmitter.  $att$  is the attenuation coefficient.

As indicated by Equation (1), the available power decreases as a function of the squares of distance and frequency. Assuming everything else is maintained equal, attenuation in free space will be much greater at 60 GHz than at lower frequencies. Moreover, this attenuation also depends on the medium of transmission, since the speed of transmission  $c$  is dependent on this factor.

The attenuation coefficient  $att$  is more frequently seen as to show the loss with units of dB, as shown in Equation (2), where it's modified for such purpose.

$$att \text{ (dB)} = -20 \log \frac{c}{4\pi d f} \quad (2)$$

The *Friis equation* predicts that operation at 60 GHz results in 22 dB of additional propagation loss when compared to transmission at 5 GHz, assuming that antenna gain, transmit power, distance and medium are maintained equal [61]. This could present a serious complication for millimetre wave systems.

This equation is extremely useful when dealing with line-of-sight (LOS) communication in one channel. We define channel as a link between transmitter and receiver [62]. However, when reflections occur on other objects, the ceiling and the ground surface, we're dealing with multipath propagation. This is the kind of system we expect for our application, as multiple surgical instruments, tables and even people will be in the room when transmission occurs, so it's certainly relevant to talk about multipath communication.

In 1991, Schäfer described the first characterization of the channel model for short-range communications at 60 GHz in the framework of the PROMETHEUS research program [63]. In this paper, propagation effects for an intervehicle radio link were theoretically examined. It was concluded that the received field is a combination of the direct LOS link, a specular component reflected by the road surface and a scattered component accounting for multiple reflections is foliage, buildings and other surrounding obstacles.

These multipath reflections of the transmitted wave caused by local scatterers are said to cause short-term fading [62], [64]. This concept is very relevant when working with indoor,

short distance communication. Short-term or small-scale fading is used to describe the rapid fluctuation of the amplitude of a radio signal over a short period of time or travel distance. Fading is caused by interference between several versions of the transmitted signal, which arrive at the receiver at slightly different times. These waves are called multipath waves and combine at the receiver antenna to give a resultant signal that can vary widely in amplitude, depending on the distribution of the intensity and relative propagation time of the waves and the bandwidth of the transmitted signal.

Statistical models for multipath channels can help predict the effects of fading and several have been suggested, in order to explain the observed statistical nature of these channels. Clarke's model [65] is based on scattering and is widely used [64]. Nevertheless, studies show that the path loss in indoor environment has very dynamic and fast changing features, which make it very unpredictable over short distances. Simple path loss rules are sometimes unsuccessful in describing indoor atmospheres [66], so it's recommended that model parameters should be derived from field measurements, rather than simplified theory.

Schafer's goal was to study outdoor communication. We're more interested in the wave's behaviour for indoor applications. In 2005, a study was conducted in the Eindhoven University of Technology for indoor channel measurement inside one single room [67]. This paper compared the characteristics of radio wave propagation in the frequencies at 58 and 2,25 GHz in both LOS and NLOS areas and concluded that the differences in penetration and reflection loss have a significant impact on the received power level at both frequencies. The study performed in [68] also proves the feasibility of indoor applications using frequencies in the 60 GHz ISM band.

In a more recent study performed by the Intel Corporation's Wireless Technology Group in [61], it was stated that the most part of the power propagated in a 60 GHz channel is through the LOS path. This requires the use of highly directional antennas to compensate the significant propagation loss and the support of the NLOS operation.

As mentioned in the previous section, a major advantage of the 60 GHz ISM band is high-frequency reuse. In fact, one major limitation of frequency assignment policy is co-channel interference experienced by cells using the same sub-band [59]. Oxygen absorption provides a natural way to separate co-channels, reducing interference between neighbour cells. In addition, as we can state from **Table 4**, collected from [69], attenuation by walls and windows is more significant in the 60 GHz band, when compared to lower frequencies. This means millimetre waves do not penetrate most solid materials very well, providing improved security and higher frequency reuse.



**Table 4** – Attenuation for different solid materials. Source: [69].

	<i>Material Thickness</i> (cm)	<i>Average Measured Attenuation (dB)</i>	
		<b>2,5 GHz</b>	<b>60 GHz</b>
<i>Drywall</i>	2,5	5,4	6,0
<i>Office Whiteboard</i>	1,9	0,5	9,6
<i>Clear Glass</i>	0,3	6,4	3,6
<i>Mesh Glass</i>	0,3	7,7	10,2

## 2.6 RFID Based on Millimetre Waves

Radio-frequency identification is an example of an application that can benefit from the use of millimetre waves, as its performance is highly dependable of the used frequency of operation.. In this section we'll discuss the implications of the choice of frequency, as well as the criteria behind our particular choice.

Literature usually divides the transmission frequencies into four categories, as shown in **Table 5** [70], [71].

**Table 5** – Transmission frequency bands used on RFID systems [14, 15].

<i>RFID Band</i>	<i>Frequency range</i>
<i>Low frequency (LF)</i>	30 – 300 kHz
<i>High frequency (HF)</i>	3 – 30 MHz
<i>Ultra-high frequency (UHF)</i>	300 MHz – 3 GHz
<i>Microwave</i>	> 3 GHz

These divisions are made because frequency can impact several different aspects of the application, such as potential size, price and read range and power consumption. A choice of frequency of operation should be carefully made, according to the main goals of the system at hand.

First of all, let's look at how the choice of a higher frequency can affect the size of the system.

The physical size of antennas is inversely proportional to the carrier frequency [72]. As a consequence, it becomes possible to build complex antenna arrays at higher frequencies, and further integrate them in *chip* or PCB.

As mentioned in section 2.5, free-space propagation depends on frequency, so higher

frequencies don't propagate as well than lower ones, thus limiting the read range of the system. However, this is only true if all other parameters (like antenna gain) are maintained equal, which can lead to a misconception about communication at higher frequencies.

The larger the effective aperture of the antenna, the larger the gain because more energy is captured from a passing radio wave, and as we've established, antennas have small apertures at high frequencies [58]. However, with these short wavelengths, more antennas can be packed in the same area compensating the "disadvantage" of free space loss. In addition, antenna arrays enable beamforming with higher gains.

The fact is that RFID systems at mm-waves have two power constraints when it comes to reading range: the reader transmission must have enough power to allow passive operation by the tag and the backscattered signal must exceed the reader's sensitivity. In [73], the authors made a comparison between passive RFID communication at 865 MHz and at 60 GHz and concluded that the first system could reach 100m, while the mm-wave system could only reach distances up to 10 m, despite of higher antenna gains. Despite this shorter range, for our specific application, 10 m can be considered sufficient.

Higher frequencies also allow for higher data rates, as a high data rate can be achieved by a combination of signal bandwidth and dynamic range [74]. The inherent security and privacy is also better at higher frequencies because of the limited range and relatively narrow beam widths than can be achieved [74].

Millimetre-wave frequencies refer to frequencies ranging from 30 GHz to 300 GHz, with wavelengths from 10 mm to 1 mm [74]. Millimetre-wave identification (MMID) updates the RFID system to millimetre waves [75] and encompasses all the advantages of the use of higher frequencies.

For an application where it is proposed to communicate between a tag placed in a surgical instrument or sponge and a reader, MMID offers the great advantage of allowing ultra-small directive antennas, providing the possibility of selecting a transponder by pointing toward it.

RFID integrated systems and tags operating in the HF and UHF bands have been widely implemented, namely in [76]–[80]. This demonstrates that there is a clear tendency to move up the spectrum towards higher frequencies.

In the next section, we will discuss this aspect further, as we take a look at small sized transmitter and receiver devices operating in the 60 GHz ISM band.

## 2.7 Examples of RFID Devices for the 60 GHz ISM Band

---

In this section, we make a small review of the existing RFID components for mm-wave operation existing in the literature. There aren't many documented works in this specific field, which demonstrates that mm-wave radio frequency identification is still considered an uncharted area.

The VTT Technical Research Centre of Finland has showed great interest in the research of this subject. In 2008, Pekka Pursula and his team of investigators expanded the RFID concept to mm-waves (MMID) and demonstrated its feasibility [75]. This paper included a comparison with devices operating in the UHF band and proved backscatter communication could be achieved in the 60 GHz band for wireless identification devices.

In 2010, Pursula *et al.* [73] extended their research in a paper that talked about the power limitations and possible applications of MMID systems. Examples included automotive radars and location sensing applications.

In the same year, Pellerano *et al.* [81] from Intel Corporation demonstrated an RFID tag operating at 60 GHz, motivated by the miniaturization of this kind of devices. The tag managed to harvest energy from an incoming mm-wave signal transmitted by the reader and used a 60 GHz free-running oscillator to transmit modulated bursts. This technique avoided the use of space consuming battery components and integrated a 60 GHz VCO and PA, as well as an input matching network and voltage multiplier in an area of  $1,3 \times 0,95 \text{ mm}^2$ .

It wasn't until 2011 that Pursula *et al.* presented the first MMID reader module for backscattering based communication [82]. This device was fabricated in 90 nm CMOS and integrated a 60 GHz oscillator, LNA, PA, and mixer on an LTCC substrate, with a total area of  $24 \times 13 \text{ mm}^2$ . Filters, power splitter and RX and TX antenna arrays were patterned on the LTCC. The reader consumed a power of 130 mW and reached an output power of 11,6 dBm. However, communication was only achieved at a range of 5 cm.

On the same year, Pursula and his team of investigators presented a novel strategy for passive operation MMID, by adding an external mixing element to a standard RFID device [83]. This element was introduced between the tag antenna and the RFID chip. Also in 2011, Pursula *et al.* [84] presented two different semipassive transponder designs for 60 GHz operation. One of them used a Schottky diode and an antenna on liquid crystal polymer (LCP), and the other used a backward tunnelling diode and antenna on LTCC. Both of them were proved feasible, the last being a lot more expensive.

In 2013, Kiuru *et al.* [85], also from the VTT Technical Research Centre of Finland, demonstrated a 30 cm link with an signal-to-noise ratio (SNR) of 20 dB with a semipassive MMID transponder. The device consisted of an antenna array connected to a mm-wave diode on a liquid crystal polymer. The diode acted as both a detector and backscattering modulator.

Proving the growing interest on RFID devices for the 60 GHz ISM band, and supporting its feasibility, Burasa *et al.* [86] from the Poly-Grame Research Centre in Montpellier presented a high efficiency rectifier for an active, yet batteryless tag. The device was fully integrated and fabricated using a 65 nm CMOS process for mm-wave to DC energy conversion.



# CHAPTER 3      AUTOMATIC IDENTIFICATION SYSTEMS

Automatic identification procedures (Auto-ID) are very popular in various service industries. They exist to provide information about people and products in transit [70]. RFID is an acronym for radiofrequency identification, which is a wireless communication technology that is used to uniquely identify tagged objects [71].

Like the widely known smart-card systems, RFID systems store data on an electronic device, the transponder. However, unlike the smart card, the power supply to the data-carrying device and the data exchange between the data-carrying device and the reader are achieved without the use of galvanic contacts, using instead magnetic or electromagnetic fields [70].

The number of companies that got involved in the RFID market on recent years proves that this technology should be taken seriously. In the year 2000, global sales of RFID systems were approximately 900 million US dollars [70]. By 2014, it's estimated that the total RFID market is worth about 9,2 billion US dollars, and it's still growing at a very large scale. According to the report presented in [87], this number should rise to 30,24 billion dollars by 2024.

RFID results from the convergence of three technologies, as their emergence and advancement allowed commercially viable RFID systems. Firstly, radiofrequency electronics made manufacturing of RFID tags and interrogators possible. These advances were made during the Second World War and the 1970s. Secondly, advances in information technology

from the 1970s up to the 90s made these systems much more attractive because they allowed networking of RFID systems. Lastly, breakthroughs in material science during the 1990s reduced the prices of tag manufacturing to symbolic values. Overcoming this barrier made RFID commercially viable [71], [88].

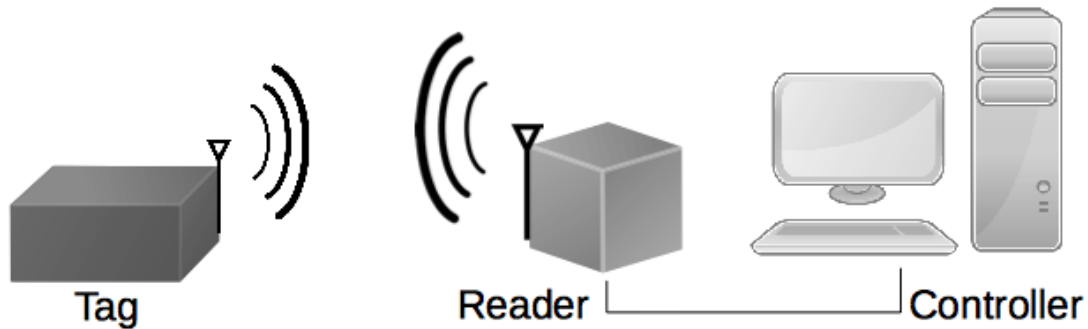


*Figure 6 – Basic components on a simple RFID system.*

A typical RFID system has two main components, as shown in **Figure 6**:

- The tag, also called the transponder, is composed of a semiconductor chip, an antenna and sometimes a battery. It's located on the object to be identified.
- The reader, or interrogator, is composed of an antenna, an RF electronics module and a control module (microcontroller).

Some authors consider the controller, or host, (normally a computer) to be a third component of an RFID system [71].

### 3.1 Types of Tags

---

The basic function on an RFID tag (or transponder) is to store data and transmit it to the interrogator. In this case, the tag placed in a surgical instrument will store a binary sequence and send it back when requested.

In its most basic form, the tag consists of an antenna connected to an electronic chip. Generally, the chip contains a memory unit (to read from, and sometimes also write) in addition to other important circuitry [71]. Also, some tags contain batteries, making the differentiation between active and passive transponders.

### 3.1.1 Active Tags

---

RFID tags are said to be active if they contain an on-board power source [71], [89]. A power source is needed for transmission, when the tag needs to send information to the interrogator and the active tag synthesizes a carrier signal using a local oscillator and crystal reference [89]. As a consequence, active tags can reach much longer ranges and communicate with less powerful interrogators; however, they are a lot bigger and more expensive. In addition, their operating time is limited to battery life.

### 3.1.2 Passive Tags

---

Passive transponders derive the power they need from the energy of the RF signal sent by the reader, as they have no independent source of electrical power [71]. They depend on the rectification of the received power from the reader to support the operation of the circuitry and backscatter the RF signal to establish communication back to the reader [89]. The absence of an independent power supply makes passive tags smaller and more affordable. On the other hand, they communicate at smaller ranges and need more powerful interrogators.

To power the tag's logic circuitry, a rectification technique is normally implemented, using a diode and a storage capacitor to generate a constant voltage [90].

Incorporating a battery to power the tag circuitry produces a semipassive tag [90]. This allows adding high-frequency amplification and other RF functions. Semipassive tags are also known as battery-assisted passive tags and despite the existence of a battery, they still use backscattered signals for the tag-to-reader communication [89], [90].

As for the backscattering principle, a simple illustration is presented in **Figure 7**. Current is induced on the receiving antenna as a result of the established link. This induced current is no different from the current on the transmitting antenna that started things out in the first place. The radiated wave can make its way back to the transmitting antenna, induce a voltage, and therefore, produce a signal that can be detected: a backscattered signal [90]. On the other hand, if instead there is a load that allows little current to flow (a large impedance) connecting the antenna to ground, little or no induced current will flow. In other words, if the antenna impedance is matched to the load, no reflection occurs at the interface [3]. The backscattered signal is modulated this way.

UHF passive tags (868-915 MHz band) are widely used for RFID systems, with different architectures for RF-to-DC conversion and backscattering modules [77], [79], [80]. However, passive transponders for the millimetre wave band have also been proven to be investigation-



worthy [84], [91].

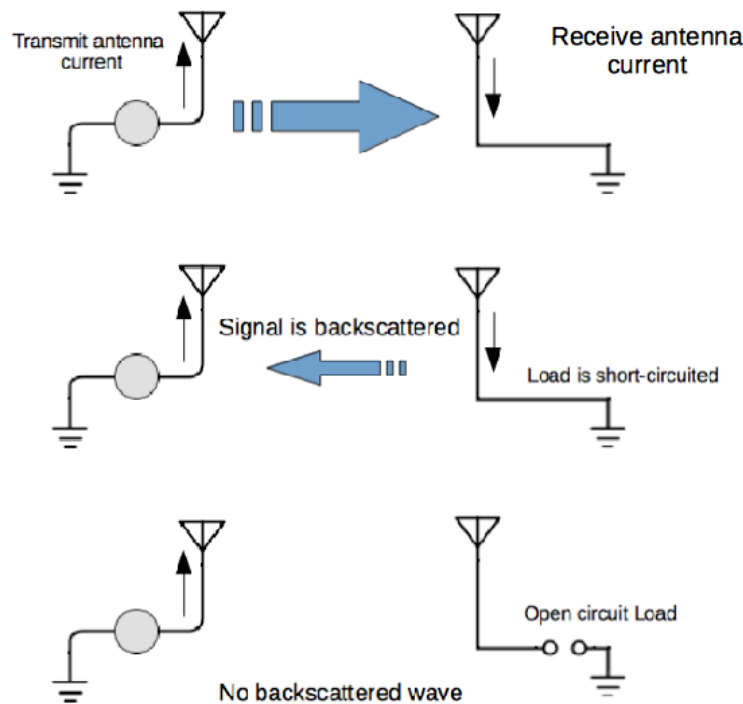


*Figure 7 - Simple representation of the backscattering principle.*

In addition, semipassive MMID tags are also successfully implemented in [85] proving to be a solution worth mentioning for communication devices in the 60 GHz ISM band.

### 3.2 Role of the Reader

The RFID reader or interrogator is the bridge connecting the tag and the user. Its main functions are to relay data from the controller, power the tag (for passive tags), send the RF signal in the tag's direction (and possibly write to it) and interpret the data sent by the tag [71]. To sum up, the reader orchestrates the communication in its interrogation zone and the transponder only responds to its commands, never acting independently [70], [89].

They are roughly composed of three main parts: an antenna, an RF electronics module and a control unit [70], [71].

A reader communicating with a passive or semipassive tag must operate in full-duplex mode, in the sense that it must transmit and receive simultaneously [89]. This can pose a problem because both signals are in the same frequency. Using separate antennas for transmission and reception can improve sensitivity, in what is called a bistatic configuration. Limitations of this configuration include price, size and complexity. The alternative is a

monostatic configuration, where a single antenna is used for both transmission and reception [89].

As for the RF module, it should be able to satisfy the communication protocol established, performing some important functions:

- Generating a high-frequency transmission signal, able to activate the tag and possibly supply it with power [70]. A voltage control oscillator normally generates this signal, which is later amplified and radiated through the antenna [89].
- Modulating the transmission signal to send data to the transponder and demodulating the received RF signal [70], [89].

Depending on the performance of the reader antenna, the input signal may be a mixture of a variety of frequencies at different power levels, as a consequence of the interference of many RF sources of energy [89]. A band filter ideally removes the undesired frequencies. The wanted frequencies are amplified and mixed with a signal originated by a local oscillator. The result (after low pass filtering, so that remaining RF and harmonics are removed) is a low-frequency signal whose amplitude is proportional to the strength of the high-frequency signal [89].

A reader module operating at 60 GHz based in backscattering communication has been designed in [82].

### **3.3 Accessing Multiple Tags Simultaneously**

---

Radiofrequency identification systems are proven powerful tools for object identification. However, if multiple tags are to be identified simultaneously, messages from the tags collide with each other and cancel each other out. Information gets lost [92], [93].

In most applications, typically a single RFID tag is recognized at a time, because it's sufficient in many cases. For example, in EAS, it's enough to identify one unpaid item in order to take the appropriate measures. In other applications, the tags are presented in a sequential order to the reader, making it unnecessary to recognize more than one item at a time.

However, in more advanced applications, the ability to recognize multiple objects at once is crucial. It would be a significant advantage if the reader could identify several retained items at once, in the OR. Therefore, it's relevant to present the existing methods and protocols used for the task at hand.

In this chapter, we present an overall review of the simplest existing multiple access protocols that can be used in radiofrequency identification systems, which include conflict-free

access protocols, but also protocols where collision is a concern.

### 3.3.1 Conflict-free Access Protocols

---

Conflict-free protocols are designed to ensure that a transmission, whenever made, is not interfered with by any other and is therefore successful. This is achieved by allocating the channel without any overlap between the portions of the channel allocated to different users [94]. The two most well-known protocols in this class are Frequency Division Multiple Access and Time Division Multiple Access.

#### 3.3.1.1 *Frequency Division Multiple Access (FDMA)*

With this protocol, the available frequency band is divided into smaller bands, each of which is handed to a single user. Therefore, each tag transmits in its unique frequency to avoid collision with other tags. As for reception, a single receiver can be implemented for the entire frequency range with a bank of band pass filters for the individual bands [94].

The main advantage of FDMA is its simplicity it does not require any coordination or synchronization among the users since each can use its own frequency band without interference. However, FDMA is not flexible; adding a new user to the network requires equipment modification (such as additional filters) in every other user [94].

#### 3.3.1.2 *Time Division Multiple Access (TDMA)*

TDMA is very similar to FDMA in concept, except predetermined users are divided into time slots, instead of being assigned different frequencies. Every user is allowed to transmit freely in a given time period, that is, all system resources are devoted to one user at a time, according to time slots. The slot assignments follow a predetermined pattern that repeats itself periodically; each such period is called a cycle or a frame [94]. For proper operation according to the TDMA scheme, all users must be synchronized and know exactly when and for how long they can transmit.

#### 3.3.1.3 *Code Division Multiple Access (CDMA)*

CDMA is an alternative to FDMA and TDMA that allows the users to share a channel, by attributing a unique code or “signature sequence” to each user. This allows the user to spread the information signal across the assigned frequency band [95].

Signals from the various users are separated at the receiver module by cross-correlation of the received signal with each of the possible signature sequences. In CDMA, users access the

channel in a random manner and transmitted signals overlap in time and in frequency.

There is an obvious drawback of conflict-free access protocols. Static channel allocation is predetermined from the beginning and does not change during the entire operation. This means that parts of the channel might be idle, despite having information to transmit. Also, every user must be known from the moment of design and their number mustn't change.

In order to overcome these drawbacks, several other protocols were designed to allow simultaneous transmission from tags to readers.

### 3.3.2 Aloha Protocols

---

The Aloha protocols are probably the most popular of multiple access protocols, mainly due to seniority, but also because they're pretty straightforward and easy to implement.

Unlike the previously discussed conflict-free protocols, successful transmission by the Aloha-protocol is not guaranteed to happen, because there is a chance that two transmissions attempt to use the same channel. In this case, collisions occur and all the information is lost. As a consequence, the signal has to be retransmitted until reception is successful [94]. Therefore, transmission scheduling is a concern in these classes of protocols.

The pure Aloha protocol was introduced in 1970 [96]. It states that a newly created package is immediately transmitted hoping for no interference and a consequent acknowledgement. In case of a collision, every colliding user schedules a retransmission for a random time in the future. This randomness is a requirement to ensure that an infinite cycle of collisions doesn't happen.

Although this protocol can work, its throughput is quite low (close to 18%) and a user can send numerous packages of data while another user isn't able to send any. This is why an improved version, called slotted Aloha, was designed [97].

This variation divides the channel of transmission into time slots, synchronizing the transmission of devices and thus improving the utilization of the shared medium.

To simplify, the slotted Aloha protocol can be divided into steps as follows [98]:

- Time is divided into slots, and each node can attempt to send one packet in each time-slot. If a node has a new packet to send, it attempts transmission during the next time-slot.
- If a node successfully transmits one packet, it can transmit a new packet in the next time-slot.

- If a node detects a collision, it retransmits the old packet in each subsequent time-slot after waiting a random amount of time until the packet is successfully transmitted.

Slotted Aloha protocols are very popular for RFID systems, as seen in [92] and [93].

The main disadvantage of the Aloha family of protocols is the (in)stability issue. We implicitly make a stability assumption when we assume that the number of users waiting to transmit a package is not growing. It's assumed that the packets are entering and leaving the system at the same rate and we can intuitively reason that this assumption is incorrect [99].

### 3.3.3 Carrier Sensing Protocols

---

Despite their popularity, the Aloha protocols exhibit poor performance as a consequence of their “impolite” behaviour, as they proceed to make a transmission without taking into consideration other users. It doesn't take much to realize that this consideration can benefit all.

In carrier sensing protocols, before transmitting, the tag will first listen to whether another user is using the channel. In this case, it will not attempt to transmit for the benefit of all, because its packet would clearly not be successfully transmitted and would disturb another user, resulting in the retransmission of other packets [94].

It is important to note that in order to ascertain if the channel is in use, the tag doesn't need to retrieve the information, making the task at hand not that demanding.

However, carrier sensing doesn't relieve us from collisions. Considering the channel is idle and two users generate a packet concurrently, each will listen to the channel, determine it is idle and attempt a transmission, which will result in a collision.

All the Carrier Sensing Multiple Access (CSMA) protocols share the same philosophy: when a new packet is generated, the user checks if the channel is idle and, if it is, transmission is initiated without further ado. If collision occurs, the transmission is rescheduled for another time in the future, at which time this operation is repeated. There are some variations of this protocol, which are due to user behaviour in which there is a wish to transmit despite finding the channel busy.

These different variations of the CSMA protocols were introduced in [100] and [101] and we present an enumeration as follows [94]:

- **Nonpersistent Carrier Sense Multiple Access (NP-CSMA):** if the user senses the channel to be busy, it refrains from transmission and behaves as if collision actually occurred, by scheduling the transmission for a random time in the future [100];

- **1-Persistent Carrier Sense Multiple Access (1P-CSMA):** if the user senses the channel to be busy, it waits until the channel is idle and sends it as soon as it is. This means the channel will always be busy as long as there are packets ready for transmission;
- **Slotted Carrier Sense Multiple Access (Slotted NP-CSMA or 1P-CSMA):** behaviour is similar to the previously mentioned CSMA protocols, except for a slotted time axes, which allows synchronization between users. When a packet is ready for transmission, the user waits for the beginning of a time slot to sense the channel and if it's idle, it proceeds to transmit. If it's not idle, the selected CSMA protocol is put into use.

### 3.3.4 Collision Resolution Protocols

---

If we look, for example, at the Aloha protocol family, we see that there is no sincere attempt to solve collisions as soon as they occur. Transmissions are rescheduled for another random time in the future in the hope a collision will not happen again. Odds are they will.

With Collision Resolution Protocols (CRP), all efforts are made to solve collisions as soon as they occur. The key here is the feedback information that is sent to users in order to control the retransmission scheduling, and solve collisions more efficiently [94].

In this family of protocols, assumptions are similar to the ones under the slotted Aloha protocol, in the sense that time is divided into slots and packets are only sent at the beginning of these slots. At the end of each slot, all users are informed of whether there was a collision or not (binary feedback).

#### 3.3.4.1 Binary Tree Protocol

Tree Search Algorithms were introduced in [101] and [102] in a generic manner to multiple access problems, but are a great alternative for RFID systems [103].

As described in [8], the search starts with the root node and, at each succeeding node, it's asked whether there are zero, one or more than one packets in the subtree stemming from each of the two emanating branches. If the answer at any of the branches is more than one, proceed to the node at the end of the branch and repeat the question. This logic continues until all the leaves are separated into sets such that it is known that each set contains at most one packet [101]. To sum up and simplify, we can define the algorithm in the following steps:

If collisions occur:

- No new packets are transmitted until collision is resolved;
- Resolve the first collision before resolving the next collisions;

- A collision in node  $n_{ij}$  is resolved by dividing the tree into two halves and, for each, retry transmission.

We say that a collision is resolved when the system's users know that all packets involved in the collision have been transmitted successfully.

### *3.3.4.2 Limited Sensing Protocols*

So far, the protocols presented require every user to be aware of the state of the channel at all times; which means they always have to be interpreting its feedback even if the user has no packet to transmit. This kind of feedback monitoring is called full-sensing [94].

This kind of operation can be impractical because if a user crashes, it will never be able to join the chain again. Also, if a user for some reason didn't receive all signals correctly, the entire system can be disturbed. This means that ideally the users only monitor the feedback during limited periods. This kind of monitoring is called limited-sensing.

The simplest protocol following this philosophy is the full-access protocol analysed in [104] and [105]. In this protocol, new packets are transmitted as soon as possible at the beginning of the slot subsequent to their arrival; thereafter, a user that transmitted a new packet monitors the feedback signals and continues operating as if he were an "old" user.

# CHAPTER 4 IMPLEMENTATION OF AN RFID SYSTEM USING MM-WAVES

In the course of this chapter, we will discuss how the RFID system was assembled, as well as the different components that compose it. **Figure 8** illustrates the different constituents that will be mentioned in the course of the chapter. Both reader and tag have a software (SW) and hardware (HW) component that communicate according to a protocol, whose behaviour will be detailed next.

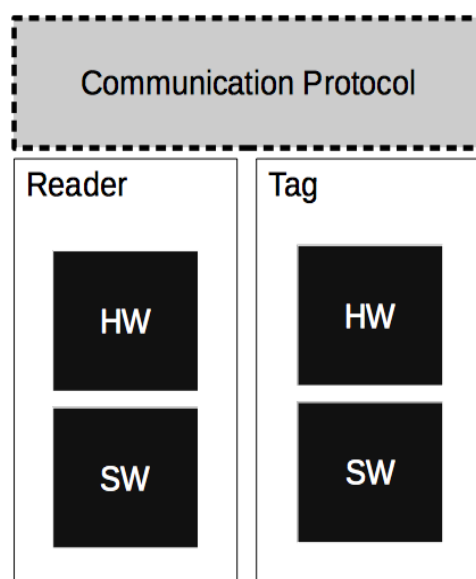


*Figure 8 – Overview of the system's components.*



## 4.1 Communication Protocol

---

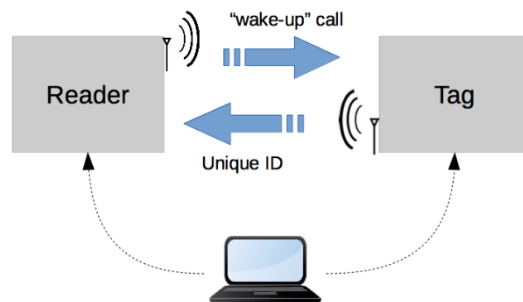


*Figure 9 – Communication diagram for a link at the 60 GHz ISM band with the assembled setup.*

As is shown in **Figure 9**, the presented system is composed of a reader and an active tag. The reader is in charge of establishing communication with the tag, while the tag can be placed on the surgical instrument. The instrument or sponge, which will be traced, has its own unique identification code. Configurations of both are defined with the help of a computer, as we'll see later on.

The chosen protocol for interrogation is illustrated in **Figure 10**, from both the reader's and the tag's standpoint and it can be ordered as follows:

1. When the system is at rest, both devices are waiting for an external element to inform them of what their next action should be;
2. The reader waits for the user to decide to start procedure through an external signal (like a push button), at which point it sends a single bit of information to the tag, only to demand its unique identification sequence;
3. After transmission, the reader waits for a response to be sent by the tag;
4. The reception of this signal by the tag triggers communication from tag to reader, which is modulated with a binary sequence;
5. After transmitting, the tag also returns to the rest state;
6. The reader is responsible for receiving and decoding this sequence;
7. After analysing the sequence, the reader also returns to the rest state.

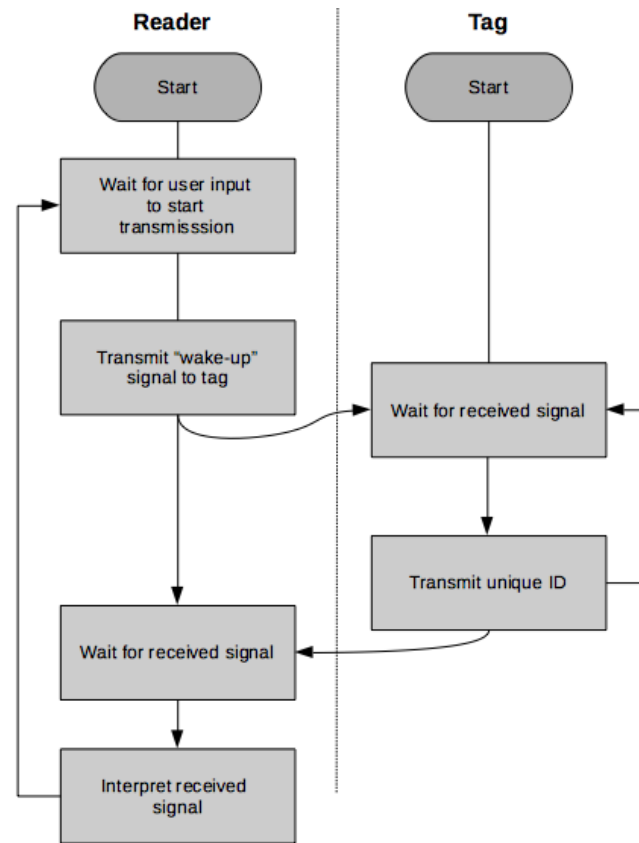


Figure 10 – Diagram of the communication protocol between reader and tag.

## 4.2 Hardware

There are five hardware components to both reader and tag modules, which will be discussed in this subchapter:

1. A VCO, which will generate an intermediate frequency (IF) signal in the 0,5 – 5 GHz range;
2. A V-band converter, responsible for converting the IF in the 0,5 – 5 GHz range to the carrier frequency, in the 60 GHz band (V-band) or vice-versa;
3. A downconverter unit that will convert the received IF signal to the 4 – 5 MHz range;
4. A rectification circuit, which will convert the 4 – 5 MHz range signal in a proportional DC voltage;
5. A control unit, responsible for logic operations.

4.2.1 Block Diagram of the RFID System

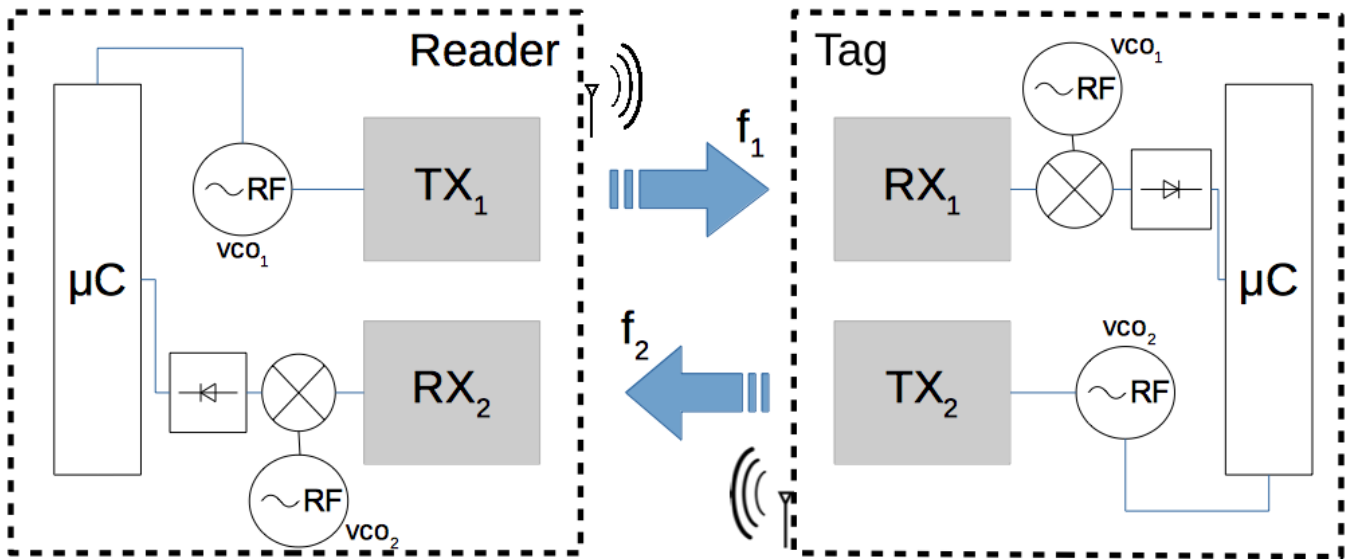


Figure 11 – Diagram showing an overview of the full RFID system.

Figure 11 shows an overview of the behaviour of the RFID system. To avoid interference between the reader-tag and tag-reader communication channels, two different frequencies were used: 58 and 62 GHz respectively.

Rectification circuits are necessary in both reception modules because DC voltage is required for communication with the microcontrollers.

In the next subsection, a theoretical power and frequency budget is presented.

4.2.1.1 Power and Frequency Budget

Firstly, the performance of both VCOs in terms of output power and frequency is presented in Table 6.

Table 6 – Power and Frequency Budget (VCOs).

Stage		Power (dBm)	Frequency (MHz)
Output VCO <sub>1</sub> (ZX95-3800A-S+)	“high”	4,44	1773,4
	“low”	4,45	2532,7
Output VCO <sub>2</sub> (ZX95-2150-VW)	“high”	2,96	864,6
	“low”	3,82	1173,0

To calculate a theoretical value for the RX IF output power, which will be the mixer’s input, Equation (3) will be used:

$$P_{out} = P_{in} + G_{TX} - FSPL - L_{O_2} + G_{RX} \quad (3)$$

where  $P_{out}$  is the IF RX output power,  $P_{in}$  is the TX IF input power,  $FSPL$  is the free-space path loss, which is calculated using Equation (2), and  $L_{O2}$  is the loss due to the effect of oxygen molecules on the propagating wave (15,5 dB/Km).  $G_{RX}$  and  $G_{TX}$  represent the gains introduced by the RX and TX converters, respectively. These last two values are the sum of their nominal gain (IF-to-RF and RF-to-IF) and the gain introduced by the aperture antennas (Equation (4) and (5)).

$$G_{RX} = G_{NRX} + G_A \quad (4)$$

$$G_{TX} = G_{NRX} + G_A \quad (5)$$

For this calculation, we will consider the maximum effective area of the aperture antenna, which is equal to its physical area. The aperture of the converter modules is a standard WR-15 waveguide, which has an area ( $A$ ) of  $3.759 \times 1.880 \text{ mm}^2$  [106]. The gain of the aperture is calculated according to Equation (6) [72].

$$G_A = \frac{4\pi}{\lambda^2} A \quad (6)$$

The nominal gains of RX and TX modules are 20 dB and 40 dB respectively.

As an example, **Figure 12** shows the chart that represents the values of  $P_{out}$  in relation to distance (5 to 505 cm), for an input of -20 dBm and a link frequency of 60 GHz. Multipath and fading effects were not accounted for.

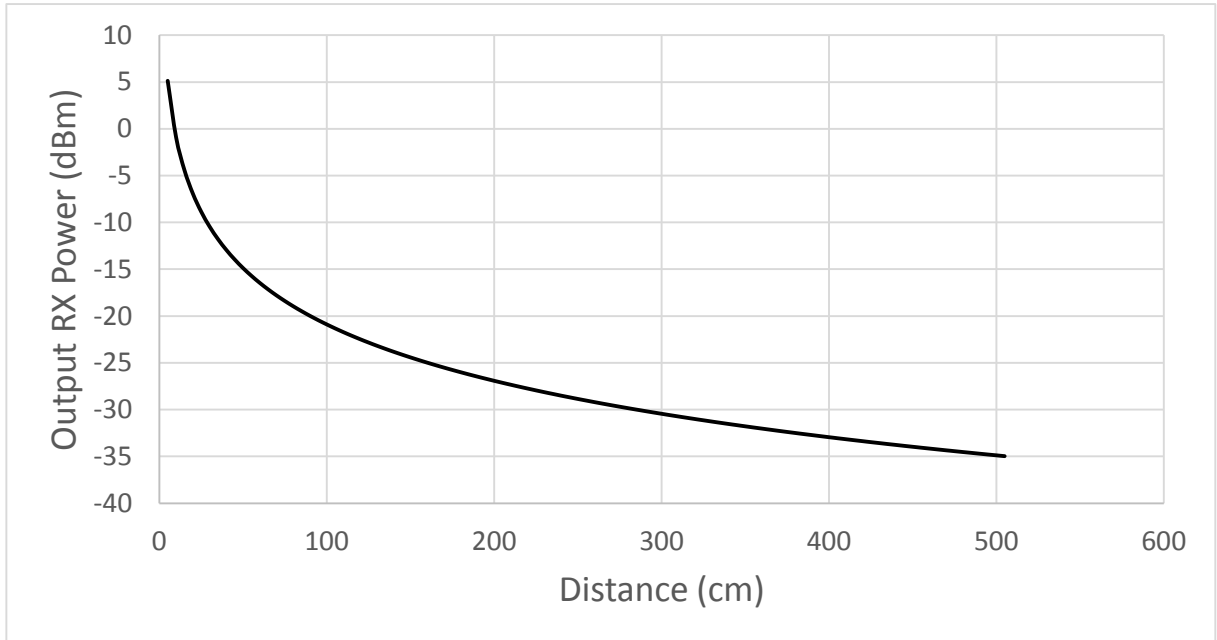


*Figure 12 – Output RX power according to distance for a power input of 20 dBm.*

An Experimental characterization of the 60 GHz link will be presented in Chapter 5.

**Table 7** presents the power budget for the downconversion unit, whose input is the output of the RX module.

*Table 7 – Power and Frequency budget (downconversion unit).*

<i>Stage</i>	<i>Loss/Gain (dBm)</i>	<i>Frequency (MHz)</i>
<i>Mixing</i>	-7,4*	5
<i>Amplification</i>	+11**	5

\*Conversion loss from mixing  
\*\*Power Amplification

#### 4.2.2 IF Signal Generation and Modulation

The IF signal is generated by a VCO, by Mini Circuits [107]. A picture of the two types VCOs used is shown in **Figure 13**.



*Figure 13 – VCOs used for signal generation.*

The use of this component is paramount to the used modulation strategy: the tune voltage will change according to the binary sequence generated by the control unit. 5 V will be called a “high” value of the sequence, or a binary 1 and 0 V a “low” value, or a binary 0. As so, the VCO’s output frequency will be different for 1s and 0s.

Two different VCOs from Mini Circuits were used: ZX95-2150-VW and ZX95-3800A-S+. For each VCO, the “low” frequency output value will be eliminated through a downconversion process.

### 4.2.3 V-band Converter by Sivers IMA

---

A V-band converter by Sivers IMA (FC1005V00) [108] was used for both reader and tag devices. This converter platform is a broadband building block for applications in the 60 GHz ISM band and integrates an upconverter and a downconverter in a single unit, which operate independently. RF bandwidth is 58 – 63 GHz, while IF bandwidth is 0,5 – 5 GHz.

In addition to the converter, one needs a control board to make the desired configurations and supply power to the main device. As so, this control board is used to interface the main device's frequency converter units with on board synthesizers and stand-alone synthesizer units, through a 20-pin I2C communication. **Figure 14** shows a photograph of the converter and the control board, as well as a pin diagram and the complete block diagram showing the integrated electronic components.

As we can see from **Figure 14c**), the I2C bus connects to the microcontroller unit (MCU), which acts as a slave unit, accepting commands from the control board. This unit makes the interface with the control board and, consequently, with the user. The MCU connects with the PA and LNA for transmitter and receiver modules respectively and this allows the user to adjust gain and power settings. In addition, it connects to the synthesizers, allowing the user to select a desired link frequency.

As we can see, the desired frequency in the V-band is the result of a multiplication of the synthesizer's frequency by four. The final 60 GHz signal is the output of an I/Q mixer.

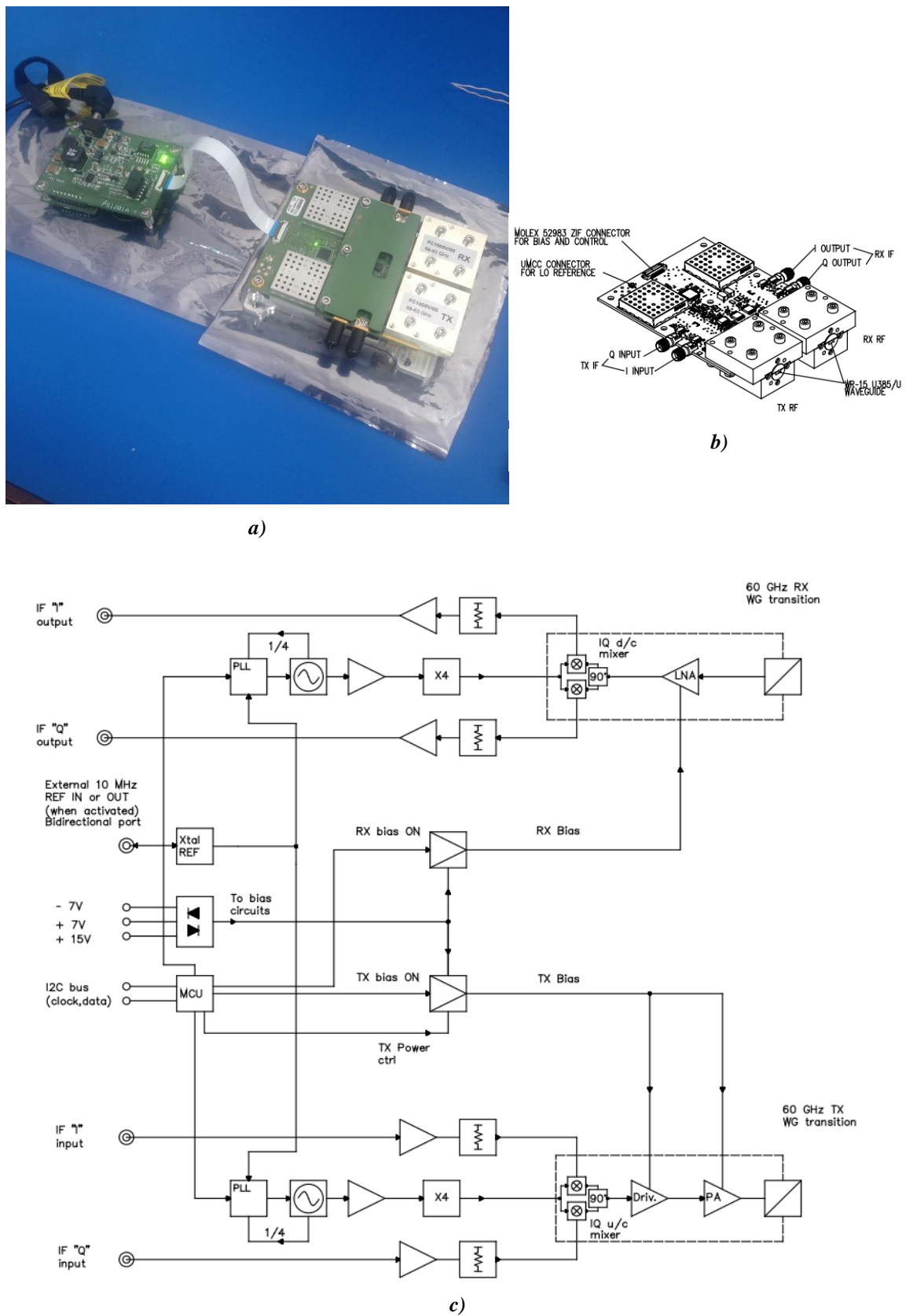
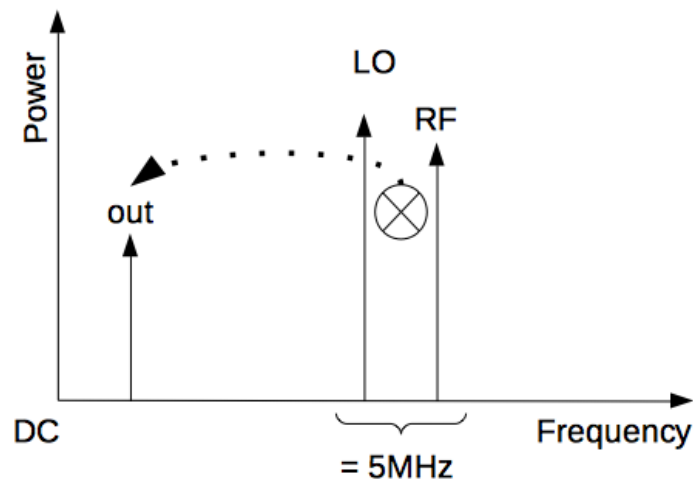


Figure 14 – a) Picture of the Siverts IMA FC1005V00 and control board; b) Sketch with pin diagram; c) Block diagram.

4.2.4 Decoding the Intermediate Frequency Signal

Decoding the signal implies finding a way to generate the original sequence produced by the control unit through the output of the converter’s RX module. This signal has a frequency in the 0,5–5 GHz range that changes according to the tune voltage of the VCO connected to the TX module.

A first important step is another frequency downconversion to a 1–5 MHz range. This step is vital because the electronic dial in-line package (DIP) components available don’t operate correctly in the 1-5 GHz range. This downconversion is accomplished through mixing. The basic principle is demonstrated in **Figure 15**.



*Figure 15 – Basic principle of downconversion.*

In this process, the local oscillator is a VCO of the same reference as the one used to generate the signal in the transmission step, with a constant tune voltage of a value a little lower than 5 V, as to allow a difference of frequencies of less than 5 MHz. The output of the mixer can be calculated through Equation (7). **Figure 16** shows a photograph of the downconversion unit.

$$f_{out} = f_{RF} - f_{LO} \tag{7}$$

This way, if the signal is “high”, the output of the mixer will be a wave of about 5 MHz, and no signal otherwise. The desired tune voltage for the LO was selected with the use of a potentiometer and a spectrum analyser.



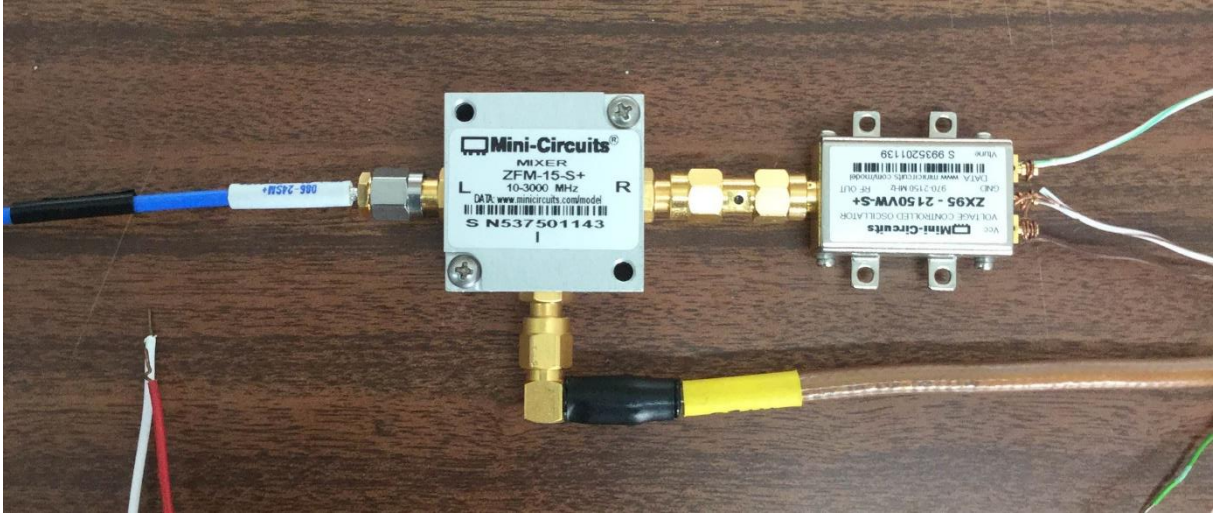


Figure 16 – Photograph of the downconversion unit.

The output signal from the mixer has very low power because of the transmission and conversion losses. So the next logical step is to amplify the signal.

Firstly, coaxial amplifiers were used (ZX60-14012L-S+ and ZFL-1000LN+ from Mini Circuits) to compensate for the mixer’s conversion loss. In addition, we used a high-speed operational amplifier IC from Linear Technology [109], with a bandwidth of 1 GHz.

Rectification and filtering will allow a constant DC output proportional to the input. A full-wave rectifier using high-speed diodes from Solid State Inc. (1N270) [110] constitutes this block. As the full-wave rectification circuit has a differential output, a differential amplifier was used as a final block. A diagram is shown in **Figure 17**.

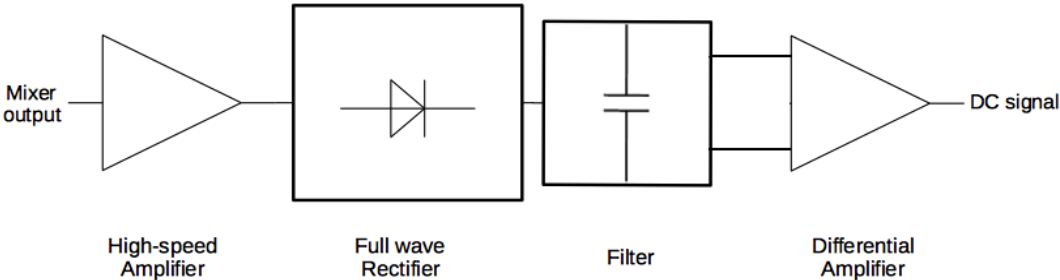


Figure 17 – Block diagram of the decoding circuit.

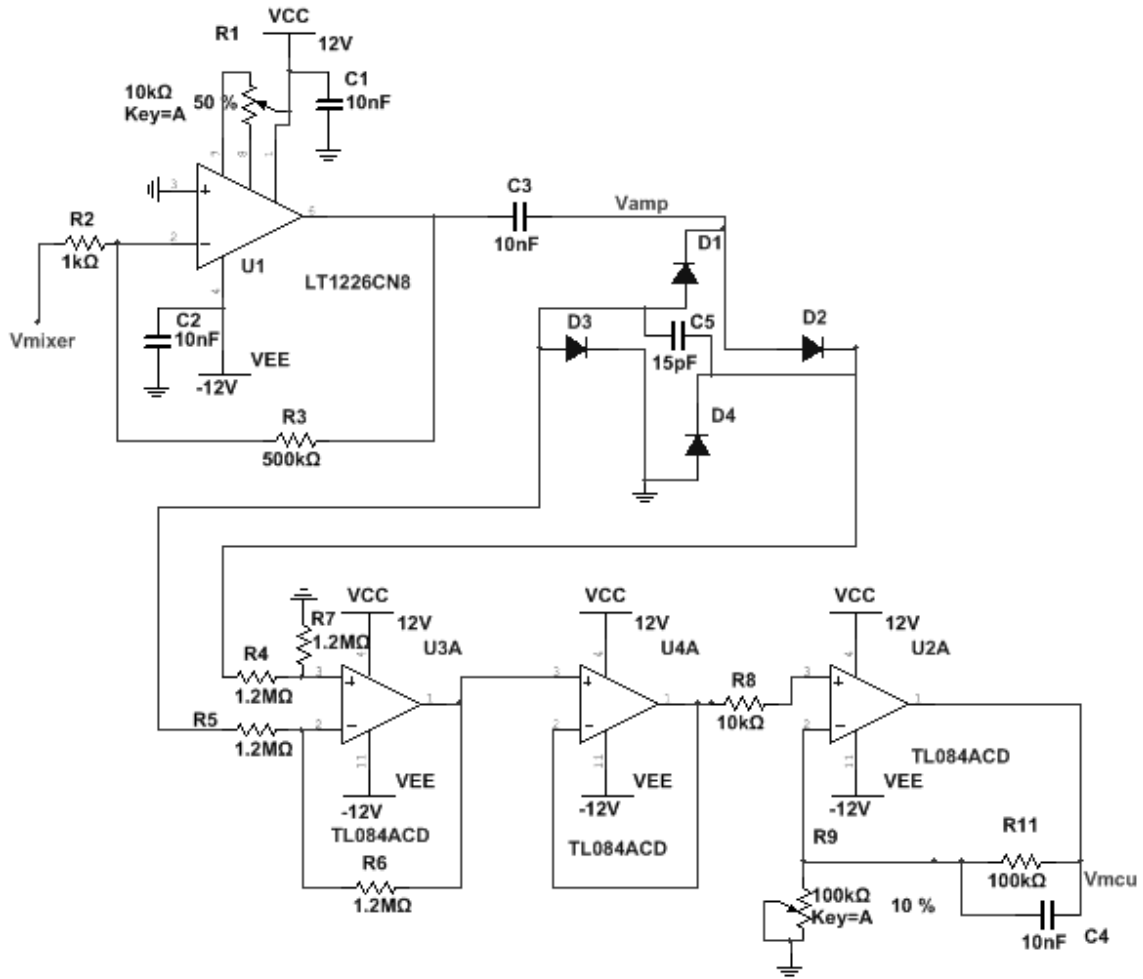


Figure 19 – Schematic of the decoding circuit.

Figure 19 presents the schematic of the electronic circuit, in which all the electronic components can be seen, as well as their dimensions. Lastly, Figure 18 presents a photograph of the implemented electronic circuit.

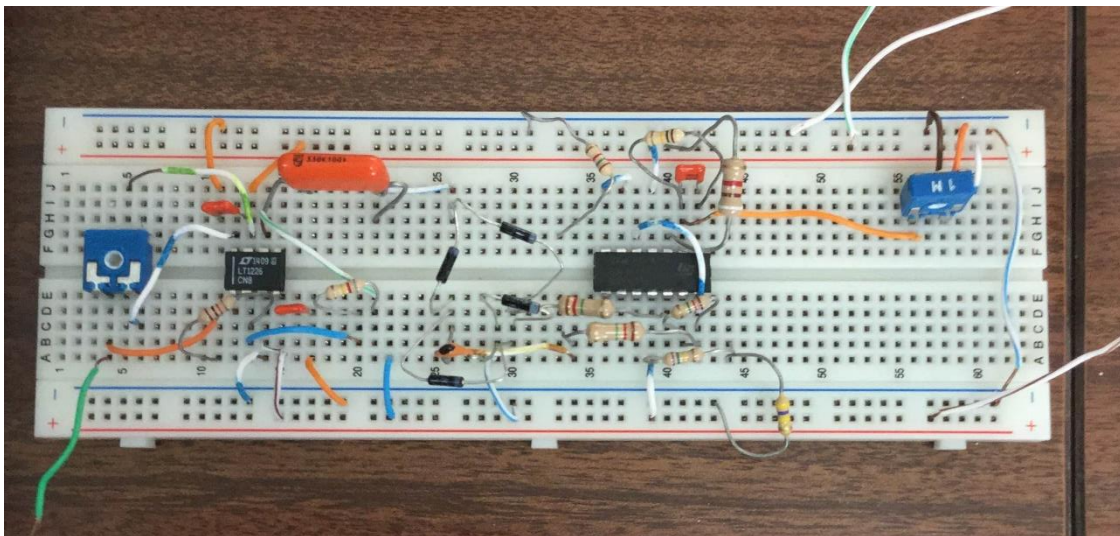


Figure 18 – Implemented DIP decoding circuit.

### 4.2.5 Control Unit of the RFID System

---

The controller unit is composed of a microcontroller both in the tag and reader modules, and for this study we used an Atmega 324 [111], from Atmel Corporation.

The component has a power supply of 5 V, meaning 5 V and ground will be the values for the VCO's voltage tune for "high" and "low" values, respectively. These values provide sufficient separation between output frequencies. The device has an internal clock of 1 MHz, which is also sufficient because we don't intend to test high data-rates.

**Figure 20** shows the connection diagram for both tag and reader control units. In these illustrations, we can see what the relevant inputs and outputs from the microcontroller units are.

In both units there are light-emitting diodes (LED) indicating if the device is transmitting or waiting for a reception from another module. The reader device also has a couple of LEDs that allow the user to conclude if the sequence sent from the tag is correct or incorrect.

In the next section, we'll discuss the software component of the system.

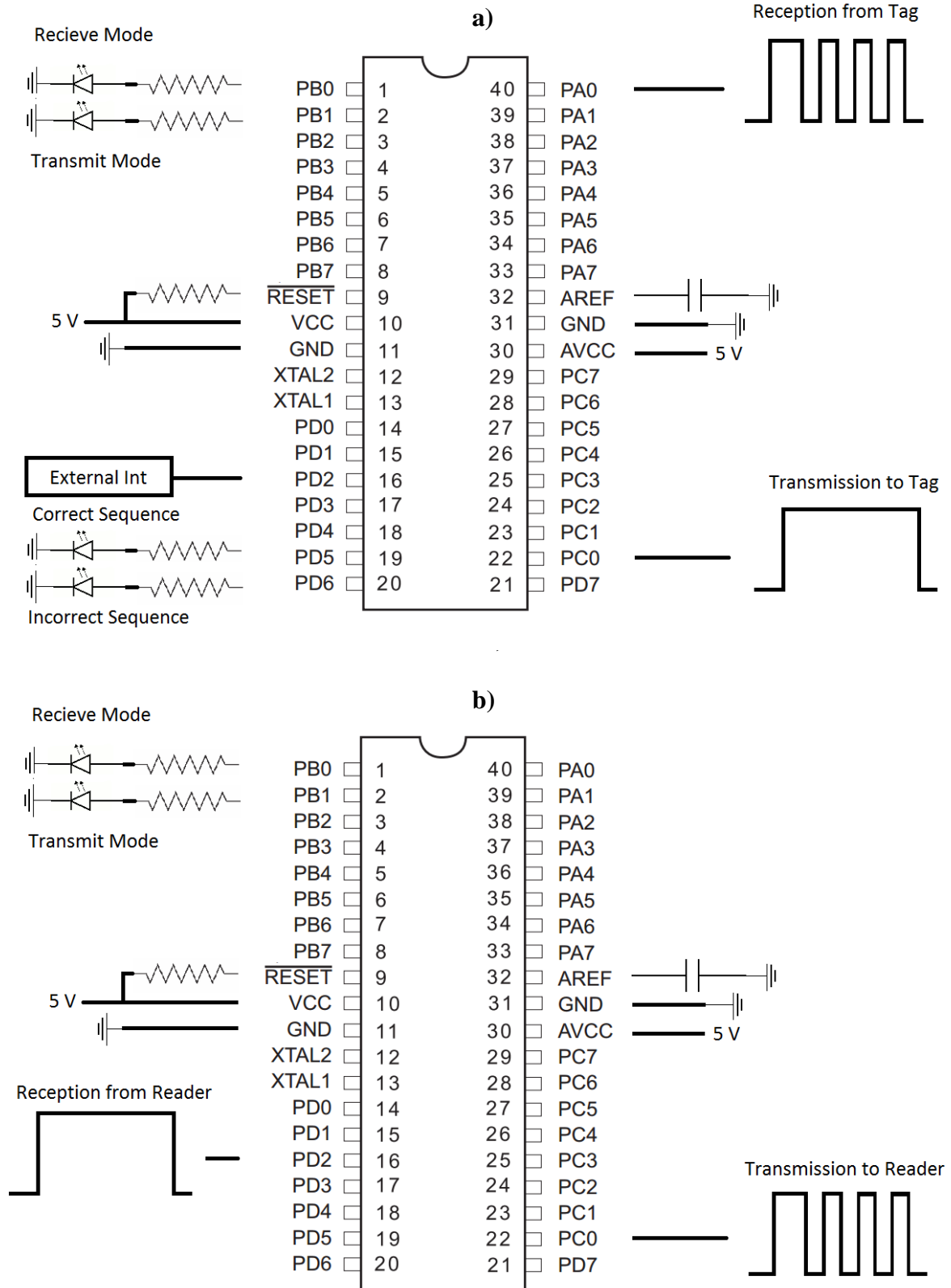


Figure 20 – Connection diagrams of the control unit: a) Reader; b) Tag.

## 4.3 Software

---

In this section, we discuss the software required to control the MMID system, which has two components:

1. Programming of the microcontrollers (tag and reader) in C language;
2. Specification of the parameters of the V-band converter, by serial communication.

### 4.3.1 Program for the Microcontrollers

---

The microcontroller serves distinct functions in the system, according to whether it belongs to the reader or tag module. For both devices, we'll go through the main tasks attributed, the interrupts assigned and the algorithm's flowchart, as to clarify how the microcontroller unit fits in the established communication protocol.

#### 4.3.1.1 Algorithms for the Reader

The main tasks assigned to the reader are the following:

1. Generate a simple "call-out" signal, only a binary '1' to communicate with the tag;
2. Successfully receive the signal sent by the tag and determine if it's an accepted sequence.

Both devices were programmed using C language and the strategy included a main program with an infinite loop, as well as several interrupt service routines (ISR).

The reader device's interrupts are detailed in **Table 8**.

*Table 8 – Interrupts of the reader device program.*

<i>Interrupt</i>	<i>Source</i>	<i>Description</i>
<i>External</i>	Rising edge of the selected pin value	Starts transmission when a “button” is pressed.
<i>Timer Compare Match</i>	Compare match with the selected timer mask	Used mainly for reception. Timer is configured with selected data rate. When the reader is receiving a sequence, the interrupt starts when a value is to be read.
<i>Pin Change</i>	Change of value of the selected pin	Starts reception, when the value of a selected pin is changed. Sent sequence from reader has to start with a binary ‘1’ for this interrupt to function correctly.

**Figure 21** shows the flowchart of the main program.

It’s important to note that there are some variables that have to be previously defined for the system to work properly. These include the data rate, or the baseband frequency, and the sequence to be transmitted/read. As the reader doesn’t have a unique sequence, it was decided that it should transmit a sequence composed only of binary ones.

The main program can function on two separate modes: the reception mode, where the device is resting and waiting to be called by another device (or reading a sequence) or by the user and the transmitting mode, where the device is outputting a signal in the tag’s direction.

As for the ISRs, **Figure 22** shows their flowcharts.

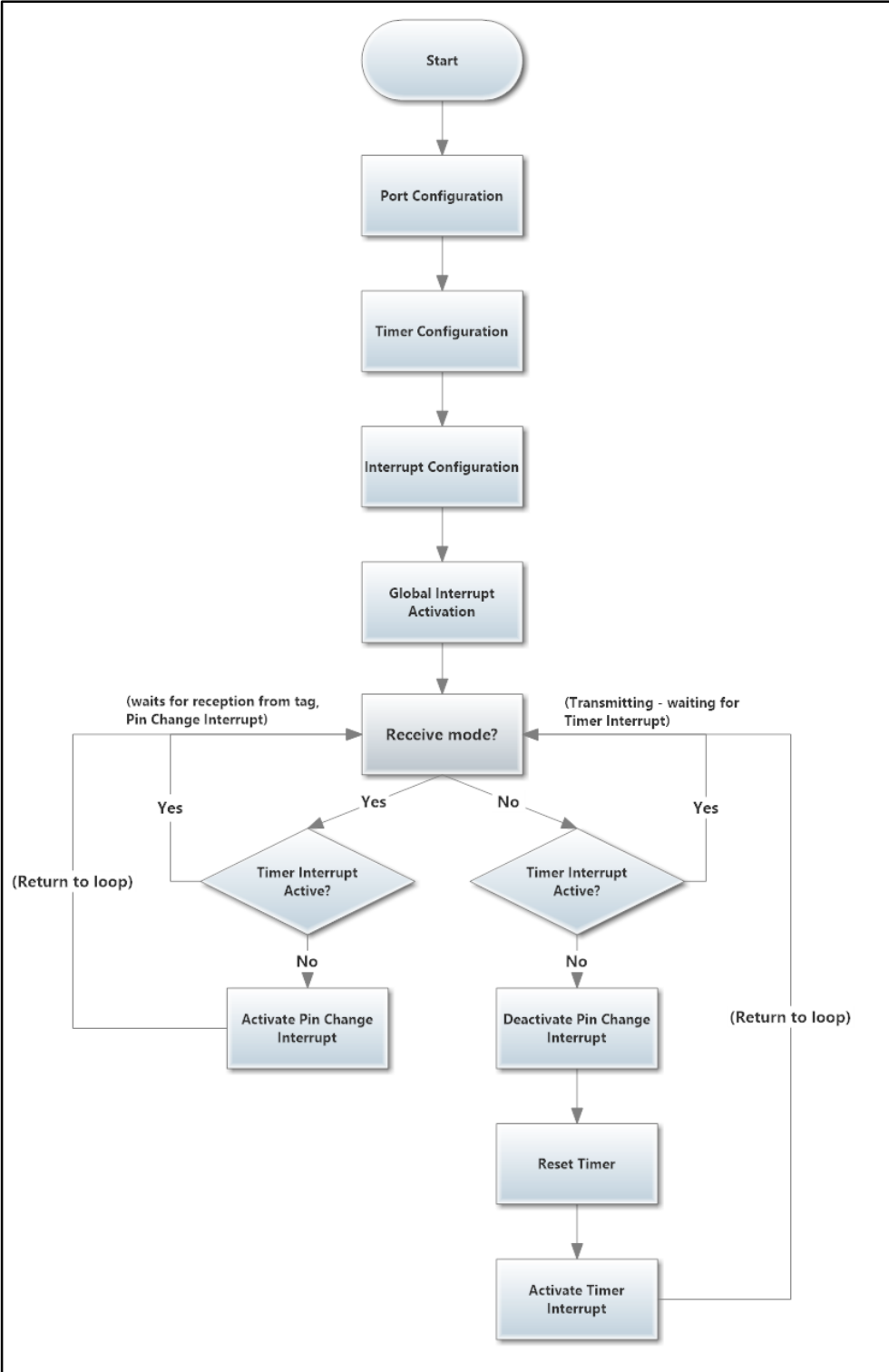


Figure 21 – Flowchart of the main function of the Microcontroller Unit (Reader).

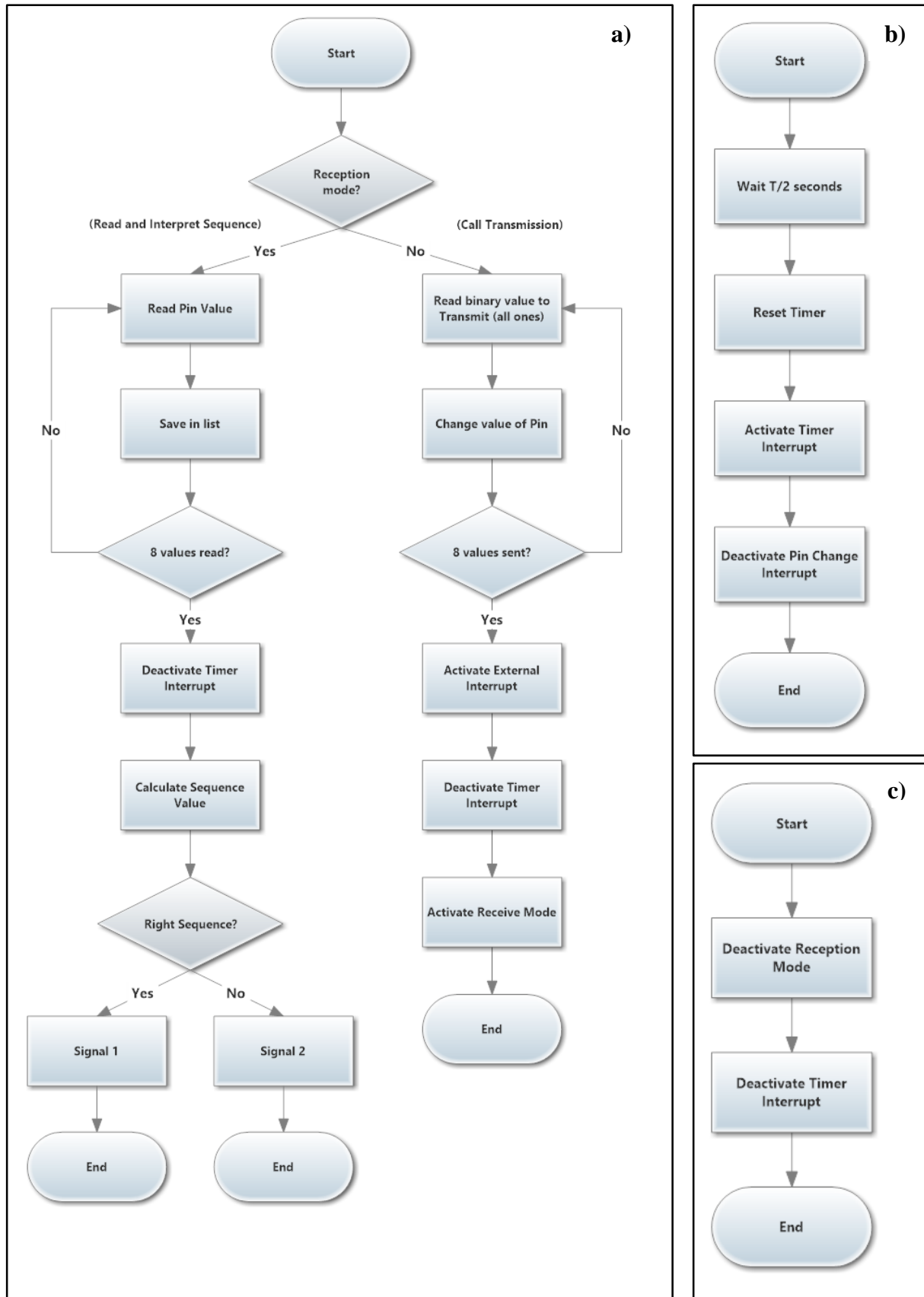


Figure 22 – Flowchart of the Interrupt Service Routines of the Microcontroller Unit (Reader): a) Timer Compare Match; b) Pin Change; c) External Interrupt.



4.3.1.2 Algorithms for the Tag

The tag’s main program was modelled after the program that was coded for the reader. Alterations were made according to what was intended for the tag.

Only the tag stores a unique binary sequence of ones and zeros. As it communicates with the reader only, the tag isn’t required to interpret a sequence, it only has to identify that the reader called it for transmission. This makes the pin change interrupt unnecessary.

The external interrupt will be activated when the reader, at the falling edge of the call signal, reaches the tag so that transmission starts only when the reader stops its transmission and is ready to receive the sequence from the tag.

The used interrupts are summarized in **Table 9**.

*Table 9 – Interrupts of the tag device program*

<i>Interrupt</i>	<i>Source</i>	<i>Description</i>
<i>External</i>	Falling edge of the selected pin value	Starts transmission when call from reader ends.
<i>Timer Compare Match</i>	Compare match with the selected timer mask	Used for transmission. Timer is configured with selected data rate. When the tag is transmitting its sequence, the interrupt starts when a value is to be sent.

Flowcharts of the main program and ISRs are shown in **Figure 23** and **Figure 24** respectively.

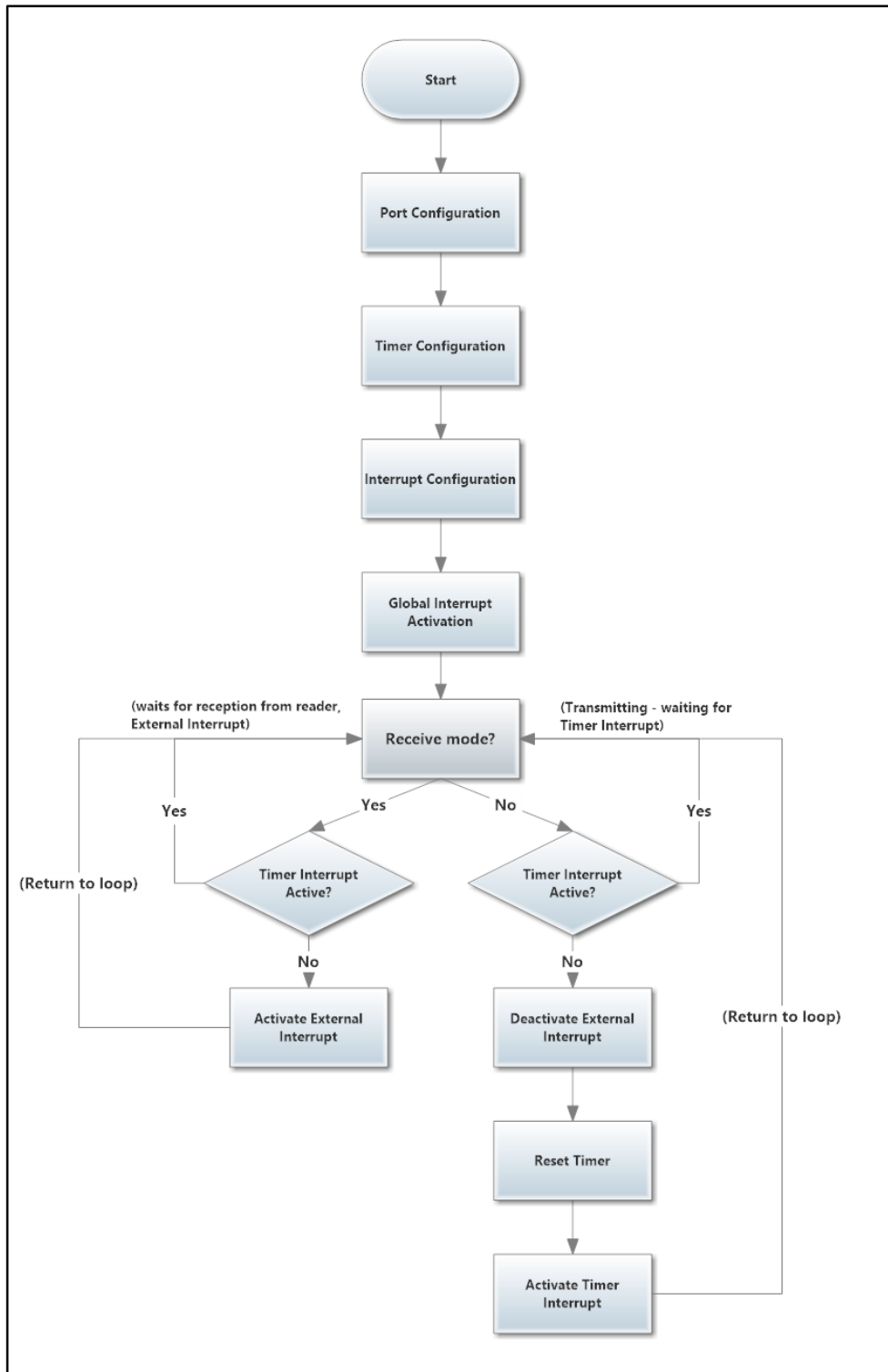


Figure 23 – Flowchart of the main function of the Microcontroller Unit (Tag)

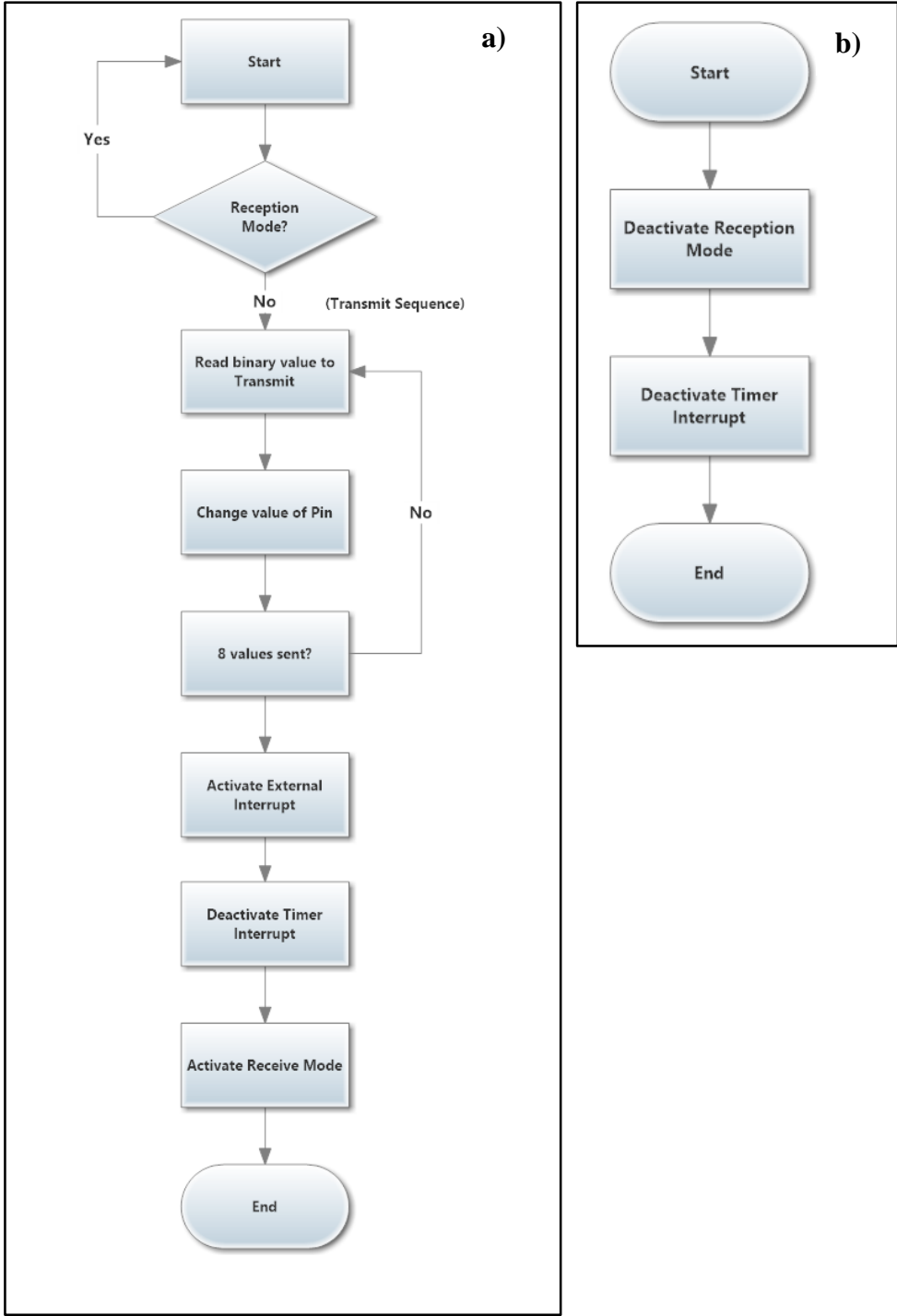


Figure 24 – Flowchart of the Interrupt Service Routines of the Microcontroller Unit (Tag): a) Timer Compare Match; b) External Interrupt.

4.3.2 Configuration of the Converter’s Control Board

As aforementioned, communication from the PC to the V-band converter’s control board is established through serial communication using a USB module. PuTTY was used as the serial console, because it’s a free and open-source application.

```

COM4 - PuTTY
conv:txon on
ACK
synt:txon on
ACK
synt:txfr 03 8A 40
ACK
█
    
```

a)

```

COM6 - PuTTY
conv:rxon on
ACK
synt:rxon on
ACK
synt:rxfr 03 8A 40
ACK
█
    
```

b)

*Figure 25 – Example of converter configuration: a) TX module; b) RX module.*

Communication is typically started by addressing the microcontroller unit to listen, and it will follow with an acknowledgement (ACK).

For the converter to complete the desired task, three commands are needed:

1. Turn converter RX/TX module ON;
2. Turn the RX/TX frequency synthesizers ON;
3. Define the RX/TX frequency synthesizers' frequency of operation.

These commands, as introduced in the *PuTTY* terminal, are exhibited in **Figure 25**. As can be seen, as input is made, it is followed by the ACK sent from the converter's MCU.

#### 4.4 Suggested Protocol for Implementation in an Operating Room

---

It's important to explain how the implemented system's communication protocol could be useful inside a real operating room and help reduce the errors of human performance.

The reader would be placed next to a wall, where it could communicate with tags placed in every location of the room. It's expected that, if the tag is placed inside the patient's body (the body is placed between tag and reader), it will be undetectable.

As for the tags, one should be attached to every instrument and sponge planned for use in the procedure. The tags would be programmed with unique sequences, which are known beforehand by the reader.

**1. An initial read should be made at the start of the procedure.**

Using multiple access protocols (section 3.3), the reader will be able to uniquely identify every tag in its reading range. This will allow for a list of all the present objects to be made and displayed. This list will be a reference for future reads.

**2. Continuous reads should be made during the course of the procedure.**

The objects in range are continuously displayed. In a similar way, and by comparison to the original list, the objects out of range should also be displayed in a separate list. The medical staff and engineers could decide what would be the optimal time interval between reads.

In this way, the nurses and other medical assistants could keep track of all the surgical instruments in real time. If an object is placed inside the patient's body, it should probably disappear from the list, but later on should return to the visible list.

**3. The instrument list should be verified before the patient is closed up.**

It's very important to verify if there are retained objects before close up. If all objects are not accounted for at this time, a search could be promptly made in all cavities, saving resources, time, and further complications.

However, there is a margin for error in this read because a tag could be reachable by the reader even if not visually accessible by the staff (cavities are still open).

**4. After the surgeon closes up the patient, verification should be made.**

A comparison is made with the initial list. If all objects are accounted for, the lists should be the same. If not, it's safe to conclude there are retained foreign bodies.

**5. After the patient leaves the room, a final verification should be made.**

As a safety measure, a final verification should be conducted after the patient leaves the room. The medical staff should gather all the instruments for a final read. If initial and final lists don't match, an RSI is very likely.

The system should only be turned off after this final verification is made.

# CHAPTER 5      RFID SYSTEM

## CHARACTERIZATION

In this chapter, we discuss performance aspects of the implementations that were presented in Chapter 4. All the different setups are explained and important results are clarified and interpreted. The main concern while testing the system was the successful establishment of a wireless link at 60 GHz, which will be the topic of the next section.

### 5.1 60 GHz Link between Tag and Reader

---

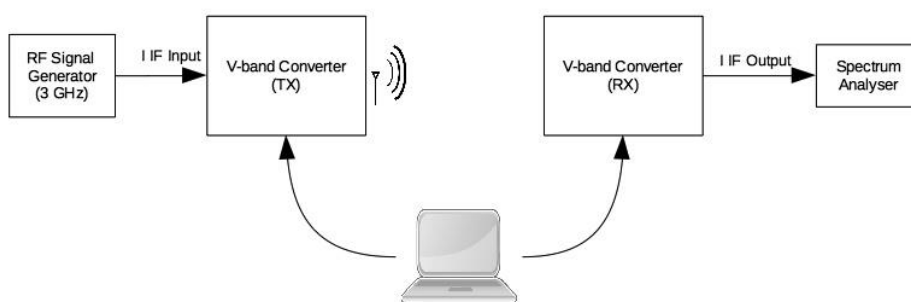


*Figure 26 – Assembled setup for a link at the 60 GHz ISM band.*

As explained in section 4.2.3, an IF input in the 0,5 – 5 GHz range is needed. The generated input signal was used for the “I” input for amplitude modulation. The “Q” input was not used. For this purpose, an RF generator was engaged (Agilent N9310A) to create a signal with 3 GHz. As an alternative, a simple VCO was also tested.

As previously stated, the used transceiver modules do not allow a direct measure of the received power, only at the IF frequency (0,5–5 GHz), but since all the transceiver settings are kept constant during measurements, the power measured at the IF frequency attends as an indirect measurement of the expected attenuation when using such frequencies. A spectrum analyser (Agilent E4404B) was used for these measurements. If the link is successful, the output signal should have the same frequency as the input. **Figure 26** shows a diagram of the setup.

A picture of the implemented setup is exhibited in **Figure 27**. To obtain data close to what will be obtained in a real scenario, the measurements were done inside the laboratory, without any particular attention to multipath, or reflections.

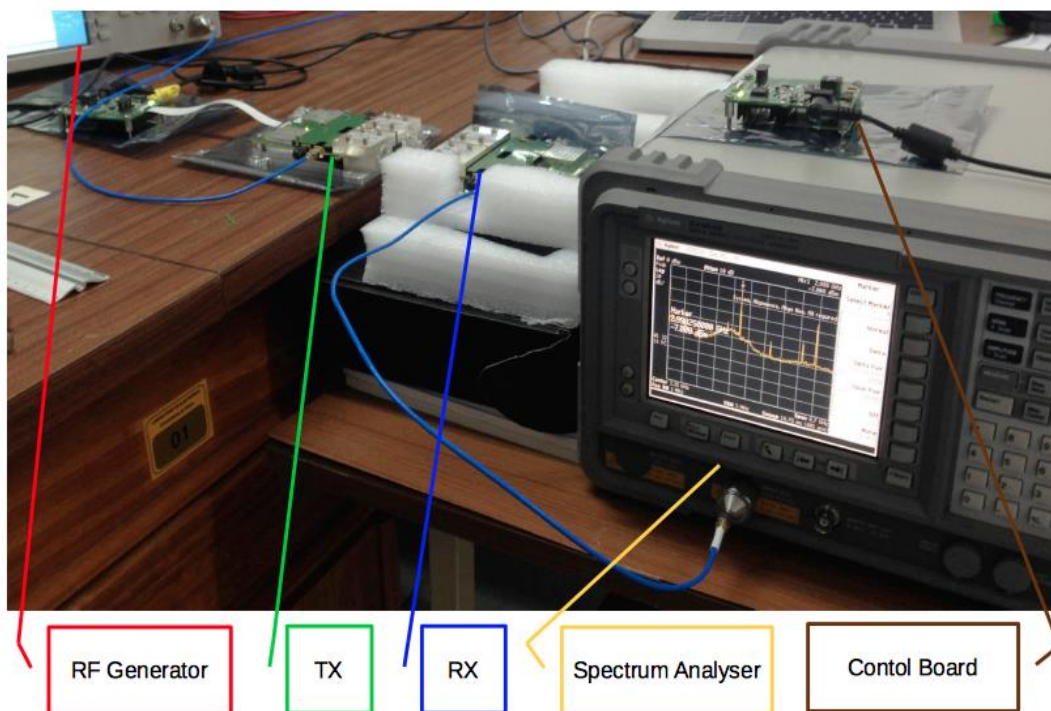


*Figure 27 – Setup used to implement the link at 58 GHz, with different blocks differentiated.*

The radiators were operating without any antenna, serving the rectangular waveguide aperture as radiation element.

Input IF signal had a power of 0 dBm and frequency of 3 GHz. Initial distance separating the reader from tag, as seen in the figure was 5 cm. As we can see from the image shown in the spectrum analyser, the link was successfully implemented, as the most powerful spectral component of the output IF signal is at 3 GHz, about -8 dBm. Other spectral components with less power are also shown, which are the result of interference of other unidentified RF sources.

After the link was achieved at a short distance, further testing was made to make sure a signal would be detected at distances and angles that will allow the implementation of a RFID system.

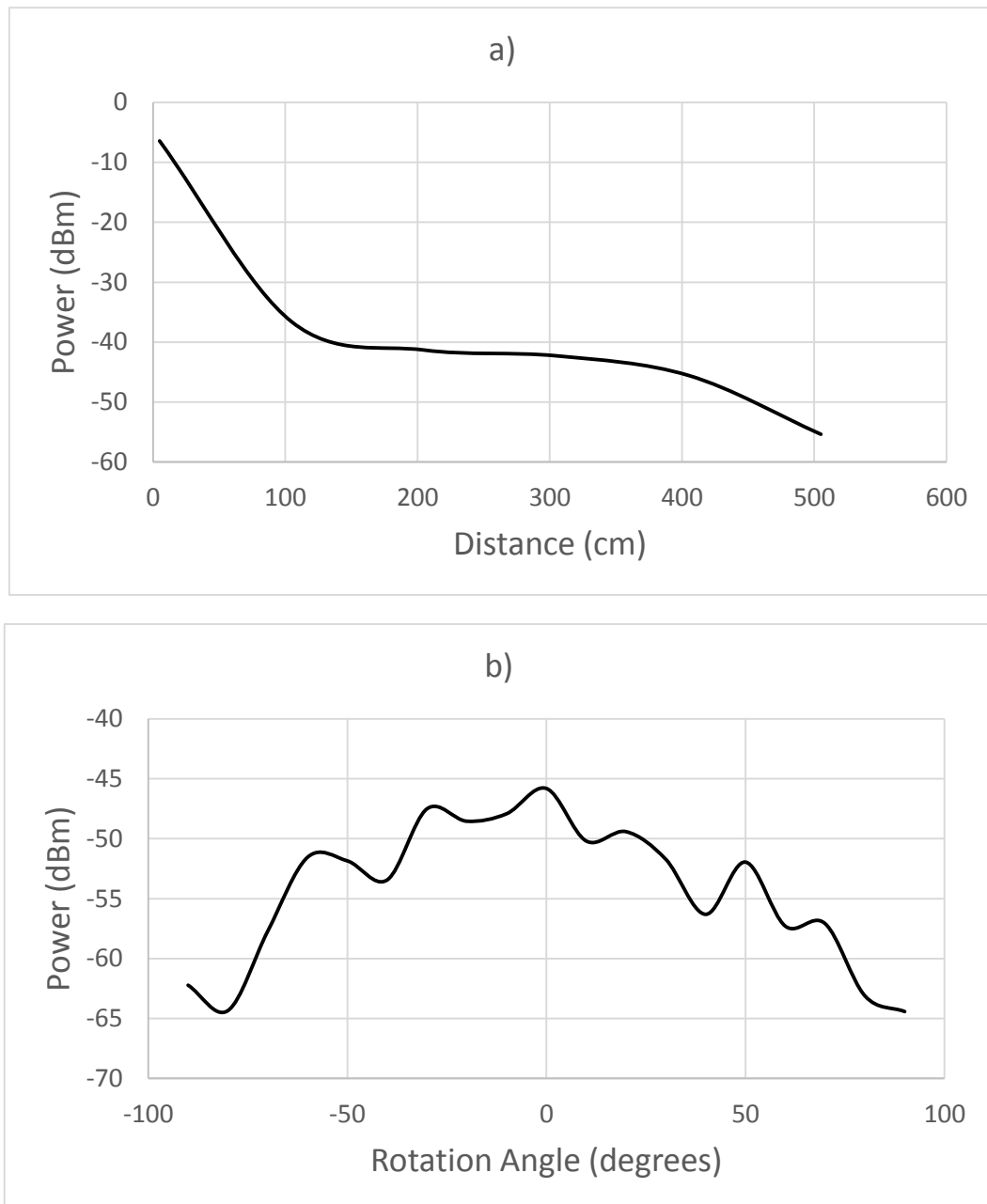


**Figure 28** – Output intermediate frequency RX power according to: **a)** Increasing distances separating tag and reader; **b)** Different rotation angles at a fixed distance of 4 m.

**Figure 28a)** shows the resulting relationship between distances and output power. For these measurements, the setup was maintained the same as previously described. The tag was moved, at the same height (reader's height) away from the reader and output IF power was collected.

From the analysis of this first graph, we can safely conclude that a link was successfully achieved at distances up to 5 m. It can also be concluded that RX power is inversely proportional to the distance separating tag and reader, which is an expected consequence of path losses.



**Figure 29** shows a comparison between the predicted RX IF output values (section 4.2.1.1) and the ones obtained experimentally. As we can conclude from its analysis, the experimental values are lower than the theoretical ones.

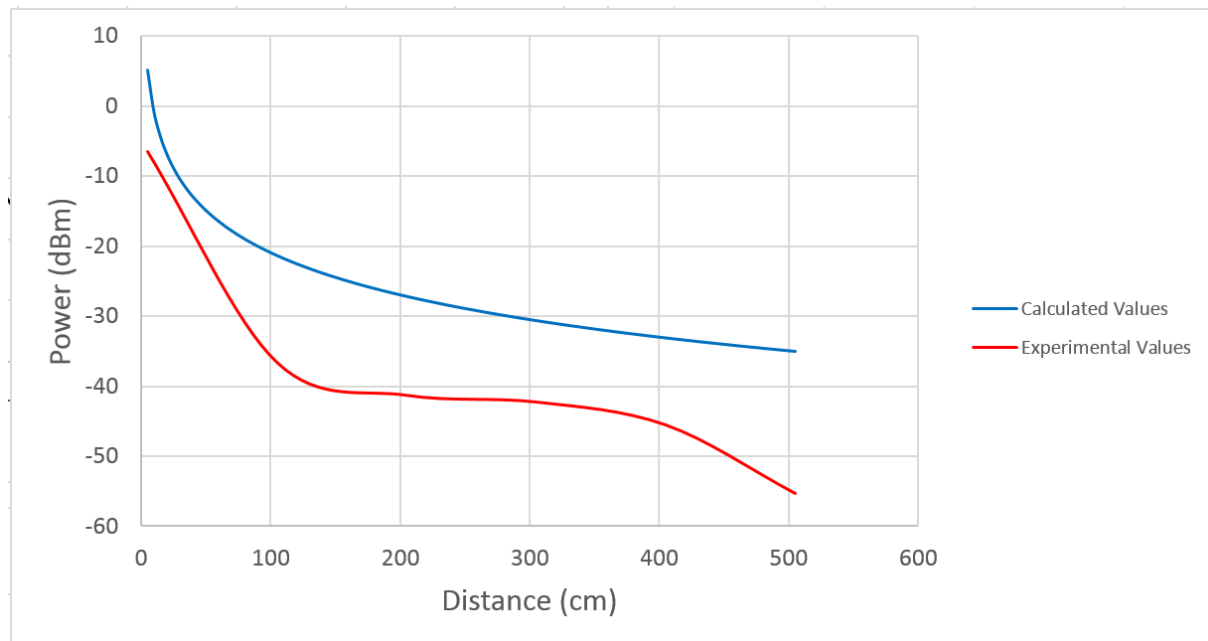


**Figure 29** – Comparison between calculated and experimental values for the RX output power according to distance.

These differences can possibly be explained by the multipath effect. The experimental plot shows faster attenuation in comparison to the calculated plot, until it reaches a “plateau” phase. After a certain distance, it starts dropping once again.

As for measurements for different angles, a rotational stepping motor (Standa 005406) was introduced into the setup in order to allow rotation of the device according to specific angles. To control this device, a microstep driver with USB interface was used (8SMC1-USBhF, also from Standa). A graphical user interface was used to control the device (SMCView for Windows). **Figure 30** shows a photograph of the modified setup. Distance from tag to reader was fixed at 4 m.

From the breakdown of the graph shown in **Figure 28b**), it's concluded that, at a distance of 4 m, a link was successfully achieved at angles from  $-90^\circ$  to  $90^\circ$ . The highest RX output power was noticed when there the devices are facing each other ( $0^\circ$ ).

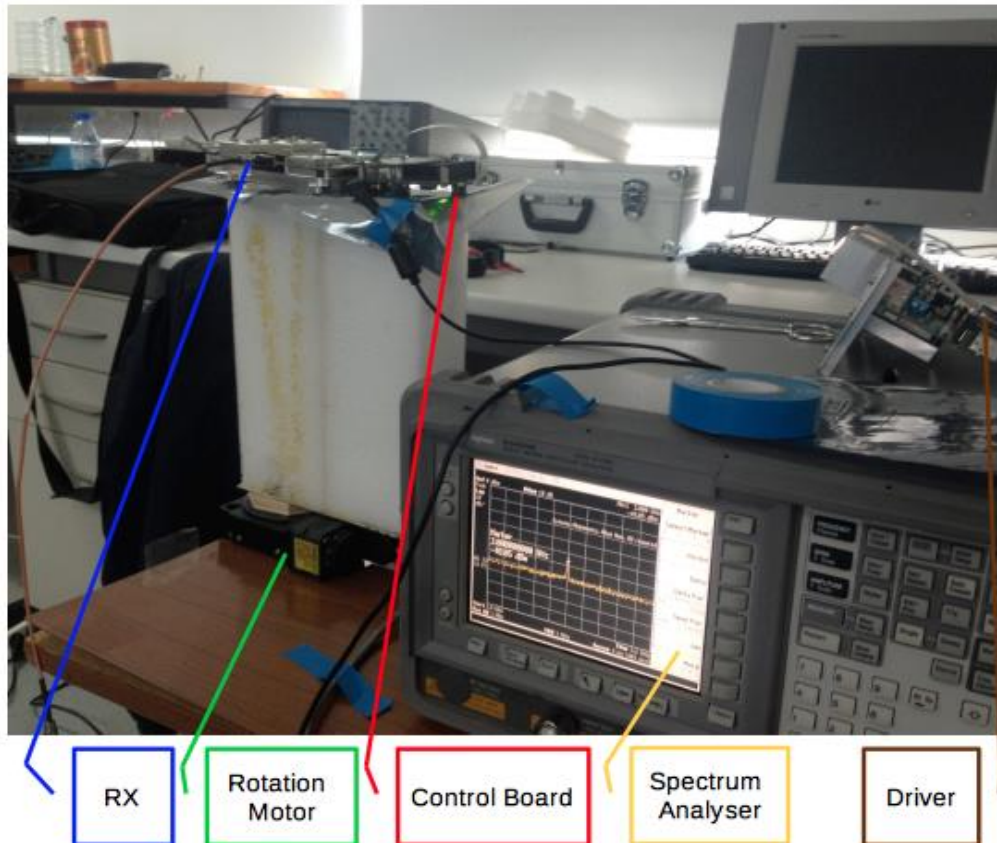


*Figure 30 – Setup used to implement the link at 58 GHz at different angles, with different blocks differentiated.*

## 5.2 Downconversion to 5 MHz and Rectification Circuit

This block of the system converts the output IF signal into a DC voltage. The goal is to reproduce the binary sequence that was generated by the control unit, at transmission. As explained in section 5.2, the first step is a downconversion from the IF frequency, outputted by the RX module, to a frequency close to 5 MHz.

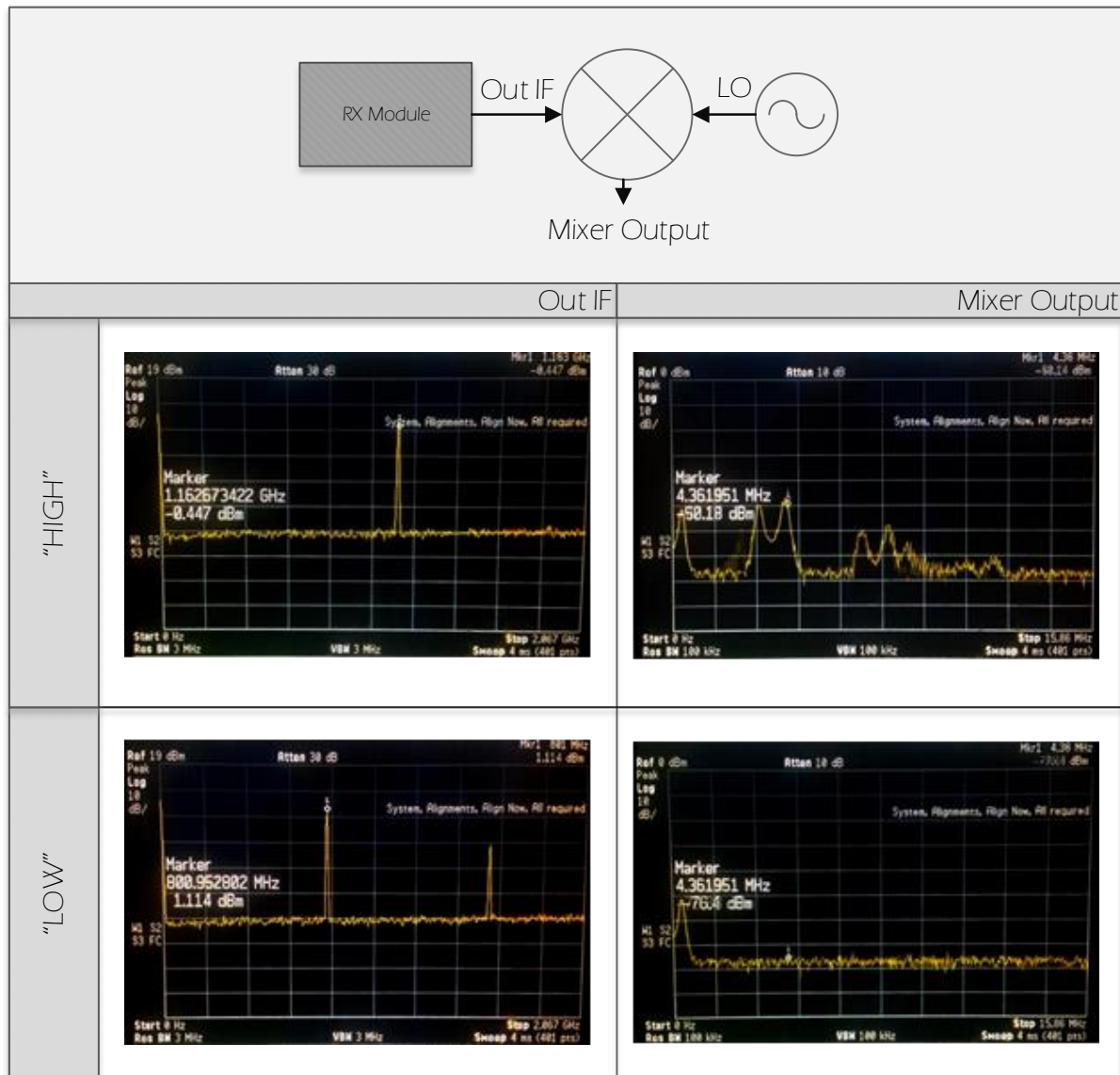


Figure 31 – Spectral Characterization of the Downconversion block.

In Figure 31 we can see the frequency spectrum of the input and output signals of the mixer. Data was collected from the spectrum analyser. We can conclude the “high” signal, which corresponds to a microcontroller output voltage of 5 V was successfully downconverted to 5 MHz, while the “low” signal has no spectral components other than DC. We can also conclude the mixing operation comes at a very high conversion loss (about 50 dB).

After amplification with coaxial amplifiers (ZX60-14012L-S+ and ZFL-1000LN+ from Mini Circuits), the next block of the system aims to output a DC voltage proportional to the amplitude of the previously mentioned downconverted signal. As so, we expect a constant voltage of 5 V (as to generate an interrupt in the microcontroller unit) if the signal is “high” and 0 V if it’s “low”.

**Figure 32** shows the output voltage waves of each circuit component. A wideband amplifier (ZX60-14012L by Mini Circuits) was introduced after the mixer to allow correct visualization of the wave in the oscilloscope (Rigol DS1102E).

The signal was successfully amplified in the first stage to an amplitude of 3,9 V (when signal is “high”), which is higher than twice the forward voltage drop of the diodes (a maximum of 1 V). This is required because of the configuration of the full-wave rectifier.

Additionally, it’s worthy of mentioning that working with high frequency waves using a breadboard and standard copper wires and components is by itself a challenge, because the length alone of the wires used was found to be influent.

We can also conclude that a DC voltage was successfully achieved, despite noticeable interference of higher frequencies. A simple amplifier with a non-inverter configuration was introduced so that this voltage would be 5 V. As for the “low” signal, we denote only residual amplitude, not sufficient for polarization of the diodes that constitute the rectifier. DC voltage is close to 0 V in the input of the control unit.

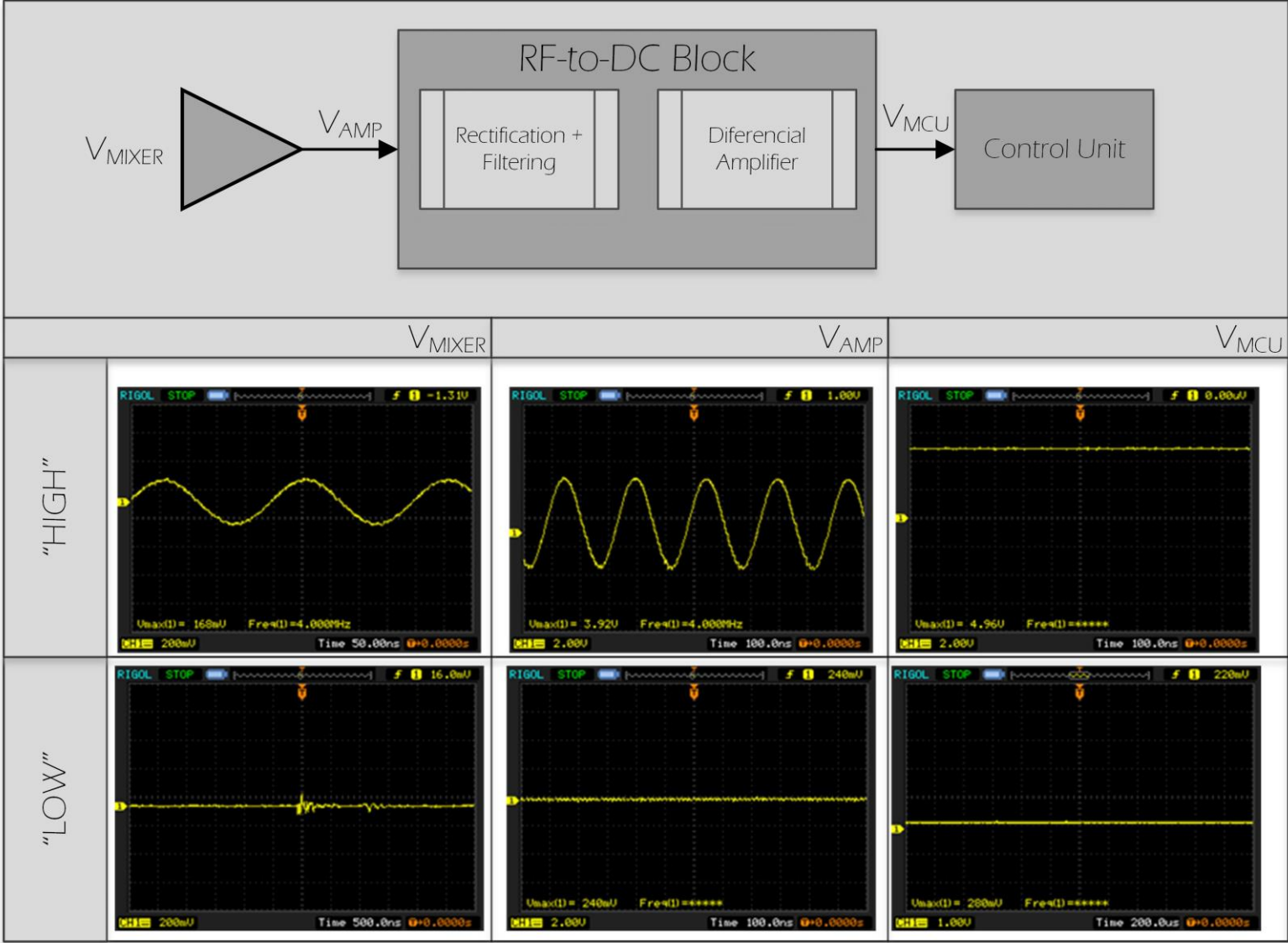
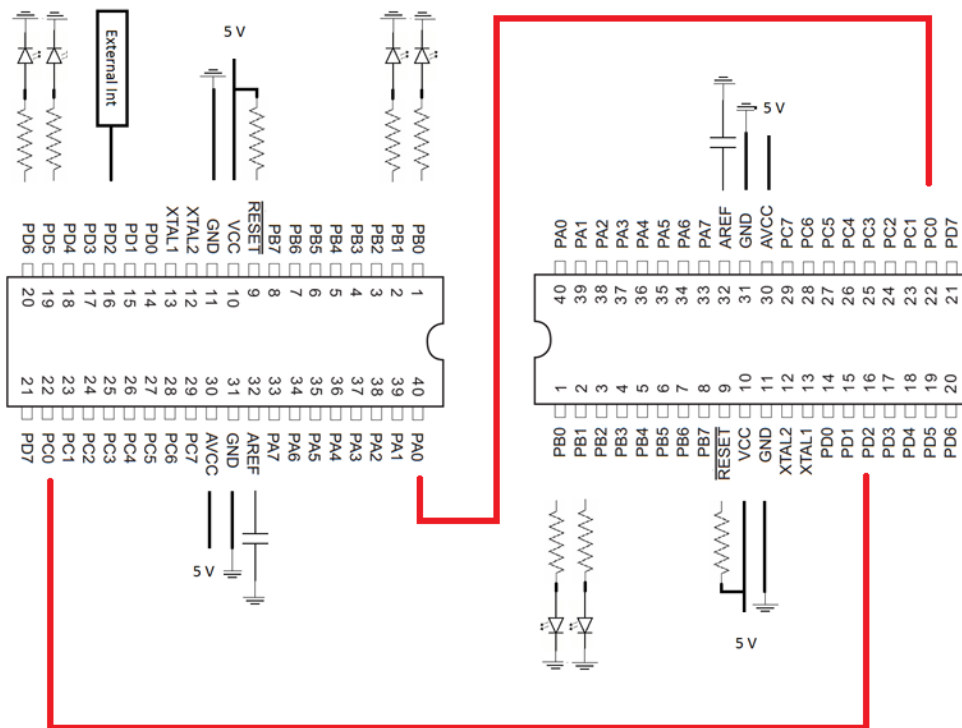


Figure 32 – Characterization of the Rectification block.

### 5.3 Microcontroller Communication

A test was made to verify if the control units of the tag and reader devices were communicating correctly with each other, that is, if the call from the reader could trigger the correct response from the tag.



**Figure 33** – Connection diagram to test the communication between control units.

The only purpose of this test was to verify if the interrupts of the microcontroller devices were working according to what was expected. As so, to perform this test, the microcontrollers were isolated and connected to each other, as illustrated by **Figure 33**, where we can see a connection diagram of the performed experiment.

As we can see from **Figure 34**, which shows the voltage outputs from both modules, the response from the tag is correctly triggered by a falling edge of the signal sent by the reader. This means the reader will be ready to read the sequence from the tag by the time it's sent.

In this example, we can see that the tag's signature sequence is "11010101".

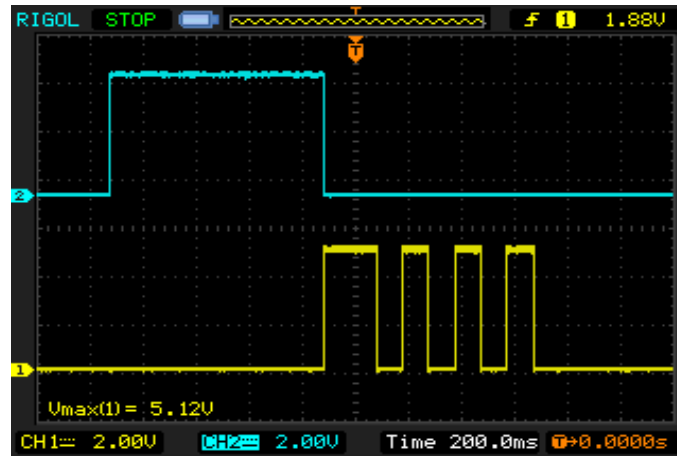


*Figure 34 – Communication between reader and tag. Channel 1: output from tag; Channel 2: output from reader.*

## 5.4 Case study

A feasibility assessment of the RFID system's ability to detect surgical sponges inside an operating room was made. This experimental procedure evaluated the usefulness and suitability of millimetre waves for RFID purposes, as well as the influence of the surgical sponge and its water content on the operation of the system.

Water was used in the experimental measurements as to simulate what the influence of blood and other bodily fluids would be. Studies have been made in the past comparing the dielectric behaviour of water and blood [112]. With the materials available in our facilities, tap water served as an acceptable substitute for blood.

To test how the tag's position inside a normal operating room can influence the ability to detect the tag attached to a sponge, representative measurements were made inside our laboratory facilities, where different objects and equipment that may interfere with the characteristics of the established link are randomly deployed. A schematic grid is shown in **Figure 35**, as to explain the eighteen total positions where the tag was placed (nine positions where the tag was placed near the ground – top picture, and another nine at the reader's height – bottom picture). The reader device was placed in position 7, at a height of 1 meter from the ground. **Figure 36** shows a picture of the laboratory facilities. Number five serves as a reference to **Figure 35**.

To establish a link in the 60 GHz ISM band, the V-band converter FC1005V00 by Sivers IMA was used. The transmitting device was placed in a fixed position, while the tag was placed in several positions around the room. To improve performance, a standard gain horn antenna (Q-par Angus Ltd, QMS-00475 [113]) was connected to the tag device. The antenna has a gain of 19 dB for the selected frequency.

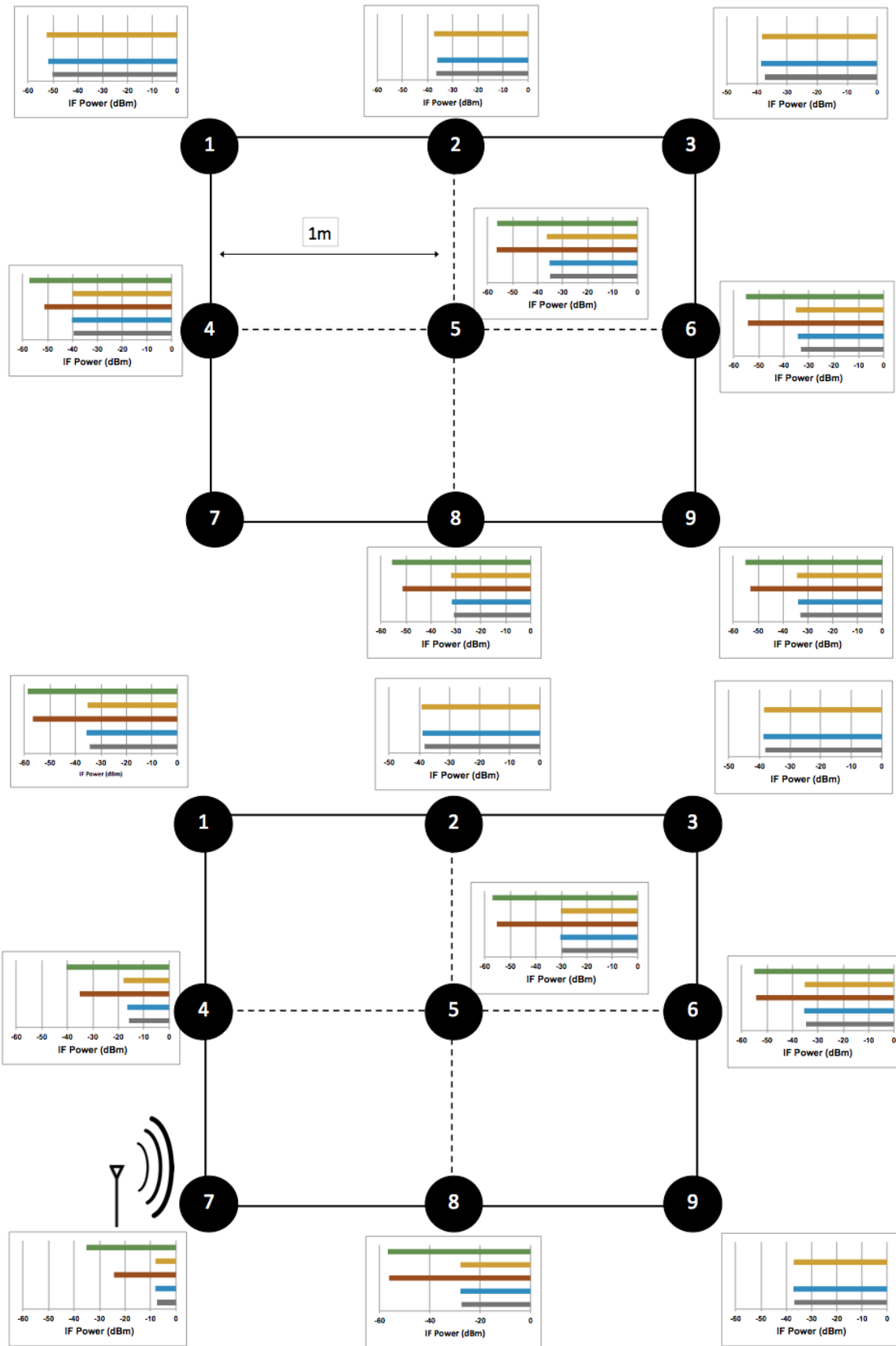


**Figure 35** – Illustration of the placement of the tags and reader. Nine positions were tested each one with two different heights, making a total of eighteen different spots. For each one, five power measurements were made. The bar charts indicate the obtained power values. The antenna was placed in position number 7, as indicated in the figure below, at a height of 1 meter from the ground





*Figure 36 – Laboratory facilities where the measurements were conducted.*

It's relevant to call to attention that the test equipment only allows for an indirect measurement of the received power, as an uplink to 58 GHz is made from an input intermediate frequency (IF) of 3 GHz at transmission, and subsequent downlink at reception. As so, the power measurements are relative to the output IF.

In addition, five different measurements were made at each position in an attempt to test the influence of two widely used materials for surgical gaze and sponges: cotton and PVA [114]:

- Direct link with no material in between reader and tag;
- Dry cotton placed in front of reader antenna;
- Cotton saturated with water in front of reader antenna;
- Dry sponge in front of reader antenna;
- Sponge saturated with water in front of reader antenna.

**Figure 37** shows the materials used in the experiment.

Also in **Figure 35**, a bar graph is shown for each position in which measurements were attempted. For a better understanding of the retrieved data, *Table 10* and *Table 11* show the power measurements for the two different heights.

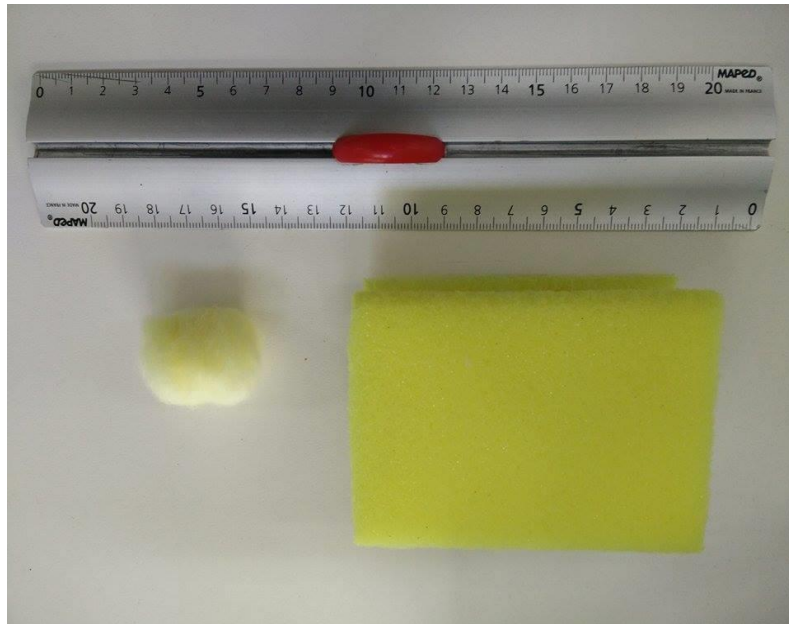


*Figure 37 – Materials used: (left) Cotton ball; (right) PVA sponge;*

As a visual aid, a colour scheme was employed to represent the five different test cases. These colours were applied to the table’s columns, as well as to the lines of the bar charts in **Figure 35**.

*Table 10 – IF output power measurements with tag placed in the ground.*

Positions	IF Output Power (dBm)				
	<i>Air</i>	<i>Dry Cotton</i>	<i>Saturated Cotton</i>	<i>Dry Sponge</i>	<i>Saturated Sponge</i>
<b>1</b>	-50,03	-51,93	UM	-52,53	NA
<b>2</b>	-36,62	-36,18	UM	-37,45	NA
<b>3</b>	-37,41	-38,6	UM	-38,32	NA
<b>4</b>	-39,48	-40,27	-51,32	-40,04	-57,36
<b>5</b>	-35,02	-35,26	-56,41	-36,35	-56,2
<b>6</b>	-33,28	-34,37	-54,35	-35,19	-55,12
<b>7</b>	UM	UM	UM	UM	UM
<b>8</b>	-30,73	-31,65	-51,4	-31,96	-55,6
<b>9</b>	-33,12	-33,91	-53,12	-34,35	-55,1

UM – Unable to measure.

*Table 11 – IF output power measurements with tag placed at reader's height.*

Positions	IF Output Power (dBm)				
	<i>Air</i>	<i>Dry Cotton</i>	<i>Saturated Cotton</i>	<i>Dry Sponge</i>	<i>Saturated Sponge</i>
1	-34,52	-35,64	-56,7	-35,2	-58,71
2	-38,27	-38,91	UM	-39,24	UM
3	-38,21	-38,73	UM	-38,55	UM
4	-15,81	-16,45	-35,12	-17,94	-40,25
5	-29,81	-30,4	-55,33	-30,18	-57,01
6	-34,52	-35,4	-54,32	-35,17	-55,07
7	-7,31	-8,1	-24,34	-8,04	-35,15
8	-27,31	-27,91	-56,3	-27,89	-56,79
9	-36,98	-37,14	UM	-37,02	UM

UM – Unable to measure. Means the received power was too low to measure.

From the collected data, it can be concluded that the received power decreases with the distance between the two devices, as was expectable. We can also state that the objects placed in between devices interfere with the received power, as the values are lower in all nine positions for the measurements with cotton or a sponge placed in between devices. When the materials are soaked with water, received power decreases significantly, in the order of 20 dB.

Another important note is that the received power is higher for the measurements made at the antenna's height, not only because the distance is shorter, but also because of the effect of the ground surface, that may reflect the signal.

From this feasibility study it was possible to conclude that the use of MMID technology presents a good prospective for application in real surgery environments, since the potential small size of the device won't offer any handling difficulties for medical staff. It was also shown that the 60 GHz band is suitable for short distance indoor communications.

# CHAPTER 6      CONCLUSIONS AND FUTURE WORK

Millimetre-wave wireless broadband systems are considered a disruptive technology trend by the investigation and corporate world. This vibrant environment has driven rapid development of standards for V-band wireless short-range communication systems. However, pricing has been the key obstacle in the path of making mm-wave devices commercially viable.

One of the main concerns of this dissertation was to investigate a possible application for 60 GHz ISM band technology, which consisted of a radiofrequency identification system. RFID systems are widely used in multiple industry sectors operating in frequencies up to 3GHz and, in this dissertation, we research the possibility of taking advantage of the benefits of higher frequencies in relation to these systems.

In addition, we exemplify how mm-wave RFID could stride to tackle a still relevant concern in hospitals worldwide: retained surgical instruments and sponges. This proves 60 GHz technology could be a factor not only when targeting broad consumer markets, but also when pursuing problems of the biomedical engineering community.

## 6.1 Conclusions

---

The mm-wave band technology holds great advantages for short-range, indoors applications such as an RFID system for object tracking in an operating room. The 60 GHz band is placed

on an oxygen absorption peak, which allows high frequency reuse and, in addition, these frequencies of operation allow manufacturing small, highly integrated devices.

The main concern of the implementation process was successfully establishing a link in the 60 GHz band in the laboratory facilities, which contains tables, chairs and several obstacles that grant it similar characteristics to an operating room.

Using a V-band converter available in the market, a link was established up to distances of 5 meters and for several azimuth angles. No particular attention was given to multipath or fading of the transmitted wave. It was undoubtedly concluded that the received power decreased as a consequence of the increasing distance separating both modules. Also, it was remarked that the received power was the highest when the devices were facing each other, in direct line-of-sight configuration.

A feasibility study was conducted to test the sponge's influence as long as it's water content in the wave propagation and overall communication. The reader device was placed in a fixed position while the tag was positioned in 18 different locations inside the laboratory facility. Two different materials were experimented, and the influence of water content was also tested.

It was concluded that the materials as well as the water content greatly affect the received power by the tag module. In spite of that, MMID showed great potential for short range communication in an indoors facility, as communication was successful in most of the positions.

A frequency multiplexing strategy was used to code a binary sequence onto the signal, by changing the tune voltage of the VCO, which was used as the source. For decoding, a rectification block was implemented using off-the-shelf and DIP components. The first staged consisted of a downconversion to 5 MHz using a frequency mixer. The downconversion was successful, despite substantial conversion loss.

A DC signal was achieved at the output of this block, using a high-speed amplifier and high-frequency diodes for rectification. However, it's relevant to point out that DIP components used in a simple breadboard are not recommended for working with radiofrequencies, as their behaviour is not as easily predicable as lower frequency waves.

The work presented inspires confidence that millimetre-wave technology could present itself as a reliable choice for short-range, indoors communication devices.

## 6.2 Future Work

First of all, as a way to improve the research about the sponge's influence of the RFID communication, new and more realistic variables could be introduced. Only water content was studied, however, blood, plasma and other tissues could present different characteristics and new challenges.

Secondly, and on a more relevant note, future work would definitely stride towards the integration of a complete miniaturized system. As was stated during the course of this dissertation, the main advantage of using mm-wave communication is the possibility of developing small-sized transceiver modules. As so, ideally, the final system would have dimensions that would allow it to be attached to surgical instruments and sponges without interfering with the performance of the medical staff.

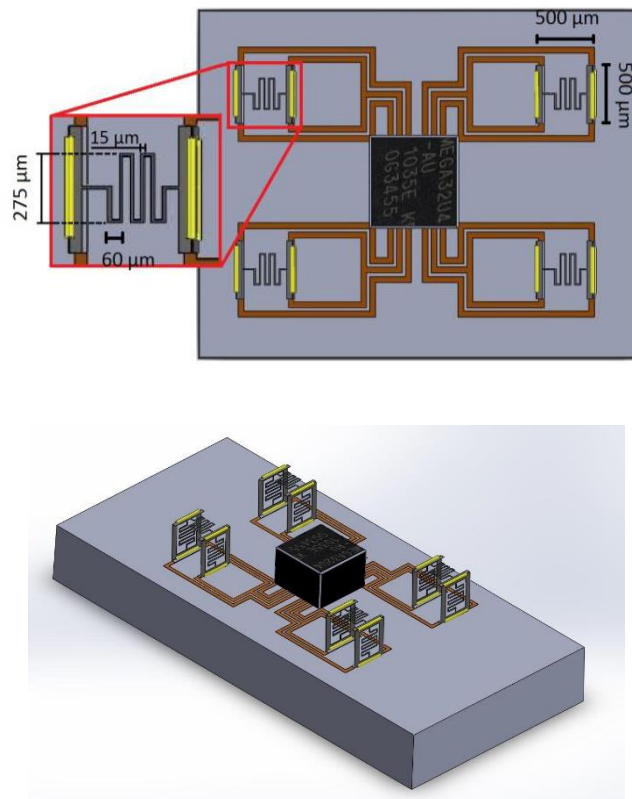


**Figure 38** – Proposed integration solution: **a)** Artistic view; **b)** Three-dimensional view

In 2012, Moroni et al. [115] from the University of Pavia in Italy successfully designed and implemented an array of distributed oscillators for millimetre-wave phased arrays, which combines LO generation and distribution. One possibility would be to integrate an on-chip

antenna on the chip designed by the Italian researchers, which is fabricated in 65nm CMOS. The chip has a small area of 6 mm<sup>2</sup>.

**Figure 38** illustrates the proposed antenna integration solution [116]. A four-antenna array is a possibility because the chip implemented in [115] has four oscillators and four RF inputs in the desired central frequency.

Integration in CMOS is undoubtedly the direction for MMID technology because it allows for high integration and small size at reasonable prices.

# REFERENCES

- [1] I. of Medicine, *To Err is Human: Building a Safer Health System*. Washington D. C.: National Academy Press, 1999.
- [2] A. A. Gawande, D. M. Studdert, E. J. Orav, T. A. Brennan, and M. J. Zinner, “Risk Factors for Retained instruments and Sponges After Surgery,” *N. Engl. J. Med.*, vol. 348, no. 3, pp. 229–235, 2003.
- [3] S. P. A. Stawicki, S. D. Moffatt-bruce, H. M. Ahmed, H. L. A. Iii, T. M. Baliya, I. Bernescu, L. Chan, L. Chowayou, J. Cipolla, S. M. Coyle, V. H. Gracias, O. L. Gunter, R. Marchigiani, N. D. Martin, J. Patel, M. J. Seamon, E. Vagedes, E. C. Ellison, S. M. Steinberg, and C. H. Cook, “Retained Surgical Items : A Problem Yet to Be Solved,” *J. Am. Coll. Surg.*, vol. 216, no. 1, pp. 15–22, 2013.
- [4] M. a. Mahran, E. Toeima, and E. P. Morris, “The recurring problem of retained swabs and instruments,” *Best Pract. Res. Clin. Obstet. Gynaecol.*, vol. 27, no. 4, pp. 489–495, 2013.
- [5] Z. H. Al-qurayshi, A. T. Hauch, D. P. Slakey, and E. Kandil, “Retained Foreign Bodies: Risk and Outcomes at the National Level,” *J. Am. Coll. Surg.*, vol. 220, no. 4, pp. 749–759, 2015.
- [6] T. F. Dagi, R. Berguer, S. Moore, and H. D. Reines, “Preventable Errors in the Operating Room-Part 2: Retained Foreign Objects, Sharps Injuries, and Wrong Site Surgery,” *Curr. Probl. Surg.*, vol. 44, no. 6, pp. 352–381, 2007.
- [7] V. C. Gibbs, F. D. Coakley, and H. D. Reines, “Preventable Errors in the Operating Room: Retained Foreign Bodies after Surgery-Part I,” *Curr. Probl. Surg.*, vol. 44, no. 5, pp. 281–337, 2007.
- [8] S. Jackson and S. Brady, “Counting difficulties: retained instruments, sponges, and needles,” *AORN journal*, vol. 87, no. 2. pp. 315–321, 2008.
- [9] R. R. Cima, A. Kollengode, J. Garnatz, A. Storsveen, C. Weisbrod, and C. Deschamps, “Incidence and Characteristics of Potential and Actual Retained Foreign Object Events in Surgical Patients,” *J. Am. Coll. Surg.*, vol. 207, no. 1, pp. 80–87, 2008.
- [10] A. Rowlands and R. Steeves, “Incorrect surgical counts: A qualitative analysis,” *AORN J.*, vol. 92, no. 4, pp. 410–419, 2010.
- [11] K. Sakhel and J. Hines, “To forget is human: The case of the retained bulb,” *J. Robot. Surg.*, vol. 3, no. 1, pp. 45–47, 2009.
- [12] C. W. Kaiser, S. Friedman, K. P. Spurling, T. Slowick, and H. a Kaiser, “The Retained Surgical Sponge,” *Ann. Surg.*, vol. 224, no. 1, pp. 79–84, 1996.



## References

---

- [13] F. Kiernan, M. Joyce, C. K. Byrnes, H. O'Grady, F. B. V Keane, and P. Neary, "Gossypiboma: A case report and review of the literature," *Ir. J. Med. Sci.*, vol. 177, no. 4, pp. 389–391, 2008.
- [14] T. H. Gallagher and W. Levinson, "Disclosing Harmful Medical Errors to Patients: a Time for Professional Action," *Arch. Intern. Med.*, vol. 165, no. 16, pp. 1819–1824, 2005.
- [15] T. L. Williams, D. K. Tung, V. M. Steelman, P. K. Chang, and M. K. Szekendi, "Retained Surgical Sponges: Findings from Incident Reports and a Cost-Benefit Analysis of Radiofrequency Technology," *J. Am. Coll. Surg.*, vol. 219, no. 3, pp. 354–364, 2014.
- [16] D. L. Feldman, "Prevention of retained surgical items," *Mt. Sinai J. Med.*, vol. 78, no. 6, pp. 865–871, 2011.
- [17] N. N. Egorova, A. Moskowitz, A. Gelijns, A. Weinberg, J. Curty, B. Rabin-Fastman, H. Kaplan, M. Cooper, D. Fowler, J. C. Emond, and G. Greco, "Managing the prevention of retained surgical instruments: what is the value of counting?," *Ann. Surg.*, vol. 247, no. 1, pp. 13–18, 2008.
- [18] C. E. Fabian, "Electronic tagging of surgical sponges to prevent their accidental retention," *Surgery*, vol. 137, no. 3, pp. 298–301, 2005.
- [19] "SurgiCount Medical | The Safety Sponge® System." [Online]. Available: <http://www.surgicountmedical.com/>. [Accessed: 07-Jun-2015].
- [20] C. C. Greenberg, R. Diaz-Flores, S. R. Lipsitz, S. E. Regenbogen, L. Mulholland, F. Mearn, S. Rao, T. Toidze, and A. a Gawande, "Bar-coding surgical sponges to improve safety: a randomized controlled trial," *Ann. Surg.*, vol. 247, no. 4, pp. 612–616, 2008.
- [21] "RF Surgical Systems Inc | Retained surgical sponge prevention | OR patient safety | RFSurg.com." [Online]. Available: <http://www.rfsurg.com/>. [Accessed: 07-Jun-2015].
- [22] V. M. Steelman, "Sensitivity of detection of radiofrequency surgical sponges: A prospective, cross-over study," *Am. J. Surg.*, vol. 201, no. 2, pp. 233–237, 2011.
- [23] C. C. Rupp, M. J. Kagarise, S. M. Nelson, A. M. Deal, S. Phillips, J. Chadwick, T. Petty, A. a Meyer, and H. J. Kim, "Effectiveness of a radiofrequency detection system as an adjunct to manual counting protocols for tracking surgical sponges: A prospective trial of 2,285 patients," *J. Am. Coll. Surg.*, vol. 215, no. 4, pp. 524–533, 2012.
- [24] S. Parlak, A. Sarcevic, I. Marsic, and R. S. Burd, "Introducing RFID technology in dynamic and time-critical medical settings: Requirements and challenges," *J. Biomed. Inform.*, vol. 45, no. 5, pp. 958–974, 2012.
- [25] "ClearCount Medical Solutions." [Online]. Available: <http://clearcount.com/>. [Accessed: 07-Jun-2015].

- 
- [26] V. C. Gibbs, "Retained surgical items and minimally invasive surgery," in *World Journal of Surgery*, 2011, vol. 35, no. 7, pp. 1532–1539.
- [27] A. Macario, D. Morris, and S. Morris, "Initial clinical evaluation of a handheld device for detecting retained surgical gauze sponges using radiofrequency identification technology," *Arch. Surg.*, vol. 141, no. 7, pp. 659–662, 2006.
- [28] V. Vidojkovic, G. Mangraviti, K. Khalaf, V. Szortyka, K. Vaesen, W. Van Thillo, B. Parvais, M. Libois, S. Thijs, J. R. Long, C. Soens, and P. Wambacq, "A low-power 57-to-66GHz transceiver in 40nm LP CMOS with -17dB EVM at 7Gb/s," *Dig. Tech. Pap. - IEEE Int. Solid-State Circuits Conf.*, vol. 55, no. 12, pp. 268–269, 2012.
- [29] K. Okada, R. Minami, Y. Tsukui, S. Kawai, Y. Seo, S. Sato, S. Kondo, T. Ueno, Y. Takeuchi, T. Yamaguchi, A. Musa, R. Wu, M. Miyahara, and A. Matsuzawa, "20.3 A 64-QAM 60GHz CMOS transceiver with 4-channel bonding," in *Digest of Technical Papers - IEEE International Solid-State Circuits Conference*, 2014, vol. 57, pp. 346–347.
- [30] K. Khalaf, V. Vidojkovic, K. Vaesen, J. R. Long, W. Van Thillo, and P. Wambacq, "A Digitally Modulated 60GHz Polar Transmitter in 40nm CMOS," *2014 IEEE Radio Freq. Integr. Circuits Symp.*, pp. 159 – 162, 2014.
- [31] H. H. Meinel, "Millimeter wave applications and technology trends," *Ann. Des Télécommunications*, vol. 47, no. 11–12, pp. 456–468, 1992.
- [32] T. S. Rappaport, J. N. Murdock, and F. Gutierrez, "State of the art in 60-GHz integrated circuits and systems for wireless communications," in *Proceedings of the IEEE*, 2011, vol. 99, no. 8, pp. 1390–1436.
- [33] A. Georgiadis, H. Rogier, L. Roselli, and P. Arcioni, *Microwave and Millimeter Wave Circuits and Systems: Emerging Design, Technologies and Applications*. Wiley, 2012.
- [34] S. Rangan, T. S. Rappaport, and E. Erkip, "Millimeter-wave cellular wireless networks: Potentials and challenges," *Proc. IEEE*, vol. 102, no. 3, pp. 366–385, 2014.
- [35] F. Boccardi, R. Heath, A. Lozano, T. L. Marzetta, and P. Popovski, "Five disruptive technology directions for 5G," *IEEE Commun. Mag.*, vol. 52, no. 2, pp. 74–80, 2014.
- [36] D. Wu, J. Wang, Y. Cai, and M. Guizani, "Millimeter-wave multimedia communications: challenges, methodology, and applications," *IEEE Commun. Mag.*, vol. 53, no. 1, pp. 232–238, 2015.
- [37] T. S. Rappaport, R. Mayzus, Y. Azar, K. Wang, G. N. Wong, J. K. Schulz, M. Samimi, and F. Gutierrez, "Millimeter Wave Mobile Communications for 5G Cellular: It Will Work!," *IEEE Access*, vol. 1, pp. 335–349, 2013.
- [38] J. Wells, "Faster than fiber: The future of multi-G/s wireless," *IEEE Microw. Mag.*, vol. 10, no. 3, pp. 104–112, 2009.
-

## References

---

- [39] T. Ninomiya, "60-GHz transceiver for high-speed wireless LAN system.," *1996 IEEE MTT-S Internat. Microw. Symp. Dig. 1996 IEEE MTT-S Internat. Microw. Symp. Dig.*, vol. 2, pp. 1171–1174, 1997.
- [40] K. Ohata, K. Maruhashi, M. Ito, S. Kishimoto, K. Ikuina, T. Hashiguchi, N. Takahashi, and S. Iwanaga, "Wireless 1.25 Gb/s transceiver module at 60 GHz-band," *2002 IEEE Int. Solid-State Circuits Conf. Dig. Tech. Pap. (Cat. No.02CH37315)*, vol. 1, no. May 2001, pp. 1597–1599, 2002.
- [41] C. H. Doan, S. Emami, A. M. Niknejad, and R. W. Brodersen, "Design of CMOS for 60GHz applications," *2004 IEEE Int. Solid-State Circuits Conf. (IEEE Cat. No.04CH37519)*, vol. 35, pp. 238–239, 2004.
- [42] C. H. Doan, S. Emami, A. M. Niknejad, and R. W. Brodersen, "Millimeter-wave CMOS design," in *IEEE Journal of Solid-State Circuits*, 2005, vol. 40, no. 1, pp. 144–154.
- [43] S. E. Gunnarsson, C. Kärnfelt, H. Zirath, R. Kozhuharov, D. Kuylenstierna, A. Alping, and C. Fager, "Highly integrated 60 GHz transmitter and receiver MMICs in a GaAs pHEMT technology," *IEEE J. Solid-State Circuits*, vol. 40, no. 11, pp. 2174–2185, 2005.
- [44] B. Razavi, "A 60-GHz CMOS receiver front-end," *IEEE J. Solid-State Circuits*, vol. 41, no. 1, pp. 17–22, 2006.
- [45] D. Alldred, B. Cousins, and S. P. Voinigescu, "A 1.2V, 60-GHz radio receiver with on-chip transformers and inductors in 90-nm CMOS," in *Technical Digest - IEEE Compound Semiconductor Integrated Circuit Symposium, CSIC*, 2006, pp. 51–54.
- [46] S. K. Reynolds, B. a. Floyd, U. R. Pfeiffer, T. Beukema, J. Grzyb, C. Haymes, B. Gaucher, and M. Soyuer, "A silicon 60-GHz receiver and transmitter chipset for broadband communications," in *IEEE Journal of Solid-State Circuits*, 2006, vol. 41, no. 12, pp. 2820–2829.
- [47] S. E. Gunnarsson, C. Kärnfelt, H. Zirath, R. Kozhuharov, D. Kuylenstierna, C. Fager, M. Ferndahl, B. Hansson, A. Alping, and P. Hallbjörner, "60 GHz single-chip front-end MMICs and systems for multi-Gb/s wireless communication," in *IEEE Journal of Solid-State Circuits*, 2007, vol. 42, no. 5, pp. 1143–1156.
- [48] T. Mitomo, R. Fujimoto, N. Ono, R. Tachibana, H. Hoshino, Y. Yoshihara, Y. Tsutsumi, and I. Seto, "A 60-GHz CMOS receiver with frequency synthesizer," in *IEEE Symposium on VLSI Circuits, Digest of Technical Papers*, 2007, pp. 172–173.
- [49] J. M. Gilbert, C. H. Doan, S. Emami, and C. B. Shung, "A 4-Gbps uncompressed wireless HD A/V transceiver chipset," in *IEEE Micro*, 2008, vol. 28, no. 2, pp. 56–64.
- [50] D. Dawn, P. Sen, S. Sarkar, B. Perumana, S. Pinel, and J. Laskar, "60-GHz integrated transmitter development in 90-nm CMOS," *IEEE Trans. Microw. Theory Tech.*, vol. 57, no. 10, pp. 2354–2367, 2009.

- 
- [51] A. Parsa and B. Razavi, "A new transceiver architecture for the 60-GHz band," *IEEE J. Solid-State Circuits*, vol. 44, no. 3, pp. 751–762, 2009.
- [52] A. Tomkins, R. A. Aroca, T. Yamamoto, S. T. Nicolson, Y. Doi, and S. P. Voinigescu, "A zero-IF 60 GHz 65 nm CMOS transceiver with direct BPSK modulation demonstrating up to 6 Gb/s data rates over a 2 m wireless link," *IEEE J. Solid-State Circuits*, vol. 44, no. 8, pp. 2085–2099, 2009.
- [53] A. Valdes-Garcia, S. T. Nicolson, J. W. Lai, A. Natarajan, P. Y. Chen, S. K. Reynolds, J. H. C. Zhan, D. G. Kam, D. Liu, and B. Floyd, "A fully integrated 16-element phased-array transmitter in SiGe BiCMOS for 60-GHz communications," *IEEE J. Solid-State Circuits*, vol. 45, no. 12, pp. 2757–2773, 2010.
- [54] A. Natarajan, S. K. Reynolds, M. Da Tsai, S. T. Nicolson, J. H. C. Zhan, D. G. Kam, D. Liu, Y. L. O. Huang, A. Valdes-Garcia, and B. A. Floyd, "A fully-integrated 16-element phased-array receiver in SiGe BiCMOS for 60-GHz communications," in *IEEE Journal of Solid-State Circuits*, 2011, vol. 46, no. 5, pp. 1059–1075.
- [55] A. Balankutty, S. Pellerano, T. Kamgaing, K. Tantwai, and Y. Palaskas, "A 12-element 60GHz CMOS phased array transmitter on LTCC package with integrated antennas," *2011 Proc. Tech. Pap. IEEE Asian Solid-State Circuits Conf. 2011, A-SSCC 2011*, vol. 2, pp. 273–276, 2011.
- [56] A. Siligaris, O. Richard, B. Martineau, C. Mounet, F. Chaix, R. Ferragut, C. Dehos, J. Lanteri, L. Dussopt, S. D. Yamamoto, R. Pilard, P. Busson, A. Cathelin, D. Belot, and P. Vincent, "A 65-nm CMOS fully integrated transceiver module for 60-GHz wireless HD applications," in *IEEE Journal of Solid-State Circuits*, 2011, vol. 46, no. 12, pp. 3005–3017.
- [57] S. Emami, R. F. Wiser, E. Ali, M. G. Forbes, M. Q. Gordon, X. Guan, S. Lo, P. T. McElwee, J. Parker, J. R. Tani, J. M. Gilbert, and C. H. Doan, "A 60GHz CMOS phased-array transceiver pair for multi-Gb/s wireless communications," *Dig. Tech. Pap. - IEEE Int. Solid-State Circuits Conf.*, vol. 40, pp. 164–165, 2011.
- [58] Z. Pi and F. Khan, "An introduction to millimeter-wave mobile broadband systems," *IEEE Commun. Mag.*, vol. 49, no. 6, pp. 101–107, 2011.
- [59] F. Giannetti, M. Luise, and R. Reggiannini, "Mobile and Personal Communications in the 60 GHz Band : A Survey \*," *Wirel. Pers. Commun.*, vol. 10, pp. 207–243, 1999.
- [60] H. T. Friis, "A Note on a Simple Transmission Formula," *Proc. IRE*, vol. 34, no. 5, pp. 254–256, 1946.
- [61] A. Maltsev, R. Maslennikov, A. Sevastyanov, A. Lomayev, A. Khoryaev, A. Davydov, and V. Ssorin, "Characteristics of indoor millimeter-wave channel at 60 GHz in application to perspective WLAN system," *Antennas Propag. (EuCAP), 2010 Proc. Fourth Eur. Conf.*, 2010.
- [62] W. C. Y. Lee, *Mobile Communications Design Fundamentals*, Second. Wiley, 1993.
-

## References

---

- [63] W. Schäfer, "Channel modelling of short-range radio links at 60 GHz for mobile intervehicle communication," in *[1991 Proceedings] 41st IEEE Vehicular Technology Conference*, 1991, pp. 314–319.
- [64] T. S. Rappaport, *Wireless communications: principles and practice*, Second. Prentice Hall, 1996.
- [65] R. H. Clarke, "A Statistical Theory of Mobile-Radio Reception," *Bell Syst. Tech. J.*, vol. 47, no. 6, pp. 957–1000, Jul. 1968.
- [66] H. Hashemi, "The indoor radio propagation channel," *Proc. IEEE*, vol. 81, no. 7, 1993.
- [67] H. Y. H. Yang, P. F. M. Smulders, and M. H. A. J. Herben, "Indoor Channel Measurements and Analysis in the Frequency Bands 2 GHz and 60 GHz," *2005 IEEE 16th Int. Symp. Pers. Indoor Mob. Radio Commun.*, vol. 1, pp. 579–583, 2005.
- [68] T. Hao Ngoc, J. Takagi, H. Oguma, S. Kameda, H. Nakase, T. Takagi, and K. Tsubouchi, "Indoor multipath propagation characteristic at 60GHz," in *IEEE Region 10 Annual International Conference, Proceedings/TENCON*, 2007, vol. 00, pp. 0–3.
- [69] C. R. Anderson and T. S. Rappaport, "In-building wideband partition loss measurements at 2.5 and 60 GHz," *IEEE Trans. Wirel. Commun.*, vol. 3, no. 3, pp. 922–928, 2004.
- [70] K. Funkenzeller, *RFID Handbook*, Third. Wiley, 2010.
- [71] V. D. Hunt, A. Puglia, and M. Puglia, *RFID: A Guide to Radio Frequency Identification*. Wiley, 2006.
- [72] C. A. Balanis, *Antenna Theory: Analysis and Design*, 3rd ed. Wiley, 2005.
- [73] P. Pursula, V. Viikari, and T. Vähä-Heikkilä, "Theory and applications of millimeter wave identification," in *Proceedings of the International Semiconductor Conference, CAS*, 2010, vol. 1, no. 1, pp. 53–56.
- [74] Y. Yu, P. G. M. Baltus, and A. H. M. van Roermund, *Integrated 60 GHz RF Beamforming in CMOS*. 2011.
- [75] P. Pursula, T. Vähä-Heikkilä, A. Müller, D. Neculoiu, G. Konstantinidis, A. Oja, and J. Tuovinen, "Millimeter-wave identification - A new short-range radio system for low-power high data-rate applications," *IEEE Trans. Microw. Theory Tech.*, vol. 56, no. 10, pp. 2221–2228, 2008.
- [76] J. P. Curty, N. Joehl, C. Dehollain, and M. J. Declercq, "Remotely powered addressable UHF RFID integrated system," *IEEE J. Solid-State Circuits*, vol. 40, no. 11, pp. 2193–2202, 2005.
- [77] Y. Yao, J. Wu, Y. Shi, and F. F. Dai, "A fully integrated 900-MHz passive RFID transponder front end with novel zero-threshold RF-DC rectifier," *IEEE Trans. Ind. Electron.*, vol. 56, no. 7, pp. 2317–2325, 2009.

- 
- [78] R. Glidden, C. Bockorick, S. Cooper, C. Diorio, D. Dressler, D. Hara, T. Hass, T. Humes, J. Hyde, R. Oliver, O. Onen, A. Pesavento, K. Sundstrom, and M. Thomas, "Design of ultra-low cost UHF RFID tags for supply chain applications," *IEEE Commun. Mag.*, vol. 42, no. 8, pp. 140–151, 2004.
- [79] R. Barnett, G. Balachandran, S. Lazar, B. Kramer, G. Konnail, S. Rajasekhar, and V. Drobny, "A passive UHF RFID transponder for EPC gen 2 with -14dBm sensitivity in 0.13 $\mu$ m CMOS," in *Digest of Technical Papers - IEEE International Solid-State Circuits Conference*, 2007, pp. 582–584.
- [80] U. Karthaus and M. Fischer, "Fully Integrated Passive UHF RFID Transponder IC with 16.7- $\mu$ W Minimum RF Input Power," *IEEE J. Solid-State Circuits*, vol. 38, no. 10, pp. 1602–1608, 2003.
- [81] S. Pellerano, J. Alvarado, and Y. Palaskas, "A mm-wave power-harvesting RFID tag in 90 nm CMOS," *IEEE J. Solid-State Circuits*, vol. 45, no. 8, pp. 1627–1637, 2010.
- [82] P. Pursula, T. Karttaavi, M. Kantanen, A. Lamminen, J. Holmberg, M. Lahdes, I. Marttila, M. Lahti, A. Luukanen, and T. Vähä-Heikkilä, "60-GHz millimeter-wave identification reader on 90-nm CMOS and LTCC," *IEEE Trans. Microw. Theory Tech.*, vol. 59, pp. 1166–1173, 2011.
- [83] P. Pursula, F. Donzelli, and H. Seppä, "Passive RFID at Millimeter Waves," *IEEE Trans. Microw. Theory Tech.*, vol. 59, no. 8, pp. 2151–2157, 2011.
- [84] P. Pursula and F. Donzelli, "Transponders for millimeter wave identification," in *Proceedings - 2011 IEEE-APS Topical Conference on Antennas and Propagation in Wireless Communications, APWC'11*, 2011.
- [85] T. Kiuru, P. Pursula, J. Rajamäki, and T. Vähä-Heikkilä, "A 60-GHz semipassive MMID transponder for backscattering communications," in *IEEE MTT-S International Microwave Symposium Digest*, 2013, pp. 9–11.
- [86] P. Burasa, N. G. Constantin, and K. Wu, "High-Efficiency Wideband Rectifier for Single-Chip Batteryless Active Millimeter-Wave Identification (MMID) Tag in 65-nm Bulk CMOS Technology," *IEEE Transactions on Microwave Theory and Techniques*, vol. 62, no. 4, pp. 1005–1011, 2014.
- [87] D. Raghu and P. Harrop, "RFID Forecasts, Players and Opportunities 2014-2024," 2013.
- [88] L. Jerry and C. Barbara, "Shrouds of Time: The History of RFID," *AIM Publ.*, p. 11, 2001.
- [89] D. Dobkin, *The RF in RFID: Passive UHF RFID in Practice*. Newnes, 2008.
- [90] J.-P. Curty, M. Declercq, C. Dehollain, and N. Joehl, *Design and Optimization of Passive UHF RFID Systems*. Springer, 2007.
-

## References

---

- [91] A. Fonte, S. Saponara, G. Pinto, and B. Neri, "Feasibility study and on-chip antenna for fully integrated  $\mu$ RFID tag at 60 GHz in 65 nm CMOS SOI," *2011 IEEE Int. Conf. RFID-Technologies Appl.*, pp. 449–454, 2011.
- [92] H. Vogt, "Efficient Object Identification with Passive RFID Tags," *Int. Conf. Pervasive Comput.*, vol. 2414, pp. 98–113, 2002.
- [93] H. Vogt, "Multiple object identification with passive RFID tags," *IEEE Int. Conf. Syst. Man Cybern.*, vol. 3, 2002.
- [94] R. Rom and M. Sidi, *Multiple Access Protocols: Performance and Analysis*. New York: Springer-Verlag, 1990.
- [95] J. Proakis and M. Salehi, *Digital Communications*, Fifth. McGraw-Hill, 2007.
- [96] N. Abramson, "The ALOHA System -- Another Alternative for Computer Communication," *Proc. AFIPS Fall Jt. Comput. Conf.*, vol. 37, pp. 281–285, 1970.
- [97] L. G. Roberts, "ALOHA packet system with and without slots and capture," *ACM SIGCOMM Comput. Commun. Rev.*, vol. 5, no. 2, pp. 28–42, 1975.
- [98] R. T. B. Ma, M. Vishal, and D. Rubenstein, "An analysis of generalized slotted-aloha protocols," *IEEE/ACM Trans. Netw.*, vol. 17, no. 3, pp. 936–949, 2009.
- [99] a. Carleial and M. Hellman, "Bistable Behavior of ALOHA-Type Systems," *IEEE Trans. Commun.*, vol. 23, no. 4, pp. 401–410, 1975.
- [100] L. Kleinrock and F. Tobagi, "Packet Switching in Radio Channels: Part I--Carrier Sense Multiple-Access Modes and Their Throughput-Delay Characteristics," *IEEE Trans. Commun.*, vol. 23, no. 12, 1975.
- [101] J. Capetanakis, "Tree algorithms for packet broadcast channels," *IEEE Trans. Inf. Theory*, vol. 25, no. 5, 1979.
- [102] J. Hayes, "An Adaptive Technique for Local Distribution," *IEEE Trans. Commun.*, vol. 26, no. 8, pp. 1178–1186, 1978.
- [103] D. R. Hush and C. Wood, "Analysis of tree algorithms for RFID arbitration," in *IEEE International Symposium on Information Theory - Proceedings*, 1998, p. 107.
- [104] G. Fayolle, P. Flajolet, M. Hofri, and P. Jacquet, "Analysis of a stack algorithm for random multiple-access communication," *IEEE Trans. Inf. Theory*, vol. 31, no. 2, pp. 244–254, 1985.
- [105] P. Mathys and P. Flajolet, "Q-ary collision resolution algorithms in random-access systems with free or blocked channel access," *IEEE Trans. Inf. Theory*, vol. 31, no. 2, pp. 217–243, 1985.

- 
- [106] “Flann Microwave - Waveguide and Flange Data.” [Online]. Available: [http://www.flann.com/Products\\_Home/Components/FmiCat07108119.pdf](http://www.flann.com/Products_Home/Components/FmiCat07108119.pdf). [Accessed: 24-Jul-2015].
- [107] “Mini Circuits - Global Leader of RF and Microwave Components.” [Online]. Available: <http://194.75.38.69/homepage/homepage.html>. [Accessed: 19-Jun-2015].
- [108] “Converters and customized transceivers – Sivers IMA.” [Online]. Available: <http://siversima.com/products/converters-customized-transceivers/>. [Accessed: 18-Jun-2015].
- [109] “Operational Amplifiers (Op Amps) - Linear Technology.” [Online]. Available: [http://www.linear.com/products/operational\\_amplifiers\\_\(op\\_amps\)](http://www.linear.com/products/operational_amplifiers_(op_amps)). [Accessed: 20-Jun-2015].
- [110] “SOLID STATE INC.” [Online]. Available: [http://www.solidstateinc.com/solid-state-inc/cat\\_111.html](http://www.solidstateinc.com/solid-state-inc/cat_111.html). [Accessed: 26-Jun-2015].
- [111] “ATmega324P.” [Online]. Available: <http://www.atmel.com/devices/ATMEGA324P.aspx>. [Accessed: 20-Jun-2015].
- [112] H. F. Cook, “A comparison of the dielectric behaviour of pure water and human blood at microwave frequencies,” *Br. J. Appl. Phys.*, vol. 3, no. 8, pp. 249–255, Aug. 1952.
- [113] “Horn Antennas | Steatite QPar Antennas.” [Online]. Available: <http://www.steatiteqpar-antennas.co.uk/products/horn-antennas.html>. [Accessed: 25-Jun-2015].
- [114] “Innovative Surgical Supplies | Products | American Surgical Company.” [Online]. Available: <http://www.americansurgical.com/products/>. [Accessed: 25-Jun-2015].
- [115] A. Moroni, R. Genesi, and D. Manstretta, “A distributed ‘hybrid’ wave oscillator array for millimeter-wave phased-arrays,” in *Proceedings of the Custom Integrated Circuits Conference*, 2012, no. 1, pp. 1–4.
- [116] M. Zamith, J. Magalhães, P. Anacleto, and P. M. Mendes, “60 GHz On-Chip Antenna Array with Efficiency Improvement Using 3D Microfabrication Technology,” in *9th European Conference on Antennas and Propagation (EuCAP2015)*, 2015.





# APPENDICES

## Appendix A: Assembling the RFID system

---

During the course of this section, it will be explained how to assemble the complete system, from the electrical connections to the software configurations.

### Digital Lab Connections

---

Two separate digital labs are necessary:

- V+ output should be fixed at 12 V;
- V- output should be fixed at -12 V;
- 5 V output will also be necessary.

### V-band Converter boards

---

The control units should be powered with a supply of 18 V using an AC adapter. Connection between control units and the main boards is made through I2C serial connection as seen in **Figure 39**.

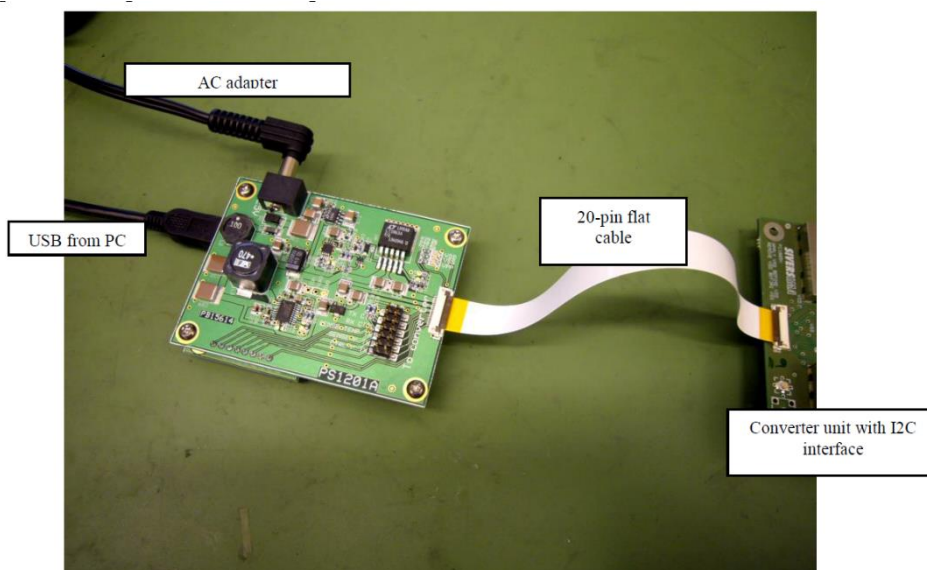


*Figure 39 – Connections of the control unit.*

Configuration of the boards is made through a serial connection between the control units and the computer, with USB interface.

Only the Windows operating system is acceptable for this configuration. Drivers should be installed when connecting the device to the computer for the first time. Necessary files are provided by Sivers IMA. Communication can be made through an open-source terminal program such as *PuTTY*.

The following steps should be followed for configuration.

- After connection with the PC, consult the Device Manager in the Control Panel to check the com-port number. The device will appear under Ports as “Sivers IMA ConverterControl”;
- In *PuTTY*, under Connection -> Serial Category, the com-port setting should be defined as described in **Table 12**. Configurations have to match in the “Session” tab;

*Table 12 – Com-port settings for converter configuration.*

<i>Bits per second</i>	<i>921600</i>
<i>Data Bits</i>	8
<i>Parity</i>	None
<i>Stop Bits</i>	1
<i>Flow Control</i>	None

- In the Terminal settings, under “Line discipline” options, Local Echo and Local line ending should be configured as “Force on”;
- After the terminal window opens, the device is ready for the configuration commands. Necessary commands include turning RX/TX synthesizer and converter modules ON and defining the synthesizer frequency, such as exemplified in **Table 13**.

*Table 13 – Configuration example for the converter boards.*

<b>RX modules</b>	<b>TX modules</b>
CONV:RXON ON	CONV:RXON ON
SYNT:RXON ON	SYNT:RXON ON
SYNT:RXFR 03 8A 40	SYNT:RXFR 03 8A 40

The last command allows for the frequency of the link to be defined. The setting is defined by number of frequency steps,  $N$ . Output frequency  $f$  relates to  $N$  as stated in Equation (8):

$$f = N \times f_{step} \quad (8)$$

where the frequency step  $f_{step}$  is a hardware parameter. For the FC1005V00 and model,  $f_{step} = 0.25$  MHz. An LO frequency of e.g. 58000 MHz thus corresponds to  $N = 58000 \text{ MHz} / 0.25 \text{ MHz} = 232000 = 0x038A40$ .

A complete description of the available commands is provided by Siverts IMA.

### Voltage Controlled Oscillators and Mixers

Two of the available VCOs, one of each modality, should be connected to the TX IF “I” input, as illustrated in **Figure 40**.

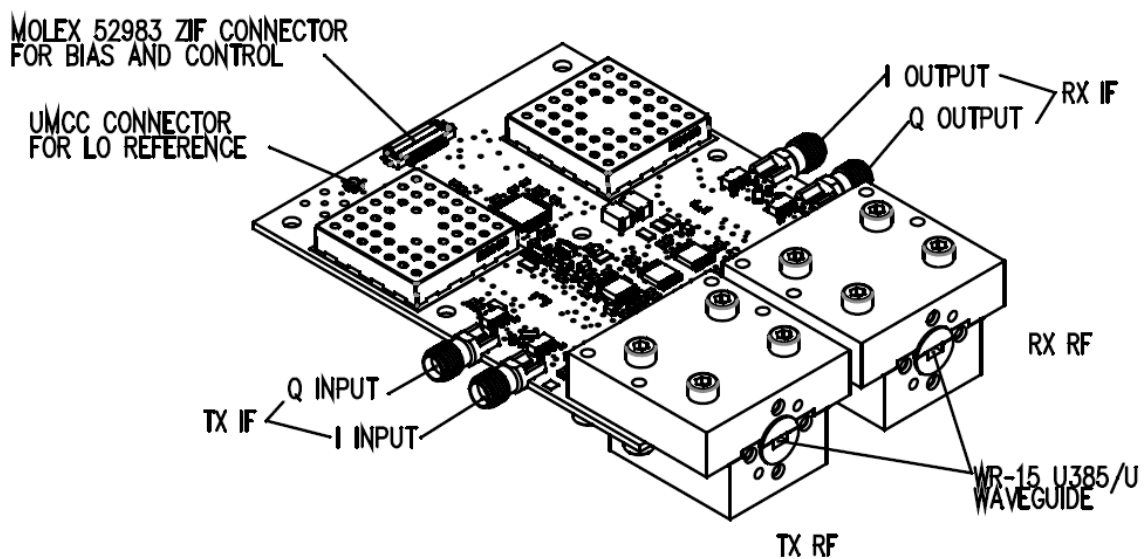


*Figure 40 – Connection diagram of the converter board.*

The remaining two VCOs should be connected to the “R” input of the mixers (Mini Circuits ZFM-15-S+).

As for power supply, the ZX95-2150-VW and the ZX95-3800A-S+ VCOs connect to 6 V and 5 V respectively. For the first, a voltage regulator (6 V) was used with a 12 V input from the digital lab. The use of a dissipater was necessary. For the last, connection was made directly to the 5 V output of the digital lab.

For the VCOs that connect directly to the TX inputs of the board, the tune voltage is defined by the microcontroller units (“high” and “low” values). These pins should be connected to the PC0 pin of the MCU (pin number 22).

As for the other two VCOs, which belong to the downconversion unit, their tune voltage should be controlled by a potentiometer. The input of the potentiometer should be 6 V (output of the aforementioned voltage regulator) and its value should be adjusted with the help of a spectrum analyser, so that the mixer’s frequency output is 5 MHz.

The “L” inputs of the mixers should be connected to the RX “I” outputs of the converter boards- The output of the mixers connect to the DIP decoding circuit, after an amplification.

All VCOs connect to ground. The mixers are passive components.

*A summary of the connections of the VCOs is presented in **Table 14** and of the mixers in*

**Table 15.**

*Table 14 – Connection summary of the VCOs.*

<i>VCO</i>	<i>V<sub>CC</sub></i>	<i>V<sub>TUNE</sub></i>	<i>GND</i>	<i>Output</i>
<i>VCO<sub>1</sub> - ZX95-2150-VW</i>	6 V – Voltage regulator (12 V input from Digital Lab)	Microcontroller output (PC0)	Digital Lab	TX IF “I” input of Converter
<i>VCO<sub>2</sub> - ZX95-3800A-S+</i>	5 V from Digital Lab	Microcontroller output (PC0)	Digital Lab	TX IF “I” input of Converter
<i>VCO<sub>3</sub> - ZX95-2150-VW</i>	6 V – Voltage regulator (12 V input from Digital Lab)	Potentiometer output	Digital Lab	“R” input of Mixer
<i>VCO<sub>4</sub> - ZX95-3800A-S+</i>	5 V from Digital Lab	Potentiometer output	Digital Lab	“R” input of Mixer

*Table 15 – Connection summary of the mixers.*

<i>Mixer</i>	<i>“L” input</i>	<i>“R” input</i>	<i>Output</i>
<i>Mixer<sub>1</sub> - ZFM-15-S+</i>	RX IF “I” output of Converter	Output of VCO <sub>3</sub>	Coaxial Amplifier
<i>Mixer<sub>2</sub> - ZFM-15-S+</i>	RX IF “I” output of Converter	Output of VCO <sub>4</sub>	Coaxial Amplifier

### Coaxial Amplifiers

Two different amplifiers should be connected to the outputs of the mixers to help compensate for the conversion loss.

The available amplifiers were ZX60-14012L-S+ and ZFL-1000LN+ from Mini Circuits, which connect to a 12 V power supply.

*Table 16 – Connection summary of the amplifiers*

<i>Amplifier</i>	<i>V<sub>CC</sub></i>	<i>GND</i>	<i>Input</i>	<i>Output</i>
<i>ZX60-14012L-S+</i>	12 V from Digital Lab	Digital Lab	Mixer output	Decoding DIP circuit
<i>ZFL-1000LN</i>	12 V from Digital Lab	Digital Lab	Mixer output	Decoding DIP circuit

### Decoding Circuit in Breadboard

As aforementioned, the output of the coaxial amplifiers connects to the input of the decoding circuit, which is the input of an inverter amplifier. Connection schematic is presented in **Figure 41**.

All integrated circuits have a power supply of  $\pm 12$  V, from the Digital Lab.

The last amplifier has a potentiometer whose resistance value should be adjusted as to allow an output of 5 V for a “high” sequence value. Its output should be connected to the microcontroller unit.

A summary of the connections is presented in **Table 17**.

*Table 17 – Decoding circuit’s connection summary*

	<i>Input</i>	<i>Output</i>
<i>Tag circuit</i>	Coaxial Amplifier connected to mixer	Microcontroller Unit (PA0)
<i>Reader circuit</i>	Coaxial Amplifier connected to mixer	Microcontroller Unit (PD2)

Microcontroller Units

The microcontrollers serve as both the initial and final units of the system, as they’re responsible for generating the sequence that is to be transmitted and interpreting the sequence that is received.

Pin diagrams explaining how all the connections should be made are presented in **Figure 20**. Nevertheless, a summary of these connections is presented in **Table 18**.

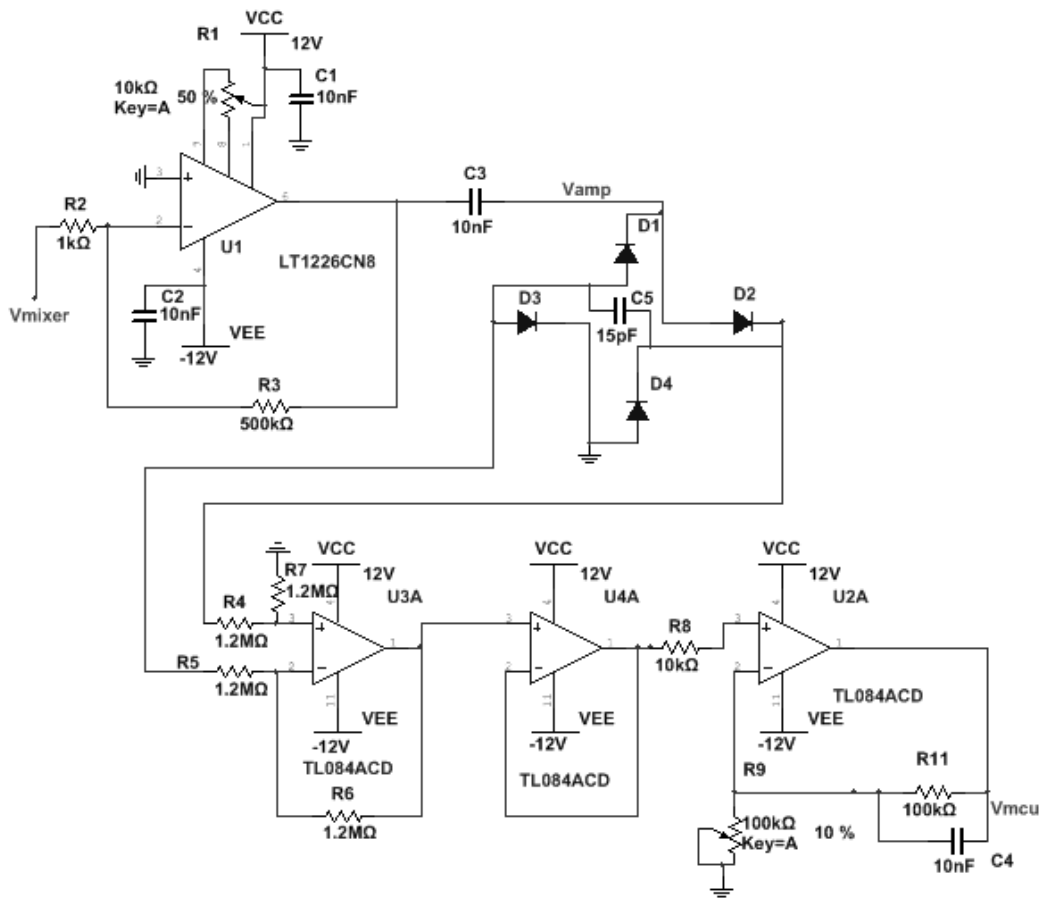


*Figure 41 – Schematic of the decoding circuit*

*Table 18 – Microcontroller units' connection summary*

-	<i>Inputs</i>	<i>Outputs</i>	<i>LEDs</i>
<i>Reader MCU</i>	PA0 – Decoding circuit output PD2 – Push button from Digital Lab	PC0 – $V_{TUNE}$ of VCO <sub>1</sub>	PB0 – Receive Mode PB1 – Transmit Mode PD5 – Correct Sequence PD6 – Incorrect Sequence
<i>Tag MCU</i>	PD2 – Decoding circuit output	PC0 – $V_{TUNE}$ of VCO <sub>2</sub>	PB0 – Receive Mode PB1 – Transmit Mode